THE IMPACT OF STEFIN B AND CYSTATIN C DEFICIENCY ON CANCER PROGRESSION AND TUMOR MICROENVIRONMENT IN A MOUSE BREAST CANCER MODEL

Petra Matjan Štefin

Doctoral Dissertation
Jožef Stefan International Postgraduate School
Ljubljana, Slovenia

Supervisor: Dr. Georgy Mikhaylov, Jožef Stefan Institute, Ljubljana, Slovenia
Co-supervisor: Prof. Dr. Olga Vasiljeva, Jožef Stefan Institute, Ljubljana, Slovenia

Evaluation Board:
Prof. DDr. Boris Turk, Chair, Jožef Stefan Institute, Ljubljana, Slovenia
Prof. Dr. Nataša Kopitar Jerala, Member, Jožef Stefan Institute, Ljubljana, Slovenia
Prof. Dr. Marko Novinec, Member, Faculty of Chemistry and Chemical Technology, University of Ljubljana, Ljubljana, Slovenia

MEDNARODNA PODIPLOMSKA ŠOLA JOŽEFA STEFANA
JOŽEF STEFAN INTERNATIONAL POSTGRADUATE SCHOOL



Petra Matjan Štefin

THE IMPACT OF STEFIN B AND CYSTATIN C DEFICIENCY ON CANCER PROGRESSION AND TUMOR MICROENVIRONMENT IN A MOUSE BREAST CANCER MODEL

Doctoral Dissertation

VPLIV ODSTRANITVE STEFINA B IN CISTATINA C NA NAPREDOVANJE RAKA IN TUMORSKO MIKROOKOLJE PRI MIŠJEM MODELU RAKA DOJKE

Doktorska disertacija

Supervisor: Dr. Georgy Mikhaylov
Co-supervisor: Prof. Dr. Olga Vasiljeva

Ljubljana, Slovenia, September 2026

Acknowledgments

I thank the Slovenian Research Agency for funding my doctoral studies.

I would like to thank my supervisor, Dr. Georgy Mikhaylov, for the supervision of my dissertation and for all the advice concerning my work. I am also thankful for the review of my doctoral thesis.

I would like to sincerely thank my co-supervisor, Prof. Dr. Olga Vasiljeva, for her guidance, advice, and supervision of my research work despite the great physical distance, and for her critical review of my doctoral thesis.

I am grateful to the head of the B1 research group, Prof. DDr. Boris Turk, for welcoming me into the group, which made this work possible. Thank you also for entrusting me with the management of the animal facility at the Jožef Stefan Institute.

I would like to thank the members of the evaluation board, Prof. DDr. Boris Turk, Prof. Dr. Nataša Kopitar Jerala, and Prof. Dr. Marko Novinec, for reviewing my doctoral dissertation and providing their expert opinion.

I would also like to thank Dr. Andreja Kozak for her guidance and all her help in my scientific work, as well as for all the professional and non-professional discussions.

I thank Ivica Štefe for her valuable technical assistance.

I would like to thank all of the B1 Department for their help and advice, and for providing a stimulating work atmosphere.

Special thanks go to my family and friends for all their support throughout the study.

Grammarly software was used for grammar checking and to improve the clarity of the text in this thesis.

Abstract

Lysosomal cysteine cathepsins participate in numerous physiological processes and are also involved in pathological conditions such as cancer and inflammation. Proteolytic activity of cysteine cathepsins is tightly regulated by endogenous inhibitors of the cystatin superfamily, among which stefin B is an intracellular, and cystatin C is an extracellular inhibitor. Altered expression of stefin B and cystatin C has been reported in multiple types of cancer; however, their combined roles in tumor progression remain unclear.

In this study, we investigated the role of stefin B (StfB) and cystatin C (CstC) in mammary tumor progression and metastasis. We established a double knockout (DKO) mouse mammary cancer model by crossing StfB and CstC-deficient mice with transgenic polyoma virus middle T oncogene (PyMT) mice that spontaneously develop mammary gland adenocarcinomas. We show that ablation of both StfB and CstC resulted in delayed tumor onset and reduced tumor growth compared to wild-type mice. Furthermore, we detected decreased proliferation and increased apoptosis in DKO tumors, along with significantly reduced pulmonary metastasis in DKO mice. These findings suggest that both inhibitors promote not only primary tumor growth but also metastatic spread.

We next investigated the impact of stefin B and cystatin C deficiency on the tumor microenvironment and immune modulation. Immunohistochemical analysis revealed increased macrophage infiltration in DKO tumors, together with a pronounced shift toward M1 polarization, while M2 populations remained unchanged. This reprogramming of the tumor microenvironment toward an anti-tumor state suggests that stefin B and cystatin C modulate immune responses to favor tumor progression.

Our findings demonstrate that stefin B and cystatin C deficiency affects tumor progression by reducing tumor burden and metastatic spread. Additionally, we showed that stefin B and cystatin C function through complementary mechanisms affecting both tumor cell-intrinsic pathways and the immune landscape.

Povzetek

Lizosomalni cisteinski katepsini sodelujejo v številnih fizioloških procesih ter so vključeni tudi pri patoloških stanjih, kot sta rak in vnetje. Njihova proteolitična aktivnost je strogo regulirana z endogenimi inhibitorji cistatinske naddružine, med katere spadata intracelularni stefin B in ekstracelularni cistatin C. Spremenjeno izražanje stefina B in cistatina C je bilo opisano pri več vrstah raka, vendar njuna kombinirana vloga pri tumorskem napredovanju še vedno ostaja nejasna.

V študiji smo raziskali vlogo stefina B (StfB) in cistatina C (CstC) pri tumorskem napredovanju in metastaziranju. Ustvarili smo mišji model raka mlečne žleze z dvojnim izbitjem (DKO) s križanjem miši brez StfB in CstC s transgenimi mišmi, ki izražajo poliomavirusni middle T onkogen (PyMT) in spontano razvijejo adenokarcinome mlečne žleze. Pokazali smo, da je izbitje StfB in CstC povzročilo kasnejši pojav tumorjev in njihovo zmanjšano rast v primerjavi z mišmi divjega tipa. Poleg tega smo odkrili zmanjšano proliferacijo in povečano apoptozo DKO tumorjev, skupaj z značilno manjšimi pljučnimi metastazami. Naše ugotovitve kažejo, da oba inhibitorja spodbujata tako rast prvotnih tumorjev kot tudi metastaziranje.

Nadalje smo raziskali tudi vpliv pomanjkanja stefina B in cistatina C na tumorsko mikrookolje in imunski odziv. Z imunohistokemijsko analizo smo dokazali povečano infiltracijo makrofagov v DKO tumorjih z izrazitim premikom v smer polarizacije M1-makrofagov, medtem ko populacija M2 makrofagov ni bila spremenjena. Preoblikovanje tumorskega mikrookolja v smer protitumorskega stanja nakazuje, da stefin B in cistatin C modulirata imunske odzive na način, ki spodbuja tumorsko napredovanje.

Naši rezultati kažejo, da pomanjkanje stefina B in cistatina C vpliva na napredovanje tumorjev z zmanjšanjem tumorskega bremena in metastaziranja. Pokazali smo tudi, da oba inhibitorja delujeta preko komplementarnih mehanizmov, ki vplivajo tako na od znotraj sprožene poti tumorskih celic kot tudi na imunsko okolje.

Contents

List of Figures **xv**

List of Tables **xix**

Abbreviations **xxi**

1 Introduction **1**
1.1 Cancer ... 1
1.1.1 Hallmarks of cancer ... 1
1.1.1.1 Tumor microenvironment ... 2
1.1.1.1.1 Tumor-associated macrophages ... 3
1.1.1.2 Metastasis ... 4
1.1.2 Breast cancer ... 5
1.1.2.1 Clinical and biological features of breast cancer ... 5
1.1.2.2 Mouse models of breast cancer ... 6
1.1.2.2.1 The MMTV-PyMT mouse model of mammary carcinoma ... 6
1.2 Proteases ... 8
1.2.1 Proteolytic enzymes in physiology and disease ... 8
1.2.2 Cysteine proteases ... 8
1.2.2.1 Lysosomal cysteine cathepsins ... 9
1.2.2.1.1 Localization and activation of cysteine cathepsins ... 9
1.2.2.1.2 Regulation of cysteine cathepsin activity ... 9
1.2.2.2 Cysteine cathepsins in cancer ... 10
1.3 Inhibitors of Cysteine Cathepsins ... 11
1.3.1 Cystatins ... 11
1.3.1.1 Type I cystatins ... 12
1.3.1.1.1 Stefin B ... 12
1.3.1.1.1.1 Stefin B in cancer ... 13
1.3.1.2 Type II cystatins ... 13
1.3.1.2.1 Cystatin C ... 14
1.3.1.2.1.1 Cystatin C in cancer ... 14
1.3.1.3 Type III cystatins ... 16
1.3.1.4 Simultaneous stefin B and cystatin C deficiency (double knockout, DKO) in breast cancer ... 16
1.3.2 Pharmacological inhibitors of cysteine cathepsins ... 16

2 Purpose of the Work **19**

3 Materials and Methods **21**
3.1 Materials ... 21
3.1.1 Equipment ... 21

3.1.2 Chemicals and commercial kits 22
3.1.3 Buffers, solutions, and media 23
3.1.4 Enzymes 24
3.1.5 Antibodies 25
3.1.6 Mammalian cell line 25
3.1.7 Animals 25
3.1.7.1 Mouse strains and genetic background 25
3.1.7.2 MMTV-PyMT mouse breast cancer model 25
3.2 Methods 26
3.2.1 Animal studies 26
3.2.1.1 Laboratory mouse breeding and housing 26
3.2.1.2 Monitoring tumor growth progression 26
3.2.1.3 LPS-induced neuroinflammation model in stefin B-deficient mice 26
3.2.2 Sample preparation and tissue processing 27
3.2.2.1 Organ collection 27
3.2.2.1.1 Organs for paraffin-embedded sections 27
3.2.2.1.2 Organs for cryo sections 27
3.2.2.1.3 Organs for mRNA isolation 27
3.2.2.1.4 Brain and cerebellar tissue collection 27
3.2.2.2 Preparation of tumor lysates 27
3.2.2.3 Preparation of brain and cerebellar tissue lysates 27
3.2.2.4 Preparation of primary PyMT tumor cells 27
3.2.3 Cell culture work 28
3.2.3.1 Cell lysates from primary PyMT tumor cells 28
3.2.3.2 BrdU cell proliferation assay 28
3.2.4 Gene expression and molecular analysis 28
3.2.4.1 Quantitative Real-Time PCR 28
3.2.5 Protein analysis and biochemical assays 28
3.2.6 Protein detection and characterization 28
3.2.6.1 Immunoblotting 28
3.2.7 Histological and imaging methods 29
3.2.7.1 Histomorphometry 29
3.2.7.2 Histopathology 29
3.2.7.3 Tumor-stroma ratio 29
3.2.7.4 Immunohistochemistry and immunofluorescence 29
3.2.7.4.1 Immunohistochemistry 29
3.2.7.4.2 Immunofluorescence 30
3.2.7.5 Microscopy and image analysis 30
3.2.8 Pharmacological inhibition of cathepsins X and B in PyMT breast cancer models 30
3.2.8.1 Inhibitors and vehicle preparation 30
3.2.8.2 FVB;PyMT transgenic mouse model and treatment 30
3.2.8.3 Orthotopic MMTV-PyMT tumor model 30
3.2.9 Statistical analysis 31

4 Results **33**
4.1 Analysis of PyMT Mammary Carcinomas 33
4.1.1 Confirmation of stefin B and cystatin C depletion in tumors from PyMT;DKO mice 33
4.1.2 Tumor size and weight assessment 35

4.1.3 Effect of stefin B and cystatin C deficiency on cell proliferation, cell death, and vascularization in PyMT mammary tumors 37
4.1.4 Evaluation of metastasis in PyMT mammary tumors 39
4.1.5 Histological characteristics of PyMT mammary carcinomas and organs 40
4.2 Analysis of PyMT Primary Tumor Cells 42
4.2.1 *In vitro* proliferation of primary PyMT tumor cells 42
4.3 Expression and Activity of Cysteine Cathepsins 43
4.3.1 mRNA expression of cathepsins 43
4.3.2 Cathepsin activity in tumor tissue 44
4.3.3 Cathepsin activity in primary cell media and tumor lysates 45
4.4 AMPK Activation in PyMT Mammary Tumors 46
4.4.1 Western blot analysis of phospho-AMPK (Thr172) and total AMPK in PyMT tumors 46
4.5 Tumor Microenvironment and Immune Cell Infiltration 48
4.5.1 Immunohistochemical assessment of macrophage infiltration 48
4.5.2 Immunohistochemical detection of M1 and M2 macrophages 48
4.6 Comparison with Single-Knockout PyMT Breast Cancer Models 50
4.6.1 Tumor onset 50
4.6.2 Cumulative tumor weight 50
4.6.3 Cell proliferation 50
4.6.4 Apoptosis 50
4.6.5 Angiogenesis 51
4.6.6 Lung metastasis 51
4.6.7 Cysteine cathepsin activity 51
4.7 Pharmacological Inhibition of Cathepsins B and X Impairs Tumor Progression in MMTV-PyMT Breast Cancer Models 53
4.7.1 Z9 and nitroxoline reduce mammary tumor burden in FVB;PyMT transgenic mice 54
4.7.2 Z9 and nitroxoline reduce pulmonary metastatic burden in FVB;PyMT transgenic mice 54
4.7.3 Pharmacological inhibition of cathepsins B and X suppresses tumor growth in an orthotopic MMTV-PyMT model 55
4.8 Stefin B deficiency and mitochondrial redox response during LPS-induced neuroinflammation 56

5 Discussion **59**

6 Conclusions **65**

References **67**

Bibliography **79**

Biography **81**

List of Figures

Figure 1: The tumor microenvironment and its role in cancer progression. Key components of the TME interact dynamically to support tumor growth, immune evasion, and metastatic dissemination (Quail & Joyce, 2013).....2
Figure 2: M1-like and M2-like macrophages in the tumor microenvironment (Qiu et al., 2022). 3
Figure 3: Progression of MMTV-PyMT mammary carcinomas through four stages: hyperplasia, intraepithelial neoplasia, early carcinoma, and late carcinoma (Attalla et al., 2021). 7
Figure 4: Stefin B and cystatin C expression in PyMT mammary tumors. (A) Western blot analysis of StfB in mammary tumors from PyMT;WT, PyMT;StfB^{-}/$^{-}$, PyMT;CstC^{-}/$^{-}$, and PyMT;DKO mice. StfB is present in PyMT;WT and PyMT;CstC^{-}/$^{-}$ tumors, but absent in PyMT;StfB^{-}/$^{-}$ and PyMT;DKO tumors. β-Actin was used as a loading control. (B) Western blot analysis of cystatin C (CstC) in the same tumor lysates. CstC is present in PyMT;WT and PyMT;StfB^{-}/$^{-}$ tumors, but absent in PyMT;CstC^{-}/$^{-}$ and PyMT;DKO tumors. β-Actin was used as a loading control. 34
Figure 5: Delayed tumor onset in PyMT;DKO female mice. The Kaplan–Meier curves of tumor-free survival for PyMT;WT (n=22; dark blue line) and PyMT;DKO (n=17, turquoise line) female mice, showing a modest but significant delay in the occurrence of the first palpable mammary tumor. Statistical analysis suggests a significant difference in tumor-free survival between the two groups ($p < 0.05$), with the PyMT;DKO group showing a delayed onset of tumors and longer survival than PyMT;WT mice. The hazard ratio (HR) for PyMT;DKO versus PyMT;WT group was 0.59 (95% CI: 0.24–0.85). Differences were analyzed using the Mantel-Cox log-rank test.....35
Figure 6: Tumor size distribution in PyMT;WT and PyMT;DKO female mice. The tumor size of two individual tumors 30 days after first detection with palpation from PyMT;WT (n=37) and PyMT;DKO (n=34) groups. $p < 0.01$ by the chi-square test. 36
Figure 7: The cumulative tumor weight in PyMT;WT and PyMT;DKO female mice at 14 weeks of age. The total tumor weight per mouse for all mammary tumors was calculated for PyMT;WT (n = 13) and PyMT;DKO (n = 12) mice after tumor excision at necropsy. Differences were analyzed using Student's t-test, $p < 0.001$.....36
Figure 8: Effect of stefin B and cystatin C deficiency on tumor cell proliferation in PyMT mammary tumors. (A) Representative Ki67 immunohistochemical staining of primary mammary tumors from PyMT;WT and PyMT;DKO female mice at 14 weeks of age (scale bar: 100 µm). (B) Quantification of Ki67-positive nuclei shows a marked decrease in the proliferation index in PyMT;DKO tumors compared with PyMT;WT controls (PyMT;WT: n=11; PyMT;DKO: n=10). Differences were analyzed using Student's t-test, $p < 0.0001$..
.....37
Figure 9: Cell death in PyMT mammary carcinomas from both genotypes, determined through TUNEL assays. Representative images (A) and quantification (B) of TUNEL-positive cells as a percentage of total cells in PyMT;WT (n=9) and PyMT;DKO (n=8) tumors. The TUNEL+ index was calculated from 10 high-power fields per tumor using

computer-assisted data analysis in ImageJ. Differences were analyzed using Student's t-test. Scale bar: 100 µm. 38
Figure 10: Tumor vascularization in PyMT;WT and PyMT;DKO mammary tumors. (A) Representative immunofluorescence images of tumor sections stained with the endothelial cell marker CD31 (red) and counterstained with DAPI (blue) from PyMT;WT and PyMT;DKO mice. Scale bar: 100 µm. (B) Quantification of CD31-positive area expressed as a percentage of total tumor area. No statistically significant difference in vascularization was observed between PyMT;WT, and PyMT;DKO tumors (n.s., not significant)..... 39
Figure 11: Effect of stefin B and cystatin C on pulmonary metastasis development in the PyMT breast cancer model. (A) Representative histological sections of lungs showing metastatic foci in PyMT;WT and PyMT;DKO female mice at 14 weeks of age (scale bar: 50 µm). (B) Histomorphometric analysis of the number of lung metastases in PyMT;WT (n=14) and PyMT;DKO (n=14) female mice at 14 weeks ($p < 0.05$). (C) Average size of individual lung metastases in PyMT;WT (n=14) and PyMT;DKO (n=14) mice, showing no statistically significant difference between genotypes (n.s., non-significant). Differences were analyzed using Student's t-test. 40
Figure 12: Tumor stroma ratio (TSR) in PyMT;WT and PyMT;DKO mammary tumors. The TSR (%) was calculated as the mean from 5 tissue sections per group, with 3 fields of view (FOV) examined per section at 10x magnification. Tumor and stroma areas were measured using CellSens software (Olympus). 41
Figure 13: Histopathological examination of major organ tissues from different genotypes. Liver, kidney, lung, and spleen sections from PyMT;WT, PyMT;DKO, PyMT;StfB^{-}/$^{-}$, and PyMT;CstC^{-}/$^{-}$ mice were stained with hematoxylin and eosin, and comparative histopathological assessment was performed. Scale bar: 100 µm. 42
Figure 14: Reduced proliferation of primary PyMT;DKO tumor cells *in vitro*. BrdU incorporation assay of primary tumor cells isolated from PyMT;WT and PyMT;DKO mice. PyMT;DKO cells showed significantly reduced proliferation compared to PyMT;WT cells. Data are presented as mean ± SEM ($p < 0.01$)..... 43
Figure 15: Expression of cysteine cathepsins in PyMT;WT (black, n=3) and PyMT;DKO (white, n=3) primary mammary tumors. Relative mRNA levels of cathepsin B (CtsB), cathepsin H (CtsH), cathepsin L (CtsL), cathepsin S (CtsS) and cathepsin Z (CtsZ) were determined by quantitative real-time PCR, normalized to reference genes (Atp5b, Ubc), and expressed relative to PyMT;WT (set to 1). Error bars represent 95% confidence intervals (CI) for expression ratios calculated by REST 2009 (randomisation test, 2000 iterations). CtsS is significantly upregulated in PyMT;DKO tumors compared with PyMT;WT (fold change 1.353, 95% CI 1.032–1.922, P(H1) = 0.011), whereas CtsB, CtsH, CtsL and CtsZ show no significant differences between genotypes. 44
Figure 16: Relative cysteine cathepsin activity in tumor homogenates in PyMT;WT and PyMT;DKO mice. Activity was measured by Z-Phe-Arg-AMC hydrolysis in the presence or absence of the cysteine cathepsin inhibitor E64. The graph is showing significantly increased activity in PyMT;DKO tumors compared with PyMT;WT controls ($p < 0.001$). 45
Figure 17: Relative cysteine cathepsin activity in conditioned media from primary PyMT;WT and PyMT;DKO tumor cells. The activity was measured by Z-Phe-Arg-AMC hydrolysis in the presence or absence of the cysteine cathepsin inhibitor E64. The graph is showing a marked increase in extracellular cathepsin activity in PyMT;DKO cultures compared with PyMT;WT controls ($p < 0.001$). 46
Figure 18: Comparison of p-AMPK expression between genotypes in PyMT mammary carcinomas. Representative Western blots show p-AMPK levels in tumors from PyMT;WT, PyMT;StfB−/−, PyMT;CstC−/−, and PyMT;DKO mice. β-actin served as a loading control. 47

Figure 19: Total AMPK expression in PYMT mammary carcinomas in different genotypes. Representative Western blots show total AMPK levels in tumors from PyMT;WT, PyMT;StfB−/−, PyMT;CstC−/−, and PyMT;DKO mice. β-actin served as a loading control. 47
Figure 20: Effect of stefin B and cystatin C deficiency on macrophage infiltration in PyMT mammary tumors. (A) Representative microscopic images of immunohistochemical staining of F4/80, a broadly used marker for macrophages, in mammary tumors from PyMT;WT and PyMT;DKO mice. Scale bar: 100 μm. (B) Quantification of F4/80-positive cells as a percentage of total cells in PyMT;WT (n=5) and PyMT;DKO (n=5) tumors. Statistical significance was determined using Student's t-test. 48
Figure 21: Effect of stefin B and cystatin C deficiency on macrophage polarization in PyMT mammary tumors. (A) Representative microscopic images of immunohistochemical staining of M1 macrophages using the CD86 marker in mammary tumors from PyMT;WT and PyMT;DKO mice with CD86 marker. Scale bar: 100 μm. (B) Quantification of CD86-positive cells as a percentage of total cells in PyMT;WT (n=5) and PyMT;DKO (n=5) tumors. (C) Representative immunohistochemical staining of M2 macrophages using the CD206 marker in mammary tumors from PyMT;WT and PyMT;DKO mice. Scale bar: 100 μm. (D) Quantification of CD206-positive cells as a percentage of total cells in PyMT;WT (n=5) and PyMT;DKO (n=5) tumors. Statistical significance was determined using Student's t-test. 49
Figure 22: Z9 and nitroxoline reduce mammary tumor burden in FVB;PyMT transgenic mice. Eleven-week-old female FVB;PyMT transgenic mice were treated intraperitoneally every other day with vehicle (5% DMSO in peanut oil), the selective reversible cathepsin X inhibitor Z9 (67.18 mg/kg), the cathepsin B inhibitor nitroxoline (40 mg/kg), or the combination of Z9 (67.18 mg/kg) and nitroxoline (40 mg/kg). Mice were sacrificed at 14 weeks of age, and all mammary tumors were excised and weighed. (A) Cumulative mammary tumor weight per mouse was significantly reduced in the Z9-, nitroxoline-, and combination-treated groups compared with vehicle-treated controls. (B) Representative images of excised mammary tumors from the respective treatment groups. Data are presented as mean ± SEM. *p≤0.05, **p≤0.01. 54
Figure 23: Z9 and nitroxoline reduce pulmonary metastatic burden in FVB;PyMT transgenic mice. At 14 weeks of age, lungs were collected from vehicle-, Z9-, nitroxoline-, and Z9/nitroxoline-treated FVB;PyMT transgenic mice. Paraffin-embedded lung sections were stained with hematoxylin and eosin, and pulmonary metastatic lesions were evaluated by histomorphometric analysis. The number of pulmonary metastases per mm^2 of lung tissue and the mean cross-sectional area of individual metastases were significantly reduced in all inhibitor-treated groups compared with vehicle-treated controls. Data are presented as mean ± SEM. *p≤0.05 55
Figure 24: Z9 and nitroxoline impair tumor growth in an orthotopic MMTV-PyMT breast cancer model. Orthotopic mammary tumors were established in female FVB mice. When tumor volume reached approximately 125 mm^3, mice were treated intraperitoneally every other day with vehicle (5% DMSO in peanut oil), Z9 (33.59 mg/kg), nitroxoline (20 mg/kg), or the combination of Z9 (33.59 mg/kg) and nitroxoline (20 mg/kg). (A) Tumor volume was measured every other day throughout treatment. Z9, nitroxoline, and combined treatment significantly reduced tumor growth compared with vehicle treatment; the table suggests the time points at which statistically significant differences relative to controls were observed. (B) Representative images of orthotopic tumors collected from each treatment group. Data are presented as mean ± SEM. *p≤0.05, **p≤0.01, ***p≤0.001. .56
Figure 25: Peroxiredoxin 3 (Prx3) expression in brain and cerebellar tissue of stefin B-deficient (StfB KO) and wild-type (WT) mice under basal conditions and during LPS-induced neuroinflammation. (A, B) Western blot analysis of Prx3 and β-actin in brain

lysates from untreated control (A) and LPS-treated (3 mg/kg, 4 h) (B) WT and StfB KO mice. (C, D) Western blot analysis of Prx3 and β-actin in cerebellar lysates from untreated (C) and LPS-treated (D) WT and StfB KO mice. (E, F) Densitometric quantification of Prx3 protein levels in brain (E) and cerebellar (F) lysates relative to β-actin. Prx3 expression is significantly increased in brain tissue of LPS-treated StfB KO mice compared with WT controls and is elevated in cerebellar tissue of StfB KO mice both under basal conditions and after LPS challenge (*$p < 0.05$)..... 57

List of Tables

Table 1: Comparison of key tumor parameters across PyMT knockout breast cancer models. Results from stefin B single-knockout (PyMT;StfB^{-}/$^{-}$; StfB KO), cystatin C single-knockout (PyMT;CstC^{-}/$^{-}$; CstC KO), and double-knockout (PyMT;DKO) PyMT breast cancer models relative to wild-type (WT) controls (Butinar et al., 2014; Matjan Štefin et al., 2026; Završnik et al., 2017).....52

Abbreviations

ABC	...	avidin-biotin complex
AMPK	...	AMP-activated protein kinase
APC	...	antigen-presenting cell
BcL-2	...	B-cell lymphoma 2
BrdU	...	5-bromo-2'-deoxyuridine
BSA	...	bovine serum albumin
CD31	...	cluster of differentiation 31
CD86	...	cluster of differentiation 86
CD206	...	cluster of differentiation 206
cDMEM	...	complemented Dulbecco's Modified Eagle Medium
CstC	...	cystatin C
CT	...	computer tomography
CTSB	...	cathepsin B
CTSH	...	cathepsin H
CTSL	...	cathepsin L
CTSS	...	cathepsin S
CTSX	...	cathepsin X
DAB	...	3,3′-diaminobenzidine
dH20	...	destilled water
DKO	...	double knockout
DMEM	...	Dulbecco's Modified Eagle Medium
DMSO	...	dimethyl sulfoxide
DNA	...	deoxyribonucleic acid
DTT	...	dithiothreitol
ECM	...	extracellular matrix
EDTA	...	ethylenediaminetetraacetic acid
EMT	...	epithelial-mesenchymal transition
EPM1	...	progressive myoclonus epilepsy type 1
FADD	...	Fas-associated protein with death domain
FBS	...	fetal bovine serum
FLIP	...	FLICE-like inhibitory protein
FOV	...	field of view
HRP	...	horseradish peroxidase
IL-10	...	interleukin-10
IL-18	...	interleukin-18
K_i	...	inhibition constant
KO	...	knockout
LPS	...	lipopolysaccharide
MMP	...	matrix metalloprotease
MMTV-PyMT	...	Mouse mammary tumor virus-Polyoma virus middle T oncogene
MRI	...	magnetic resonance imaging

NK	...	natural killer
NLRP3	...	NOD-, LRR- and pyrin domain-containing protein 3
PBS	...	phosphate-buffered saline
PBST	...	phosphate-buffered saline with Tween-20
PECAM-1	...	platelet endothelial cell adhesion molecule-1
PEG	...	polyethylene glycol
Prx3	...	peroxiredoxin 3
PyMT	...	polyoma middle T antigen
RNA	...	ribonucleic acid
SDS-PAGE	...	sodium dodecyl sulfate-polyacrylamide gel electrophoresis
StfB	...	stefin B
TAM	...	tumor-associated macrophage
TME	...	tumor microenvironment
TSR		tumor-stroma ratio
WT		wild-type

Chapter 1

Introduction

1.1 Cancer

Cancer is one of the most fatal and complex diseases. It was the leading cause of death globally in 2022, with 20 million people diagnosed as new cases and 9.7 million deaths recorded that year (Bray et al., 2024). However, its burden is distributed unequally due to differences in cancer incidence and mortality rates that vary significantly by geography, socioeconomic status, and access to healthcare. Although major advances in early cancer detection, surgery, radiotherapy, chemotherapy, and targeted biological therapies have substantially improved outcomes for several cancer types, many patients still progress to metastatic disease, for which treatment options remain limited and are rarely curable (Bray et al., 2024; Sung et al., 2021). Therefore, much effort has been put into a deeper understanding of the molecular mechanisms responsible for tumor growth and metastasis to develop novel therapeutic strategies and to optimize the use of current ones (Hanahan & Weinberg, 2011).

Cancer develops when cells start to divide uncontrollably and escape the regulatory mechanisms that maintain tissue homeostasis. In most cases, this is driven by the gradual accumulation of genetic and epigenetic alterations over time that disrupt key pathways regulating cell growth, survival, and differentiation. A major reason cancer remains such a challenging and complex disease is its remarkable diversity (Hanahan, 2022; Hanahan & Weinberg, 2011). Across different tissues, tumors can exhibit significant differences in their molecular profiles, growth patterns, and responses to therapy, and sometimes these differences even exist within a single tissue (Hanahan & Weinberg, 2011; McGranahan & Swanton, 2017). Despite this heterogeneity, researchers have identified a group of shared biological characteristics, known as the hallmarks of cancer, that provide a comprehensive framework for understanding malignant transformation across diverse tumor types (Hanahan, 2022; Hanahan & Weinberg, 2011).

1.1.1 Hallmarks of cancer

In 2000, Hanahan and Weinberg introduced the concept, which proposes that malignant cells, regardless of tumor type, acquire a common set of functional properties during their evolution (Hanahan & Weinberg, 2000). The original six hallmarks are sustaining proliferative signaling, evading growth suppressors, resisting cell death, enabling replicative immortality, inducing angiogenesis, and activating invasion and metastasis (Hanahan & Weinberg, 2000). Additionally, deregulated cellular energetics, evasion of immune destruction, genome instability, tumor-promoting inflammation, and recently discovered phenotypic plasticity and non-mutational epigenetic reprogramming, all contribute to the

ability of tumor cells to adapt to hostile microenvironments and resist therapy (Hanahan, 2022; Hanahan & Weinberg, 2011).

1.1.1.1 Tumor microenvironment

The tumor microenvironment (TME) is the dynamic ecosystem surrounding and supporting cancer cells within a tumor. It consists of a diverse group of non-malignant cells, including cancer-associated fibroblasts, endothelial cells, pericytes, and immune cells such as macrophages, dendritic cells, T cells, and natural killer cells, all embedded within constantly remodeled extracellular matrix (ECM) (Hanahan & Coussens, 2012; Quail & Joyce, 2013). The TME plays an important role throughout every stage of tumor development and progression, from initiation and local growth to invasion and distant metastasis (Quail & Joyce, 2013). Paracrine signaling between tumor cells and stromal components maintains the supply of growth factors, creates metabolic and oxygen gradients, and fosters chronic tumor-promoting inflammation. All factors together are thus creating an environment that is enabling disease progression (Hanahan & Coussens, 2012; Quail & Joyce, 2013).

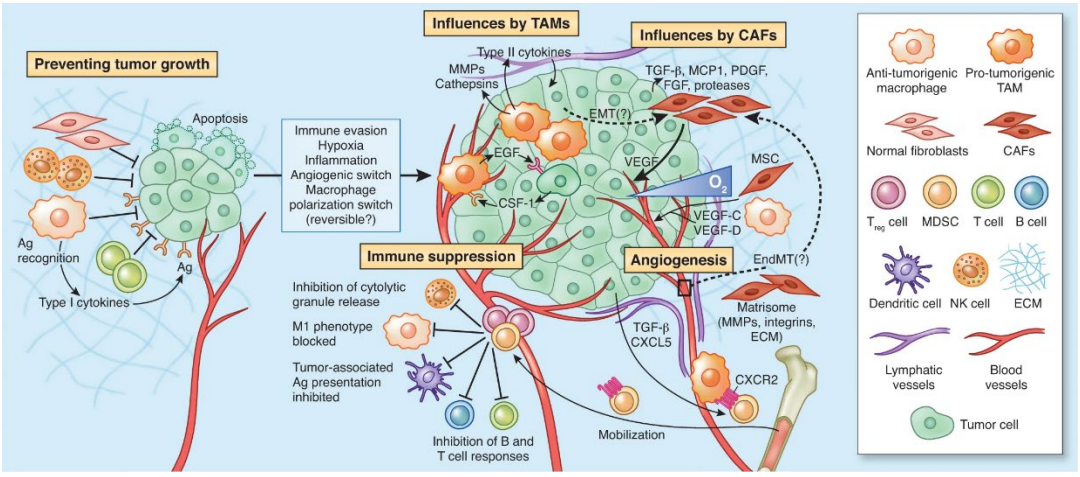


Figure 1: The tumor microenvironment and its role in cancer progression. Key components of the TME interact dynamically to support tumor growth, immune evasion, and metastatic dissemination (Quail & Joyce, 2013).

A particularly important component of the TME is its immune compartment. In the early stages of tumor development, innate and adaptive immune cells both recognize and destroy those malignant cells through a process referred to as immunosurveillance (Hanahan & Coussens, 2012). However, as tumors evolve over time, they acquire mechanisms to escape immune destruction. They downregulate immunogenic antigens, recruit immunosuppressive cells such as regulatory T cells and M2-polarized macrophages, and secrete cytokines and growth factors that suppress the effector functions of cytotoxic T lymphocytes and natural killer cells (Hanahan & Coussens, 2012; Quail & Joyce, 2013). The balance between pro-inflammatory, tumor-suppressive, and anti-inflammatory, tumor-promoting signals within the TME is, therefore, an important determinant of disease outcome and response to therapy. Proteolytic enzymes and their endogenous inhibitors are key modulators of this balance as they influence multiple layers of TME biology by processing cytokines and chemokines, controlling antigen presentation, and regulating the activation state of tumor-infiltrating immune cells (Mohamed & Sloane, 2006; Radisky, 2024; Vasiljeva et al., 2006).

1.1.1.1.1 Tumor-associated macrophages

Macrophages are one of the most abundant immune cell types in the breast tumor microenvironment and show high functional diversity (Sami & Raza, 2024; Stavrou & Constantinidou, 2024). They can adopt different activation states, from pro-inflammatory (tumor-suppressive) to anti-inflammatory (tumor-promoting) phenotypes. The states they exhibit depend on signals they receive from tumor and stromal cells (Huang, Kang, & Chen, 2024). In breast cancer, high number of tumor-associated macrophages (TAMs) is often found in more aggressive tumors and is linked with higher tumor grade, increased metastasis, and poor prognosis (Allison, Edirimanne, Matthews, & Fuller, 2023; Munir et al., 2021; C. Wang et al., 2022). Notably, high numbers of $CD163^+$ M2-like TAMs predicted worse overall, breast cancer-specific, and disease-free survival in breast cancer, with a particularly strong adverse impact in HER2-positive tumors (Jääskeläinen et al., 2024).

Most TAMs originate from circulating monocytes that enter into the tumor by the help of chemokines and growth factors such as CCL2 and M-CSF (Munir et al., 2021; Stavrou & Constantinidou, 2024). After entering the tumor, these cells acquire specific functional properties from the local microenvironment (Munir et al., 2021). Macrophages are generally divided into two phenotypes: classically activated M1-like macrophages and alternatively activated M2-like macrophages (Figure 2). M1-like macrophages produce pro-inflammatory cytokines, present antigens, and can kill tumor cells, whereas M2-like macrophages secrete anti-inflammatory mediators, stimulate angiogenesis, support tissue remodeling, and suppress anti-tumor immune responses (R. Huang et al., 2024; Munir et al., 2021; Qiu, Zhao, Luo, Qiu, & Li, 2022).

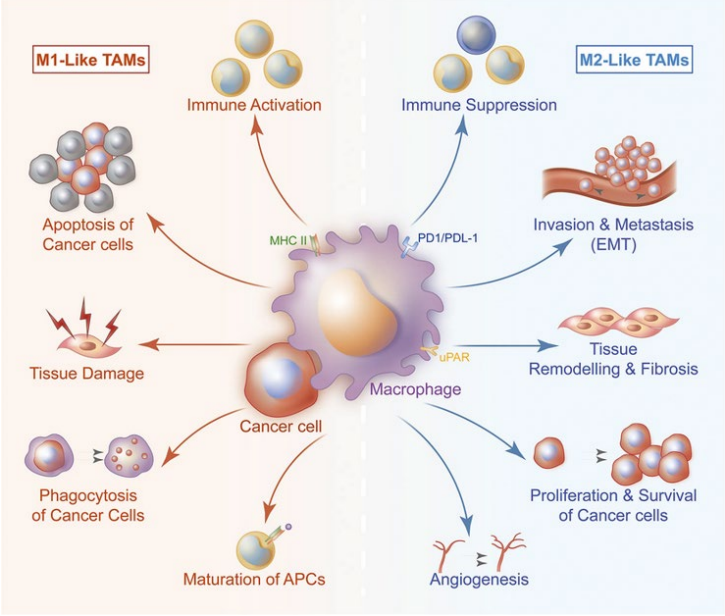


Figure 2: M1-like and M2-like macrophages in the tumor microenvironment (Qiu et al., 2022).

In most breast cancers, TAMs are shifted towards an M2-like, tumor-promoting phenotype (Munir et al., 2021; Stavrou & Constantinidou, 2024). These cells support tumor growth in several ways. They promote proliferation, invasion, and epithelial–mesenchymal transition (EMT) of tumor cells, enhance cancer stem-cell properties, stimulate the formation of new blood vessels, and inhibit cytotoxic T-cell activity (Munir et al., 2021; Sami & Raza, 2024; Stavrou & Constantinidou, 2024). Clinically, high numbers of $CD68^+$ or $CD163^+$ TAMs, especially in the tumor stroma, correlated with shorter overall survival

of patients in different breast cancer cohorts (Allison et al., 2023; C. Wang et al., 2022). Especially in triple-negative and HER2-positive breast cancers, which have a worse prognosis, M2-like TAMs were particularly enriched (Jääskeläinen et al., 2024; Stavrou & Constantinidou, 2024).

In many studies, mouse models of breast cancer have helped to clarify the role of TAMs in tumor progression. In the MMTV-PyMT model and other murine breast cancer models, macrophages accumulated in early stages of tumor development and promoted the transition from pre-malignant lesions to invasive carcinoma (Hüsemann et al., 2008; E. Y. Lin et al., 2003). They supported angiogenesis, remodeling of the ECM, and intravasation of tumor cells into blood vessels (Hüsemann et al., 2008; Munir et al., 2021). Interfering with macrophage recruitment or survival, for example, by blocking the M-CSF/CSF1R pathway or by pharmacological reprogramming of TAMs, can delay tumor progression and reduce metastasis in experimental breast cancer models. These findings show that TAMs clearly play a mainly pro-tumorigenic role in mammary tumor models (Munir et al., 2021; Stavrou & Constantinidou, 2024).

Yet studies in human breast cancers suggest that higher numbers of M1-like macrophages or an increased M1/M2 ratio are linked with more active anti-tumor immunity, although the impact on survival may depend on tumor subtype and treatment (Allison et al., 2023; Sami & Raza, 2024). The available data suggest that TAMs are important regulators of breast cancer progression and represent attractive therapeutic targets (Stavrou & Constantinidou, 2024). Potential strategies include depletion of TAMs themselves, inhibition of their recruitment into the tumor, or reprogramming of existing TAMs towards a more M1-like, tumor-suppressive phenotype (He et al., 2025; Munir et al., 2021; Stavrou & Constantinidou, 2024).

1.1.1.2 Metastasis

Metastasis is the spread of cancer cells from the primary tumor to distant organs, most commonly the liver, lungs, brain, and bones. Since the vast majority of cancer-related deaths are due to metastatic disease, it remains the greatest challenge in oncology (Li et al., 2025; Liu et al., 2024). The metastatic cascade involves a series of biological processes: from local invasion of the cancer cells of the surrounding stroma, their intravasation into blood or lymphatic vessels, survival in the circulation, extravasation at a distant site, and finally their colonization of a microenvironment in a distant tissue (Li et al., 2025; Liu et al., 2024). However, the majority of cells that enter circulation are unable to complete each of these steps. Only a very small number of disseminated tumor cells finally form clinically detectable metastatic lesions (Li et al., 2025). Furthermore, those cancer cells that have spread from the primary site may remain dormant in distant organs as single cells or as micrometastatic clusters before they eventually proliferate and form macrometastases (Diepenbruck & Christofori, 2016).

For successful local invasion, malignant cells must breach the basement membrane and remodel the surrounding ECM. This is enabled by the epithelial-mesenchymal transition (EMT), a process in which epithelial tumor cells acquire a mesenchymal phenotype. On a cellular level, they lose their epithelial markers, which are replaced by mesenchymal markers, such as vimentin and N-cadherin (Christofori, 2006; Ribatti, 2017). This transition enhances the ability of tumor cells to migrate, become more invasive migration and invasiveness to cells, and also allows them to detach from the primary tumor and penetrate the surrounding stroma. EMT is induced by the presence of multiple growth factors in the TME, including transforming growth factor-β (TGF-β), epidermal growth factor (EGF), and fibroblast growth factors (Christofori, 2006). A complete EMT rarely occurs in cancer. Instead, tumor cells frequently exist within intermediate hybrid

epithelial/mesenchymal (E/M) states that have migratory and proliferative characteristics. This partial EMT is increasingly recognized as the phenotype with the greatest metastatic capacity (Jolly et al., 2015; Nieto, Huang, Jackson, & Thiery, 2016). Moreover, it is thought that reversal of EMT through mesenchymal-to-epithelial transition (MET) at the distant site supports metastatic colonization and outgrowth (Bakir, Chiarella, Pitarresi, & Rustgi, 2020). It has also been reported that although EMT is not strictly necessary for metastasis, cells that have undergone an EMT are more resistant to conventional chemotherapeutic agents than cells that have not, which makes this transition clinically significant beyond its role in metastasis (Fischer et al., 2015).

ECM remodeling during tumor cell invasion is driven by the coordinated action of multiple protease families, including matrix metalloproteinases, serine proteases, and cysteine cathepsins (Liu et al., 2024; Vizovišek, Fonović, & Turk, 2019). These enzymes degrade structural matrix proteins and process growth factors, cytokines, and adhesion molecules that help tumor cells to migrate and enable their intravasation (Mohamed & Sloane, 2006; Vizovišek et al., 2019). Cysteine cathepsins have therefore been shown to contribute to several stages of this cascade in multiple preclinical tumor models (Joyce et al., 2004; Mohamed & Sloane, 2006; Vasiljeva et al., 2006).

1.1.2 Breast cancer

Breast cancer is the most commonly diagnosed malignancy in women and ranks among the leading causes of cancer-related mortality worldwide. In 2022, an estimated 2.3 million new cases and approximately 666,000 deaths from breast cancer were recorded (Bray et al., 2024; Kim et al., 2025).

1.1.2.1 Clinical and biological features of breast cancer

Breast carcinomas clinically appear as a spectrum from non-invasive in situ lesions to locally invasive and metastatic disease. The most widely used molecular classification of breast cancer consists of four major subtypes based on the expression of estrogen receptor (ER), progesterone receptor (PR), and human epidermal growth factor receptor 2 (HER2):

- luminal A (ER/PR-positive, HER2-negative, low Ki-67),
- luminal B (ER/PR-positive, HER2-variable, high Ki-67),
- HER2-enriched (HER2-positive, ER/PR-negative), and
- triple-negative (ER/PR/HER2-negative) (Harbeck et al., 2019; Marra, Trapani, Viale, Criscitiello, & Curigliano, 2020).

These subtypes differ in their prognosis, typical sites of metastasis, and response to treatment. Luminal A tumors tend to be slow-growing and respond well to endocrine therapy. In contrast, triple-negative breast cancers (TNBCs) are characterized by rapid growth, with a higher tendency for visceral metastasis. Also, they lack a targetable hormone or HER2 receptors, which limits treatment options to cytotoxic chemotherapy and, more recently, immunotherapy (Harbeck et al., 2019; Marra et al., 2020).

The TME plays an important and subtype-specific role in breast cancer biology. For example, in HER2-positive and triple-negative subtypes, TME contains high immune infiltration. This is associated with improved outcomes and predicts the response to immunotherapy. On the other hand, in luminal tumors, the TME is more immunosuppressive and contains more M2-polarized macrophages and regulatory T cells (Harris et al., 2024).

1.1.2.2 Mouse models of breast cancer

For studying the processes of cancer initiation, progression, metastasis, and approaches to therapy *in vivo*, experimental animal models are invaluable to the field of oncology. The laboratory mouse (*Mus musculus*) is highly appropriate for cancer research because of its small size, rapid reproduction, similarities to human physiology and molecular biology, and a fully sequenced genome (Frese & Tuveson, 2007). We can broadly divide mouse models of human breast cancer into three groups: xenograft models using human tumor cell lines or patient-derived xenografts (PDX) in immunodeficient mice; syngeneic orthotopic transplantation models using murine mammary tumor cells in immunocompetent hosts; and genetically engineered mouse models (GEMMs), which comprise transgenic and gene knockout lines (Attalla, Taifour, Bui, & Muller, 2021; Frese & Tuveson, 2007).

1.1.2.2.1 The MMTV-PyMT mouse model of mammary carcinoma

The FVB/N-Tg(MMTV-PyVT)634Mul transgenic mouse model, commonly referred to as MMTV-PyMT, was first described in 1992 (Guy, Cardiff, & Muller, 1992). The rapid development of tumors along with extensive pulmonary metastasis, and accessibility from commercial sources make this model the most widely used GEMM in the field of mammary cancer research to date (Attalla et al., 2021; Guy et al., 1992). In this murine model, the polyoma virus middle T antigen (PyMT) oncogene is expressed under the control of the mouse mammary tumor virus (MMTV) long terminal repeat promoter, which drives transgene expression selectively in the mammary epithelium. The MMTV promoter is hormonally regulated and is highly active during pregnancy, although it expresses in a mosaic expression pattern throughout the mammary gland (Pattengale et al., 1989; Shen & Brown, 2005). PyMT antigen itself is a membrane-associated scaffold protein encoded by a small DNA polyomavirus. It activates multiple oncogenic signaling cascades: the Src kinase family, the Ras/MAPK pathway, c-Myc, and the PI3K/Akt axis. Each of these pathways is similarly dysregulated in human breast cancer (Attalla et al., 2021; Fluck & Schaffhausen, 2009).

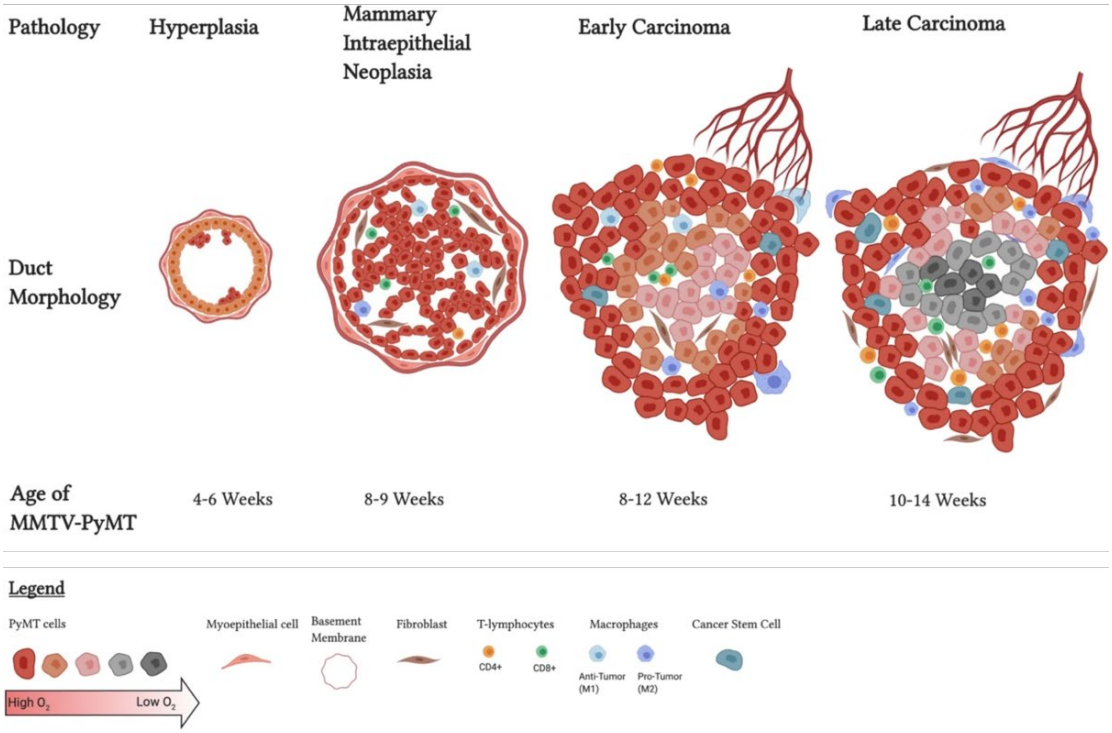


Figure 3: Progression of MMTV-PyMT mammary carcinomas through four stages: hyperplasia, intraepithelial neoplasia, early carcinoma, and late carcinoma (Attalla et al., 2021).

Female MMTV-PyMT mice spontaneously develop multifocal mammary tumors in all ten mammary glands. The hyperplasia of the first tumors usually occurs around 4 weeks of age. Following this initial stage, the tumors develop in four consistent stages: hyperplasia, adenoma or intraepithelial neoplasia, early carcinoma, and late-stage carcinoma (Figure 3). Each of these stages very closely mirrors the histopathological stages seen within human breast cancer. Mammary tumors also develop in MMTV-PyMT males, but their growth is distinctly impaired (Attalla et al., 2021; E. Y. Lin et al., 2003). Most female mice develop pulmonary metastases by 14–16 weeks of age. Furthermore, at 4-6 weeks of age, disseminated tumor cells and micrometastases have been detected in the bone marrow, when primary tumors are already in the hyperplastic stage. These data suggest that even pre-malignant cells can disseminate and initiate metastasis (Attalla et al., 2021; Hüsemann et al., 2008). At the molecular level, MMTV-PyMT tumors lose expression of ER and PR progressively, and β1-integrin and overexpress ErbB2/Neu and cyclin D1 along with disease progression. This is also a characteristic of human luminal B and HER2-enriched breast cancer subtypes, both of which have poor prognosis (Attalla et al., 2021; Lapidus, Nass, & Davidson, 1998; E. Y. Lin et al., 2003; Maglione et al., 2001). Additionally, in late-stage carcinomas, heavy infiltration of the tumor stroma with various immune cells, such as macrophages and T-cells, contributes to progression and metastasis (DeNardo et al., 2009; E. Y. Lin et al., 2003; E. Y. Lin, Nguyen, Russell, & Pollard, 2001; Wyckoff et al., 2007).

1.2 Proteases

1.2.1 Proteolytic enzymes in physiology and disease

Proteases or proteolytic enzymes are proteins that catalyze one of the essential biochemical reactions, the hydrolysis of the peptide bond. Among all enzymes, they represent one of the most abundant and functionally diverse groups in biology. Proteases regulate various normal biological processes and function in virtually every cellular compartment, including the cytoplasm, the nucleus, and the extracellular space. They are essential in protein degradation, protein and lipid metabolism, autophagy, antigen presentation, growth factor receptor recycling, cellular stress signaling, and lysosome-mediated cell death (Radisky, 2024; V. Turk et al., 2012). Additionally, they are involved in embryogenesis, where protease-dependent tissue remodeling drives organogenesis, and in hemostasis, where proteases of the coagulation cascade convert fibrinogen to fibrin (V. Turk et al., 2012). Proteases are classified into five major mechanistic classes: serine, cysteine, aspartic, threonine, and metalloproteinases, based on the chemical nature of the nucleophile that attacks the peptide bond. In serine, cysteine, and threonine proteases, this nucleophile is an active-site amino acid residue, whereas in aspartic and metalloproteinases it is a water molecule, activated either by two aspartate residues or by a divalent metal ion cofactor, usually zinc (Radisky, 2024; V. Turk et al., 2012).

Proteases function within a highly interconnected network, termed the "protease web". Their activity is tightly regulated at multiple levels, including transcriptional and post-translational control, compartmentalization, and mainly zymogen activation and inhibition by endogenous protein inhibitors (Radisky, 2024; V. Turk et al., 2012). Dysregulation of proteolytic activity is associated with numerous diseases, from neurodegeneration, inflammatory, cardiovascular, and autoimmune disorders, osteoporosis, and cancer. In cancer, the deregulation of proteases promotes tumor invasion and metastasis through ECM breakdown and activation of pro-tumorigenic growth factors and cytokines (Olson & Joyce, 2015; V. Turk et al., 2012; Vasiljeva et al., 2007).

1.2.2 Cysteine proteases

In the hydrolysis of peptide bonds, cysteine proteases make use of a cysteine residue at the active site as the primary nucleophile. The catalytic mechanism involves a catalytic dyad, most commonly cysteine paired with histidine, and proceeds through a covalent acyl-enzyme intermediate. In mammals, the major cysteine protease families include the papain-like lysosomal cathepsins, the caspases involved in apoptosis and inflammation, and the calpains, which are cytoplasmic proteases activated by calcium (V. Turk et al., 2012). Cysteine cathepsins are localized in the slightly acidic endolysosomal compartment, which is essential for their optimal activity. At neutral pH levels, however, they are mostly unstable and become inactivated rapidly (Kramer, Turk, & Turk, 2017; V. Turk et al., 2012; Yadati, Houben, Bitorina, & Shiri-Sverdlov, 2020). Most cysteine cathepsins are endopeptidases, but some also act as exopeptidases. Cathepsin H has additional aminopeptidase activity, cathepsin B can act as a carboxypeptidase, and cathepsins C and X function primarily as exopeptidases. Cathepsins have a relatively broad substrate specificity, and they cleave substrates preferentially after basic or hydrophobic residues (Stoka, Vasiljeva, Nakanishi, & Turk, 2023; V. Turk et al., 2012).

1.2.2.1 Lysosomal cysteine cathepsins

Lysosomal cysteine cathepsins are members of the papain-like superfamily. There are 11 human cysteine cathepsins: B, C, F, H, K, L, O, S, V, W, and X/Z (V. Turk et al., 2012). The majority of these are expressed within nearly all human tissues, but others exhibit more restricted cell- or tissue-specific localization. Cathepsin K is most highly expressed in osteoclasts, where it mediates bone matrix degradation, while cathepsin S is most abundant in antigen-presenting cells (Mohamed & Sloane, 2006; V. Turk et al., 2012). They are the main proteases responsible for the degradation of proteins delivered via endocytosis, phagocytosis, or autophagy, and are essential for MHC class II-mediated antigen presentation (Jakoš, Pišlar, Jewett, & Kos, 2019; V. Turk et al., 2012).

1.2.2.1.1 Localization and activation of cysteine cathepsins

Cysteine cathepsins are synthesized in the endoplasmic reticulum as inactive preproenzymes. There, the signal peptide is cleaved and yields the inactive proenzyme or zymogen. The propeptide occupies the active site cleft and acts as a reversible inhibitor, preventing premature proteolysis. After N-glycosylation in the Golgi apparatus, procathepsins are then transported to late endosomes and lysosomes, where activation occurs through autocatalytic processing at low pH or through the action of other proteases, including pepsin and cathepsin D (V. Turk et al., 2012; Vidak, Javoršek, Vizovišek, & Turk, 2019).

While traditionally considered to exist only within lysosomes, cathepsins have also been found within other subcellular compartments, including the nucleus, cytoplasm, plasma membrane, and also in the extracellular space. There, they participate in signaling, ECM remodeling, and immune modulation (V. Turk et al., 2012; Vidak et al., 2019). Active cathepsins can be secreted into the extracellular milieu through regulated lysosomal exocytosis or vesicular export. In tumor cells and activated immune cells, cathepsins are highly upregulated. Their redistribution into extra-lysosomal compartments is particularly important in the TME. There, they directly promote matrix remodeling, growth factor processing, and modulate the immune response (Mohamed & Sloane, 2006; Olson & Joyce, 2015; Radisky, 2024; Vidak et al., 2019).

1.2.2.1.2 Regulation of cysteine cathepsin activity

Since cathepsins are highly potent proteases, their tight regulation is essential and occurs at multiple levels. Under physiological conditions, their basal expression is controlled by developmental and homeostatic signaling pathways. However, pathological stimuli such as hypoxia, inflammatory cytokines, oncogenic signaling, and epigenetic alterations can markedly induce cathepsin transcription and thus largely contribute to their frequent upregulation in tumors (Olson & Joyce, 2015; V. Turk et al., 2012). Post-translationally, the activity of cathepsins is regulated by zymogen activation, glycosylation, and cofactor interactions; for example, glycosaminoglycans such as heparan sulphate and chondroitin sulphate can either activate or inhibit specific cathepsins depending on the enzyme and the species of GAG involved (V. Turk et al., 2012). The most important regulatory mechanism at the protein level is inhibition by endogenous inhibitors. They are essential guardians of proteolytic activity (B. Turk, Turk, & Salvesen, 2002, 2005). The cystatin superfamily represents the principal class of endogenous cysteine cathepsin inhibitors. It ensures tight control of proteolytic activity, whether occurring intracellularly or extracellularly (Breznik, Mitrović, T, & Kos, 2019; V. Turk, Stoka, & Turk, 2008). This balance between cathepsin activity and inhibition regulated by cystatins is a critical determinant of the cellular proteolytic environment. Its disruption has been linked to the development and progression

of multiple diseases, including cancer (Breznik et al., 2019; Cox, 2009; B. Turk et al., 2002; V. Turk et al., 2012).

1.2.2.2 Cysteine cathepsins in cancer

In cancer, cysteine cathepsins are often dysregulated in both expression and activity. Elevated levels of cathepsins B, L, S, H, K, and X have been reported in many tumor types, including breast, lung, gastric, prostate, colorectal, and pancreatic carcinomas, and in association with disease progression, lymph node involvement, metastasis, and poor clinical outcome (Mohamed & Sloane, 2006; Olson & Joyce, 2015; Stoka et al., 2023). However, tumor cells are certainly not the only cells that secrete cathepsins. Cancer-associated fibroblasts, macrophages, dendritic cells, endothelial cells, and tumor-infiltrating lymphocytes also all actively produce and secrete cathepsins into the TME, where they promote pro-tumorigenic processes (Jakoš et al., 2019; Mohamed & Sloane, 2006).

Cysteine cathepsins contribute to tumor progression through several interconnected pathways. They can degrade key ECM components, including laminin, fibronectin, tenascin C, and type IV collagen, leading to loosening of tissue architecture and enabling local invasion and intravasation of tumor cells (M. Fonović & Turk, 2014; Löser & Pietzsch, 2015; Vizovišek et al., 2019). Additionally, cathepsins activate other proteases, such as urokinase-type plasminogen activator (uPA). They inactivate adhesion molecules, such as E-cadherin, which promotes tumor cell detachment and migration (Mohamed & Sloane, 2006). Cathepsins also modulate important signaling pathways, including TNF-α/MAPK, TGF-β1, and PI3K, that control tumor cell proliferation, survival, and migration (Gogineni, Gupta, Nalla, Velpula, & Rao, 2012; Tummalapalli et al., 2007; G. P. Zhang, Yue, & Li, 2020). While within immune cells in tumor stroma, cathepsins drive antigen processing and MHC class II-mediated presentation, but in the tumor context, their dysregulation can reprogram the immune response from tumor-suppressive to tumor-supportive (Jakoš et al., 2019; Vasiljeva & Turk, 2008). Hypoxia and the associated glycolytic metabolism make the TME acidic, which are favorable conditions for cathepsin activation and stabilization of their extracellular activity (Vidak et al., 2019; Yadati et al., 2020). Through these mechanisms, cysteine cathepsins not only support invasion and immune escape but also contribute to tumor neovascularization by processing pro- and anti-angiogenic factors (Mohamed & Sloane, 2006; Olson & Joyce, 2015; Stoka et al., 2023).

Studies in mouse models demonstrate the functional importance of cathepsins in breast cancer. Deletion of cathepsin B in the MMTV-PyMT model delayed tumor onset and reduced tumor burden compared with wild-type animals (Vasiljeva et al., 2008; Vasiljeva et al., 2006). Cathepsin B contributed to tumor growth in both tumor cells and stromal cells, and its depletion alone reduced the volume of pulmonary metastasis by approximately 65% (Vasiljeva et al., 2006). Combined deletion of cathepsins B and Z further delayed tumor development. It markedly decreased the number and size of pulmonary metastases, highlighting complementary roles for these proteases in metastatic dissemination (Sevenich et al., 2010). This cooperative relationship is also seen at the pharmacological level. Pharmacological inhibition of cathepsin B with nitroxoline significantly reduced tumor growth, angiogenesis, and metastasis in LPB fibrosarcoma and MMTV-PyMT breast cancer models *in vivo* (Mirković et al., 2015). In addition, selective inhibition of cathepsin X with the nitroxoline-derived triazole-based compound Z9 significantly reduced tumor progression in the transgenic MMTV-PyMT and orthotopic MMTV-PyMT breast cancer models. Simultaneous inhibition of cathepsins B and X also exerted a synergistic effect on impairing tumor cell migration and spheroid growth *in vitro*, further underscoring their functional interdependence as therapeutic targets (Mitrović et al., 2022). Other mouse tumor models also support tumor-promoting functions of cathepsins. In the RIP1-Tag2

pancreatic neuroendocrine neoplasia model and the $Apc^{Min/+}$ intestinal cancer model, loss of cathepsins was associated with impaired angiogenesis, delayed tumor progression, or reduced tumor burden (Gocheva et al., 2010; Gocheva et al., 2006; Gounaris et al., 2008). In contrast, loss of cathepsin L in the K14-HPV16 skin and cervical cancer model accelerated tumor progression, indicating that cathepsin L can act as a tumor-suppressive protease in this specific context (Dennemärker et al., 2010). In the 4T1 syngeneic murine breast cancer model, pharmacological inhibition or cathepsin-targeted nanocarriers likewise reduced tumor growth and metastatic spread, which supports the translational relevance and importance of targeting cathepsins (G. Mikhaylov et al., 2014; Georgy Mikhaylov et al., 2011; Reinheckel, Peters, Krüger, Turk, & Vasiljeva, 2012; Withana et al., 2012). Together, these studies identify cysteine cathepsins as influential drivers of malignant progression and emphasize their strong potential as therapeutic targets and markers in cancer biology (Olson & Joyce, 2015).

1.3 Inhibitors of Cysteine Cathepsins

The activity of cysteine cathepsins is regulated by a family of potent endogenous protein inhibitors – the cystatins. They are reversible, tight-binding inhibitors of papain-like (C1 family) cysteine proteases and broadly conserved across eukaryotes (Abrahamson, Alvarez-Fernandez, & Nathanson, 2003; V. Turk et al., 2008). Although propeptides, thyropins, and cross-class serpins each contribute to the fine-tuning of cathepsin activity in specific physiological contexts, cystatins remain the principal and most extensively characterized endogenous regulators of papain-like cysteine cathepsins in mammals (B. Turk et al., 2005). The following sections therefore focus on the cystatin superfamily, and in particular on stefin B and cystatin C, the two inhibitors we investigated in this study.

1.3.1 Cystatins

In humans, cystatins are divided into three major families according to their molecular structure, subcellular distribution, and the presence and number of the disulfide bonds. Type I cystatins (stefins) are small and primarily intracellular inhibitors. Type II cystatins (cystatins C, D, E/M, S, SA, and SN) are secreted and mainly located extracellularly whereas kininogens or type III cystatins are large multifunctional plasma glycoproteins (Abrahamson et al., 2003; V. Turk et al., 2008).

The structure of cystatins shares a characteristic fold, termed the “cystatin fold”, which consists of five antiparallel β-strands wrapped around a central five-turn α-helix (Abrahamson et al., 2003). Within this scaffold, inhibition of the target protease is based on three conserved regions: the N-terminal segment containing a conserved glycine residue (Gly-11), a central hairpin loop (Gln55–Gly59), and a C-terminal Pro-Trp dipeptide present in type II and III cystatins, which is replaced by His or Gly in type I stefins (Abrahamson et al., 2003; Vito Turk & Bode, 1991). These elements form a wedge-shaped surface that docks into the active-site cleft of papain-like cysteine proteases and thereby prevents access of physiological substrates (Abrahamson et al., 2003; V. Turk et al., 2008). While cystatins are generally non-selective with respect to papain-like endopeptidases, they are still able to differentiate between endo- and exopeptidases and inhibit their targets in the nano- to picomolar range (V. Turk et al., 2008). The activity of individual cystatins is further modulated by their local concentration, post-translational modifications, subcellular compartmentalization, and interactions with binding partners – all of which together enable tight control of cathepsin activity in different tissues and disease settings (V. Turk et al., 2008; V. Turk et al., 2012).

1.3.1.1 Type I cystatins

Type I cystatins or stefins represent the simplest members of the cystatin superfamily. They are small (~11 kDa), nonglycosylated proteins that lack both a signal peptide and disulfide bonds. Stefins are found mostly within the cytosol, nucleus, and mitochondria (Abrahamson et al., 2003; V. Turk et al., 2008). In humans, two stefins are expressed: stefin A (cystatin A) and stefin B (cystatin B), which inhibit cathepsins B, H, L, and S within a nanomolar to subnanomolar range (Abrahamson et al., 2003; B. Turk et al., 2002). They primarily protect the cell from the accidental release of lysosomal cathepsins into the cytoplasm during oxidative stress, lysosomal membrane permeabilization (LMP), or cell death (Kopitar-Jerala, 2015b). Stefin A is predominantly located in stratified squamous epithelia, whereas stefin B is more widely expressed across many cell types and tissues, making it the main intracellular cathepsin inhibitor in most cells (Abrahamson et al., 2003; Kopitar-Jerala, 2015b).

1.3.1.1.1 Stefin B

Stefin B (cystatin B; gene *CSTB*) is an intracellular protein composed of 98 amino acid residues and with a molar mass of approximately 11 kDa. It is a potent and reversible inhibitor of lysosomal cysteine cathepsins B, H, L, and S, lacks both a signal peptide and disulfide bonds, and is unglycosylated. It is distributed across the cytosol, nucleus, and mitochondria (Abrahamson et al., 2003; Kopitar-Jerala, 2015b). Stefin B binds with histone proteins in the nucleus and influences cell cycle progression, pointing to regulatory functions beyond protease inhibition (Čeru et al., 2010). Under physiological conditions, stefin B defends the integrity of the lysosomal membrane and limits the accumulation of active cathepsins within the cytoplasm that can occur during oxidative, mechanical, or chemical stress of lysosomes. Furthermore, if these processes are left unchecked, LMP and cathepsin-mediated cell death are triggered (Kopitar-Jerala, 2015b; K. Maher et al., 2014).

Beyond its inhibitory effect, stefin B has a number of protease-independent roles. For instance, it limits oxidative damage by maintaining mitochondrial membrane potential and reducing mitochondrial reactive oxygen species (ROS) production, a cytoprotective mechanism demonstrated both in neuronal cells and in breast cancer models (Kopitar-Jerala, 2015b; Lehtinen et al., 2009; K. Maher et al., 2014). Stefin B also suppresses NOD-like receptor family pyrin domain-containing 3 (NLRP3) inflammasome activation via the AMP-activated protein kinase/mechanistic target of rapamycin (AMPK–mTOR) signalling axis: increased stefin B expression downregulates mitochondrial ROS generation and promotes autophagy, thereby restraining excessive inflammasome-driven inflammation in macrophages (Katarina Maher et al., 2014; Trstenjak-Prebanda et al., 2023). Additionally, stefin B displays chaperone-like properties by binding amyloid-β peptides and suppressing their aggregation (Škerget et al., 2010), and it modulates innate immune responses, including nuclear factor kappa-light-chain-enhancer of activated B cells (NF-κB)-dependent cytokine production (Kopitar-Jerala, 2015b).

The prominent role of stefin B in neuronal homeostasis is underscored by loss-of-function mutations in CSTB, which lead to a condition known as progressive myoclonus epilepsy type 1 (EPM1/Unverricht–Lundborg disease) (Lalioti, Antonarakis, & Scott, 2003; Pennacchio et al., 1998). In stefin-B-deficient mice, the impaired redox balance and neuroinflammation have been revealed as essential for disease progression, highlighting the critical role of stefin B in maintaining redox balance in the nervous system (Kopitar-Jerala, 2015b; Trstenjak Prebanda, Matjan-Štefin, Turk, & Kopitar-Jerala, 2021). In this model, altered expression of redox-sensitive proteins has been observed, including increased mitochondrial peroxiredoxin 3 (Prx3) expression in stefin B-deficient brain and cerebellar tissue, particularly following an inflammatory LPS challenge (Trstenjak Prebanda et al.,

2021). Interestingly, upregulation of type II cystatin C in these mice partially restores cathepsin activity. Additionally, cystatin C has been shown to act as a neuroprotector and improve clinical signs of ECM1 mice, suggesting some degree of functional compensation between the two inhibitors (Kaur et al., 2010).

1.3.1.1.1.1 Stefin B in cancer

Stefin B has a complex and highly context-dependent role in cancer (Čeru et al., 2010; J. Kos & Lah, 1998; V. Turk et al., 2012). In the MMTV-PyMT breast cancer murine model, stefin B deficiency reduced tumor burden primarily by sensitizing tumor cells to apoptosis caused by oxidative and lysosomal stress. In this study, stefin B was shown to have anti-apoptotic and pro-survival functions (Butinar et al., 2014). Mechanistically, stefin B is proposed to stabilize lysosomal and mitochondrial membranes under oxidative stress, prevent cathepsin leakage into the cytosol, and limit cleavage of pro-apoptotic B-cell lymphoma 2 (Bcl-2) family members. Stefin B also stabilizes cellular FLICE-like inhibitory protein (FLIP) and attenuates death receptor signaling by competing with caspase-8 for Fas-associated protein with death domain (FADD) binding (Yang et al., 2010).

In contrast, increased levels of stefins have been associated with disease progression and unfavorable prognosis in several human cancers. In hepatocellular carcinoma, increased expression of stefin B in tumor tissue correlated with larger tumor size and lymph node metastasis. Stefin B is identified as an independent risk factor for nodal involvement, suggesting that high stefin B levels contribute to tumor progression and dissemination (J. Kos & Lah, 1998; Y. Y. Lin et al., 2016; V. Turk et al., 2012). Similar, although not entirely consistent, associations between altered stefin expression and poor outcome have been reported in colorectal and head and neck cancers. In colorectal cancer and several other solid tumors, elevated levels of cysteine cathepsin inhibitors, including stefins, were linked to advanced cancer stage and reduced survival, supporting a tumor-promoting role of these inhibitors (Janko Kos et al., 2000; J. Kos & Lah, 1998).

Studies in head and neck squamous cell carcinoma have oppositely shown that stefins can also act as tumor suppressors. Downregulation of stefin A and stefin B in tumor tissue compared with matched non-tumorous mucosa identified a subgroup of patients at high risk of recurrence and poor disease-free and disease-specific survival, indicating that loss of stefins is associated with a more aggressive clinical course (J. Kos & Lah, 1998; Strojan et al., 2007). Collectively, stefin B may function as either a tumor promoter or tumor suppressor depending on tumor type, staging, and the balance between its protease-dependent and protease-independent activities (J. Kos & Lah, 1998; Matjan Štefin et al., 2026; V. Turk et al., 2012).

1.3.1.2 Type II cystatins

Type II cystatins are extracellular inhibitors of cysteine cathepsins with molecular masses of 13–14 kDa (Abrahamson et al., 2003). Unlike stefins, they have an N-terminal signal peptide that directs them into the secretory pathway, enabling their release into the extracellular space where they act as the primary regulators of secreted and extracellular cathepsins (V. Turk et al., 2008). Structurally, type II cystatins contain two disulfide bonds near the C-terminus that provide stability and inhibitory activity. Some family members are N-glycosylated (Abrahamson et al., 2003). In humans, there are cystatin C (CST3), D, E/M, F, S, SA, and SN, which differ in tissue distribution, inhibitory selectivity, and additional non-inhibitory functions. Together they represent the main extracellular regulatory layer of cysteine cathepsin activity in interstitial fluid, blood plasma, and other body fluids, with cystatin C being the most abundant and ubiquitously expressed member of the type II cystatin family in humans (Abrahamson et al., 2003; V. Turk et al., 2008).

1.3.1.2.1 Cystatin C

Cystatin C (gene *CST3*), previously known as gamma-trace protein, was first characterized by Grubb and Löfberg, who determined its primary structure from monkey and human pituitary gland in 1982 (Grubb & Löfberg, 1982). The mature, active human form of cystatin C consists of 120 amino acid residues with a molecular mass of approximately 13 kDa. It is a non-glycosylated secreted protein produced by almost all nucleated cells and is considered to be the most potent extracellular inhibitor of cysteine cathepsins (Abrahamson et al., 2003; Mussap & Plebani, 2004). Among all known endogenous inhibitors, it also has the broadest spectrum of cathepsin inhibition. It inhibits cathepsins L and S at picomolar concentrations and cathepsins B, H, and C at nanomolar concentrations (V. Turk et al., 2008). In addition, cystatin C can also inhibit legumain (B. Turk et al., 2002). During biosynthesis, two cystatin C molecules temporarily associate into a dimer in the endoplasmic reticulum, which likely prevents premature intracellular cathepsin binding. In secretory vesicles, the dimers then dissociate, and only active monomers are released extracellularly, where cystatin C is present in most compartments (Janowski et al., 2001; Mussap & Plebani, 2004). Because of its small size, it can undergo free filtration through the glomerular membrane in the kidneys and serves clinically as a sensitive biomarker of glomerular filtration rate and renal function (Coll et al., 2000; Mussap & Plebani, 2004). A point mutation in *CST3* (Leu68Gln) causes hereditary cystatin C amyloid angiopathy (HCCAA). It is characterized by deposition of amyloid fibrils in cerebral blood vessels, leading to repeated hemorrhages, paralysis, dementia, and early death, typically before the age of 30, occurring almost exclusively in Iceland (Olafsson & Grubb, 2000).

Like stefin B, cystatin C also features important protease-independent functions connected to tissue homeostasis and disease. In the nervous system, for example, cystatin C promotes neuroprotection by inducing autophagy via mechanistic target of rapamycin (mTOR) inhibition, supporting neurogenesis, and suppressing amyloid-β aggregation, through mechanisms independent of its cathepsin inhibitory activity (Kaur et al., 2010; Tizon et al., 2010). In the cardiovascular system, cystatin C modulates elastolytic protease activity in atherosclerotic lesions and has been independently associated with cardiovascular disease risk in epidemiological studies (Mussap & Plebani, 2004; Taglieri, Koenig, & Kaski, 2009). A recent study has further shown that cystatin C is an important regulator of inflammatory responses during endotoxemia, as cystatin C deficiency in mice increased susceptibility to LPS-induced sepsis and led to elevated caspase-11 expression, enhanced NLRP3 inflammasome activation, and impaired autophagy in bone marrow-derived macrophages (Biasizzo et al., 2021). Cystatin C also has an important role in the immune system, since it influences dendritic cell maturation and cytokine-mediated polarization of T-helper cells and shapes both innate and adaptive immune responses (Biasizzo et al., 2021; Kopitar-Jerala, 2015a; W. Zhang et al., 2019). Together, these diverse activities show that cystatin C is not only a protease inhibitor but also a regulator in broader signaling networks.

1.3.1.2.1.1 Cystatin C in cancer

The role of cystatin C in cancer is multifactorial and strongly context-dependent (J. Kos & Lah, 1998; V. Turk et al., 2012). Changes in its expression occur in a broad spectrum of human cancers, and its correlation with clinical outcome varies in different tumor types. In glioma, low cystatin C expression together with high cathepsin B levels was significantly connected with high tumor grade, Ki-67 proliferation index, and tumor recurrence, which suggests a tumor-suppressive function (Konduri et al., 2002; Nakabayashi, Hara, & Shimuzu, 2005). In prostate cancer, decreased cystatin C expression was associated with

poorer patient survival and increased tumor cell invasion through mitogen-activated protein kinase / extracellular signal-regulated kinase pathway (MAPK/Erk) and androgen receptor pathways (Wegiel et al., 2009). In preclinical studies of skin cancer, cystatin C levels progressively decreased from normal skin to premalignant lesions and invasive tumors. Deletion of cystatin C in K14-HPV16 transgenic mice accelerated the development of skin tumors, together with increased cathepsin activity, enhanced tumor cell proliferation, and elevated angiogenesis compared with controls, thus confirming a tumor-suppressive role in this model (Yu et al., 2010). In bladder cancer, cystatin C is significantly downregulated in tumor tissue, and its low levels independently predicted worse overall survival and also disease-specific survival (Li et al., 2025). In contrast, cystatin C levels were elevated in ovarian cancer cyst fluid and are significantly higher in malignant lesions compared with benign serous tumors, indicating a tumor-promoting role in that context (Kolwijck et al., 2010). In a large prospective cohort, higher serum cystatin C concentrations have been independently associated with increased cancer-specific mortality across multiple tumor types, including lung, breast, and liver cancer, further supporting its tumor-promoting potential at the systemic level (C. Huang et al., 2024). When overexpressed *in vivo*, cystatin C reduced pulmonary metastasis of fibrosarcoma cells and also inhibited invasion and migration of B16 melanoma cells, demonstrating its tumor-suppressive activities under selective experimental conditions (Ervin & Cox, 2005; Kopitz, Anton, Gansbacher, & Krüger, 2005).

In the MMTV-PyMT breast cancer model, cystatin C deficiency was shown to reduce tumor growth and tumor cell proliferation, with increased phosphorylated p-38. Cystatin C has been shown to function as a tumor-promoting factor, demonstrating its involvement in proliferative signaling pathways unrelated to direct protease inhibition (Završnik et al., 2017). In the RIP1-Tag2 transgenic pancreatic cancer model, cystatin C deficiency resulted in enhanced tumor cell proliferation, increased angiogenesis, collagen degradation, and elevated pro-tumorigenic cytokine levels, illustrating its tumor-suppressive capacity in this experimental context (B. Wang et al., 2006). Mechanistically, growing evidence has revealed that cystatin C promotes tumor progression through at least two cathepsin-independent pathways. First, cystatin C acted as a novel transforming growth factor beta (TGF-β) type II receptor antagonist that inhibited TGF-β binding and signaling in normal and cancer cells. Loss of cystatin C activity thus restores TGF-β -mediated inhibition of EMT, and therefore reduces cell invasion and migration (Sokol, Neil, Schiemann, & Schiemann, 2005; Sokol & Schiemann, 2004). Second, cystatin C is glucocorticoid-responsive and regulates the recruitment of immunosuppressive triggering receptor expressed on myeloid cells 2 (TREM2$^+$) tumor-associated macrophages into the TME. Cystatin C knockout tumors exhibited significantly reduced growth and, additionally, diminished recruitment of TREM2$^+$ macrophages, providing a direct connection between cystatin C levels and remodeling of the immune microenvironment (Kleeman et al., 2023). Furthermore, oligomeric cystatin C enhanced the immunosuppressive activity of myeloid cells by engaging inhibitory receptors leukocyte immunoglobulin-like receptor subfamily B member 2 (LILRB2) and leukocyte immunoglobulin-like receptor subfamily B member 5 (LILRB5) on their surface, resulting in T-cell suppression and accelerated tumor progression, with phosphatase signaling downstream of the cystatin C–LILRB2 interaction being a key mechanism (C. Zhang et al., 2025). Primary macrophages from cystatin C-deficient mice exhibited altered cytokine profiles, further underscoring its immunomodulatory role in shaping myeloid cell function within the TME (Završnik et al., 2017). While part of cystatin C's tumor-promoting effect can be explained by the inhibition of extracellular cathepsin activity, these findings collectively point to cathepsin-independent mechanisms. Modulation of TGF-β signaling, EMT, and direct myeloid cell immunosuppression through LILRB2/LILRB5 and TREM2$^+$

macrophage recruitment importantly contributes to its complex impact on tumor growth, progression, and metastasis (Kleeman et al., 2023; V. Turk et al., 2012; C. Zhang et al., 2025).

1.3.1.3 Type III cystatins

Type III cystatins, also known as kininogens, are large plasma glycoproteins (~70–120 kDa), predominantly found in blood plasma. They serve as precursors of vasoactive kinins such as bradykinin. High- and low-molecular-weight kininogen (HMW and LMW kininogen) are the two main human forms, synthesized primarily in the liver and circulating at relatively high plasma concentrations. A third type, T-kininogen, is restricted to rats (Lalmanach, Naudin, Lecaille, & Fritz, 2010). Their cysteine cathepsin inhibitory activity resides in N-terminal cystatin-like domains within a larger multidomain structure; of the three cystatin-like domains present, only two retain functional, tight-binding inhibitory activity (Abrahamson et al., 2003; Lalmanach et al., 2010). Kininogens also participate in the contact activation system of blood coagulation, in platelet activation, and in the modulation of inflammatory responses via kinin release (DeLa Cadena & Colman, 1991).

1.3.1.4 Simultaneous stefin B and cystatin C deficiency (double knockout, DKO) in breast cancer

While the individual roles of stefin B and cystatin C have previously been studied *in vivo* (Butinar et al., 2014; Završnik et al., 2017), the effects of their simultaneous loss on tumor biology remained unknown until recently. Studies on single-knockouts in the MMTV-PyMT model have revealed that stefin B and cystatin C do contribute to breast cancer progression through complementary, largely non-overlapping mechanisms (Butinar et al., 2014; Završnik et al., 2017). Stefin B deficiency led to a reduction of tumor burden mainly by increasing tumor cell sensitivity to oxidative and lysosomal stress-induced apoptosis, without notable effect on proliferation or metastasis (Butinar et al., 2014). In contrast, deficiency of cystatin C reduced tumor growth mainly by decreasing tumor cell proliferation and increasing extracellular cathepsin activity, with relatively minor effects on apoptosis (Završnik et al., 2017). Such contrasting phenotypes suggest that stefin B mainly regulates intracellular stress resistance while cystatin C controls extracellular proteolytic and proliferative signaling. Based on these previous observations, it was reasonable to propose that simultaneous ablation of both inhibitors might result in cumulative or even synergistic tumor-suppressive effects.

Our main aim of the present study was therefore to investigate the combined roles of stefin B and cystatin C in breast cancer by studying the effects of their simultaneous deficiency in the MMTV-PyMT model. We focused on tumor growth, cell proliferation, apoptosis, angiogenesis, metastasis, and the tumor immune microenvironment, complemented by pharmacological inhibition studies targeting cathepsins B and X directly, described below.

1.3.2 Pharmacological inhibitors of cysteine cathepsins

In addition to endogenous regulation by cystatins, cysteine cathepsin activity can be modulated pharmacologically, offering a complementary strategy to genetic approaches for studying and therapeutically targeting the cysteine cathepsin system in cancer. Lysosomal cysteine cathepsins, in particular cathepsins B and X, have been implicated in multiple steps of tumor progression, including degradation of the extracellular matrix, regulation of cell migration and invasion, and modulation of the tumor microenvironment (Mohamed & Sloane, 2006; Olson & Joyce, 2015). Genetic studies in the MMTV-PyMT breast cancer

model demonstrated that ablation of cathepsin B reduces tumor growth and pulmonary metastasis, and that combined deficiency of cathepsins B and Z further suppresses tumor progression, indicating complementary functions of these proteases (Sevenich et al., 2010; Vasiljeva et al., 2008).

Nitroxoline (8-hydroxy-5-nitroquinoline) is an established antibiotic that was identified as a potent reversible inhibitor of cathepsin B endopeptidase activity. In experimental tumor models, nitroxoline reduced tumor growth, angiogenesis, and metastatic spread, supporting pharmacological inhibition of cathepsin B as a potential anticancer strategy (Mirković et al., 2015). Cathepsin X (also known as cathepsin Z; gene CTSZ; CatX/Z) has distinct substrate specificity and cellular functions compared with cathepsin B, and functional interactions between the two proteases have been reported in tumor cells. Z9 is a selective reversible inhibitor of cathepsin X that was shown to reduce tumor cell migration and invasion and to impair tumor progression in breast cancer models (Mitrović et al., 2022).

In this thesis, pharmacological inhibition of cathepsins B and X with nitroxoline and Z9 was included as an additional approach to investigate how direct modulation of cysteine cathepsin activity affects primary tumor growth and pulmonary metastasis in MMTV-PyMT transgenic and orthotopic breast cancer models.

Chapter 2

Purpose of the Work

While numerous studies have reported the role of cysteine cathepsins in cancer development and progression, only a few have investigated the involvement of endogenous inhibitors in these processes. Therefore, we have decided to illustrate the effects of simultaneous depletion of two endogenous inhibitors, stefin B and cystatin C, on breast cancer development and tumor microenvironment in the MMTV-PyMT breast cancer mouse model. Specifically, we have determined how the deficiency of these inhibitors influences tumor growth, tumor cell proliferation and death, proteolytic activity, and the tumor microenvironment, and how these alterations affect metastatic burden. To place these genetic findings in a broader context, we additionally examined the effects of pharmacological inhibition of cathepsins B and X in the complementary MMTV-PyMT breast cancer models.

Although the main focus of this dissertation was to investigate the role of stefin B and cystatin C deficiency in breast cancer progression, a complementary part of the work addressed the broader biological consequences of stefin B deficiency in a non-tumor inflammatory setting. Stefin B has been implicated in the regulation of oxidative stress and inflammatory responses, processes that are relevant not only to neuroinflammatory disorders but also to the tumor microenvironment. We therefore examined the mitochondrial redox response in brain and cerebellar tissue of stefin B deficient mice during LPS-induced neuroinflammation. This complementary analysis was included to broaden the functional characterization of stefin B deficiency and to provide additional mechanistic context for its stress- and inflammation-related functions investigated in the tumor model.

The hypotheses of this research were:

1. Combined deletion of stefin B and cystatin C (double knockout) in the MMTV-PyMT breast cancer model will accelerate tumor progression, resulting in earlier tumor onset, faster tumor growth, increased tumor cell proliferation, and enhanced metastatic spread compared with wild-type mice.
2. We expect that simultaneous stefin B and cystatin C deficiency will exert complementary effects on tumor progression and metastasis in the MMTV-PyMT breast cancer model, resulting in a more pronounced tumor-suppressive phenotype than that previously reported for either single stefin B or cystatin C knockout in the same model.

The main goals of our research were:

1. Determine how the combined deficiency of stefin B and cystatin C affects primary tumor development in the MMTV-PyMT breast cancer model by assessing:

- Tumor onset, tumor growth kinetics, and cumulative tumor weight in PyMT double knockout (PyMT;DKO) mice in comparison to wild-type mice,
- Angiogenesis, tumor cell proliferation, and apoptosis in primary tumors.

2. Study the impact of the simultaneous depletion of stefin B and cystatin C on the tumor microenvironment and metastatic spread by:
   - Evaluating the incidence, number, and size of pulmonary metastases in the PyMT;DKO cohort versus wild-type cohort.
   - Analyzing the infiltration of tumor-associated macrophages in the PyMT;DKO, and wild-type tumors.
3. To compare key parameters we obtained in this study with previously published data from single knockout PyMT models and place the effects of stefin B and cystatin C double knockout into context.
4. As a complementary approach to the genetic strategy above, to assess the effect of pharmacological inhibition of cathepsins B and X with nitroxoline and Z9 on breast cancer progression by determining primary tumor growth in FVB;PyMT transgenic mice and in an orthotopic MMTV-PyMT breast cancer model treated with vehicle, nitroxoline, Z9, or their combination, and by quantifying the number and mean size of pulmonary metastases in inhibitor-treated versus control PyMT mice.
5. As an additional complementary aim, determine whether stefin B deficiency alters mitochondrial redox homeostasis in a non-tumor inflammatory setting by assessing peroxiredoxin 3 (Prx3) expression in the brain and cerebellum under basal conditions and following LPS-induced neuroinflammation.

Chapter 3

Materials and Methods

3.1 Materials

3.1.1 Equipment

- 1.5 mL and 2 mL micro tubes (Sarstedt)
- 10 cm and 15 cm tissue culture dishes (TPP)
- 15 mL and 50 mL centrifuge tubes (BD Biosciences)
- 96-well microtiter black plate (Greiner)
- 96-well microtiter cell culture black plate with transparent bottom (Corning)
- 96-well microtiter cell culture transparent plate (TPP)
- 96-well microtiter transparent plate (Costar)
- Automatic pipettes (Eppendorf)
- Cell line incubator (Binder)
- Centrifuges (Eppendorf)
- Dissection scissors and forceps (Elcon, Dewimed, FST)
- iBright imaging system (Thermo Scientific)
- ImageJ software (Fiji)
- Imaging software CellSense (Olympus)
- Inverted microscope Olympus IX81 (Olympus)
- Laminar air flow cabinet for cell culture BSB 4A (Gelaire Flow Laboratories)
- Microplate reader TECAN Infinite M1000 (Tecan)
- Microscope coverslips (Brand)
- Microscope slides (Eprenia)
- Microtome for paraffin sections (e.g., MICROM 315, Thermo Scientific)
- Nitrocellulose membrane
- Paraffin embedding station (Thermo Scientific MICROM)
- PCR thermal cycler 2720 (Applied Biosystems)
- pH meter MP 220 (Mettler Toledo)
- Power supply Western Lightning Volt OSP-300 (Thermo Scientific)
- Tissue homogenizer Bullet Blender (Next Advance)
- Tissue processor Slee MTP for paraffin processing of tissues
- Vertical Electrophoresis Lab Apparatus MiniProtean Tetracell (Biorad)
- Western blot transfer apparatus TE22 Mighty Small Transphor Unit (GE Healthcare)

3.1.2 Chemicals and commercial kits

- 3,3′-diaminobenzidine, DAB (Sigma-Aldrich)
- Absolute ethanol (Carlo Erba)
- Amphotericin B solution (Sigma-Aldrich)
- Bovine serum albumin, BSA (Sigma-Aldrich)
- Canadian balsam (Sigma)
- Citric acid, powder (Sigma-Aldrich)
- Dimethyl sulfoxide, DMSO (Merck)
- Dithiothreitol, DTT (Sigma-Aldrich)
- Dulbecco's phosphate-buffered saline, DPBS (PAA)
- E-64 (L-trans-epoxysuccinyl-Leu-4-guanidinobutylamide)
- ECL chemiluminescent detection reagent (GE Healthcare)
- Eosin (Sigma-Aldrich)
- Ethanol 75%
- Ethanol 96%
- Fetal bovine serum, FBS (Sigma-Aldrich)
- Glacial acetic acid (Applichem)
- GlutaMAX (Gibco-Invitrogen)
- Hydrogen peroxide 30% (H_2O_2; Sigma-Aldrich)
- Lipopolysaccharide (LPS) from Escherichia coli O55:B5 (Sigma-Aldrich)
- Magnesium chloride, $MgCl_2$
- Mayer's hematoxylin (Sigma-Aldrich)
- Methanol (Merck)
- Nitroxoline (nitroxoline; Sigma-Aldrich)
- NP-40 (non-ionic detergent)
- PageRuler Prestained Protein Ladder (MBI Fermentas)
- Paraffin (Leica)
- Penicillin/Streptomycin (Sigma-Aldrich)
- Polyethylene glycol, PEG (Fluka)
- Protease inhibitor cocktail (Sigma-Aldrich)
- Protein concentration reagent (Bio-Rad)
- Skimmed milk powder (Pomurske mlekarne)
- SlowFade Gold antifade reagent with DAPI (Invitrogen)
- Sodium chloride, NaCl (Serva)
- Sodium dodecyl sulfate, SDS (Serva)
- SYBR Green (Qiagen)
- TEMED (N,N,N′,N′-tetramethylethylenediamine; Merck)
- Tissue freezing medium (Jung)
- Tris(hydroxymethyl)aminomethane, Tris (Serva)
- Trisodium citrate dihydrate (Sigma-Aldrich)
- Triton X-100 (Serva)
- Trypan Blue (Sigma-Aldrich)
- TrypLE Select trypsin (Gibco-Invitrogen)
- Tween-20 (Sigma-Aldrich)
- VECTASTAIN ABC Kit Rabbit IgG (PK-4001, Vector Laboratories)
- VECTASTAIN ABC Kit Rat IgG (PK-4004, Vector Laboratories)
- Xylene (Sigma-Aldrich)
- Z-Phe-Arg-AMC (N-benzyloxycarbonyl-L-phenylalanine-L-arginine-7-amido-4-methylcoumarin; Bachem)

3.1.3 Buffers, solutions, and media

- BANA buffer
  16 mM Na_2HPO_4
  88 mM KH_2PO_4
  3 mM EDTA
  0,1% PEG
  pH 6.0

- Citrate antigen retrieval buffer
  2 mM citric acid
  7.5 mM trisodium citrate dihydrate
  pH 6.0

- Blocking solution for endogenous peroxidase
  10% methanol
  3% H_2O_2

- Phosphate-buffer saline (PBS)
  6.6 mM Na2HPO4
  13.4 mM NaH2PO4
  150 mM NaCl
  pH 7.0

- PBST
  PBS
  0.005% Tween-20

- Solution for SDS-PAGE stacking gel
  1.33 mL 40% acrylamide-bisacrylamide
  2.5 mL 0.5 M Tris/HCl (pH 6.8)
  6.4 mL H2O
  0.1 mL 10% SDS
  0.05 mL 10% APS
  0.025 mL TEMED

- Solution for SDS-PAGE resolving gel
  3.75 mL 40 % acrylamide-bisacrylamide
  2.5 mL 1 M Tris-HCl (pH 8.8)
  3.6 mL H2O
  0.1 mL 10% SDS
  0.05 mL 10% APS
  0.005 mL TEMED

- SDS-PAGE loading buffer (6x)
  375 mM Tris-HCl
  6% SDS
  48% glycerol
  100 mM DTT
  0.03 % bromophenol blue
  pH 6.8

- SDS-PAGE buffer
  25 mM Tris
  192 mM L-Gly
  0.1 % SDS

- Western transfer buffer
  25 mM Tris
  192 mM L-Gly
  15 mM SDS
  20% methanol

- Tissue lysate buffer
  250 mM Tris-HCl, pH 7.0
  5 mM EDTA
  1% Triton X-100

- RIPA buffer
  150 mM NaCl
  50 mM Tris-HCl, pH 7.4
  1% Triton X-100
  0.5% sodium deoxycholate
  0.1% SDS

- Phosphate buffer for activity assays
  1 mM EDTA
  0.1% (v/v) PEG
  1 mM DTT
  pH 6.0

- Fixative for organs
  4% formaldehyde in dH_2O

- Complemented DMEM (cDMEM)
  DMEM (Sigma)
  10 % FBS
  1 % Penicillin/Streptomycin
  2 mM Glutamine

- Dulbecco's PBS (PAA)

3.1.4 Enzymes

- Deoxyribonuclease I, DNase I (Sigma Aldrich)
- Hyaluronidase (Sigma Aldrich)
- Collagenase (Sigma Aldrich)
- Papain (Sigma Aldrich)
- Proteinase K (Sigma Aldrich)

3.1.5 Antibodies

- Rabbit monoclonal anti-Ki-67 antibodies (M724901, Dako)
- Rat monoclonal anti-F4/80 antibodies (NB600-404, Novus Biologicals)
- Rabbit monoclonal anti-CD86 antibodies (19589S, Cell Signaling Technology)
- Rabbit monoclonal anti-CD206 antibodies (24595, Cell Signaling Technology)
- Rabbit monoclonal anti-CD31 antibodies (550274, BD Pharmingen)
- Mouse monoclonal anti-stefin B (StfB) antibodies (MAB1409, R&D Systems)
- Rabbit monoclonal anti-cystatin C (CstC) antibodies (ab109508, Abcam)
- Rabbit monoclonal anti-phospho-AMPK alpha (Thr172) antibodies (2535, Cell Signaling Technology)
- Rabbit polyclonal anti-peroxiredoxin 3 (Prx3) antibodies (ab73349, Abcam)
- Mouse monoclonal anti-β-actin antibodies (A1978, Sigma-Aldrich)
- HRP-conjugated goat polyclonal anti-rabbit IgG antibodies (Jackson Immunoresearch)
- HRP-conjugated goat polyclonal anti-mouse IgG antibodies (Jackson Immunoresearch)

3.1.6 Mammalian cell line

- PyMT primary murine tumor cells from PyMT-MMTV mammary gland adenocarcinoma:
  - PyMT;WT primary tumor cells
  - PyMT;DKO primary tumor cells.

3.1.7 Animals

3.1.7.1 Mouse strains and genetic background

FVB/N mice were obtained from The Jackson Laboratory (Maine, USA) and used as the genetic background for all experiments. This strain is suitable for genetic manipulation, generating transgenic lines, and maintains good fertility with large litter sizes. Cystatin C-deficient ($CstC^{-}/^{-}$) mice on the C57BL/6 background were kindly provided by Dr. Anders Grubb, and stefin B-deficient ($StfB^{-}/^{-}$) mice by Dr. Richard M. Myers. Both single-knockout lines were backcrossed onto the FVB/N PyMT transgenic background for multiple generations before establishing double knockout lines. Mice were bred and maintained under controlled environmental conditions in accordance with institutional and national animal welfare regulations.

3.1.7.2 MMTV-PyMT mouse breast cancer model

Mammary tumors were studied in the MMTV-PyMT transgenic breast cancer model on the FVB/N background, in which the Polyoma virus middle T (PyMT) oncogene is expressed under the control of the MMTV promoter (FVB/N-Tg(MMTV-PyVT)634Mul) in mammary epithelium. Female mice develop multifocal mammary tumors that progress through defined premalignant and malignant stages, from hyperplasia to invasive adenocarcinoma, and develop pulmonary metastases spontaneously (Guy et al., 1992). Two genotypes were used in this study:

- PyMT;WT (MMTV-PyMT FVB/N wild-type)
- PyMT;DKO (MMTV-PyMT FVB/N stefin B and cystatin C double knockout; $PyMT;StfB^{-}/^{-}CstC^{-}/^{-}$).

3.2 Methods

3.2.1 Animal studies

3.2.1.1 Laboratory mouse breeding and housing

Female PyMT transgenic mice on the FVB/N background were bred and kept in the animal facility at the Jožef Stefan Institute under standard conditions. Animals were housed under specific-pathogen-free conditions with controlled temperature (20–24 °C), relative humidity (50–65%), and a 12 h light/dark cycle. Up to five mice were housed together per cage, with sterilized bedding, and ad libitum access to standard laboratory feed and water. All phenotypically normal female mice carrying the PyMT transgene on either a wild-type or stefin B and cystatin C double knockout background (PyMT;WT and PyMT;DKO, respectively) were included in the study. We did not exclude any animals or data points during the study. Mice were followed longitudinally and euthanized at 14 weeks of age for endpoint analyses. All experimental procedures involving animals were conducted in accordance with Slovenian animal welfare legislation, FELASA recommendations, and the "Guide for the Care and Use of Laboratory Animals". Procedures and experiments were approved by the Ethics Committee of the Administration of the Republic of Slovenia for Food Safety, Veterinary and Plant Protection (ethical approval codes U34401-35/2014/2, U34401-28/2017/5, U34401-6/2019/5, and U34401-5/2022/15). According to protocols, mice were euthanized by cervical dislocation followed by exsanguination.

3.2.1.2 Monitoring tumor growth progression

From the age of 30 days onward, female mice were regularly examined three times per week across all 10 mammary glands to detect mammary tumors with digital palpation, without the knowledge of genotype. Tumor diameters were measured with a digital caliper 30 days after the first tumors were detected. Animals were sacrificed at 14 weeks of age. Mammary tumors then were excised, individually measured, and weighed.

3.2.1.3 LPS-induced neuroinflammation model in stefin B-deficient mice

To assess the effect of stefin B deficiency on the mitochondrial redox response during systemic inflammation, wild-type (WT) and stefin B-deficient (StfB KO) mice fully backcrossed onto the FVB/N background were used. Stefin B-deficient mice were generated as described previously. Male and female mice aged 8–12 weeks were included in the experiment.

Systemic inflammation was induced by intraperitoneal injection of lipopolysaccharide (LPS) from Escherichia coli O55:B5 (Sigma-Aldrich, St. Louis, MO, USA) at a dose of 3 mg/kg body weight. Age-matched untreated WT and StfB KO mice served as controls. Animals were anesthetized according to the approved protocol using a ketamine/xylazine/acepromazine mixture and sacrificed 4 h after LPS administration. At least three animals per genotype and treatment condition were used in the experiments.

All animal studies, maintenance, and breeding were conducted in accordance with the Administration of the Republic of Slovenia for Food Safety, Veterinary and Plant Protection and the Guide for the Care and Use of Laboratory Animals. The procedures were approved by the Veterinary Administration of the Republic of Slovenia and the Government Ethical Committee (ethical protocol code: 34401-49/2014/7).

3.2.2 Sample preparation and tissue processing

3.2.2.1 Organ collection

3.2.2.1.1 Organs for paraffin-embedded sections

Mammary tumors, lungs, liver, kidneys, and spleen from PyMT;WT, and PyMT;DKO mice were collected at the endpoint. Tissues were fixed in 10% neutral-buffered formalin overnight, processed, and embedded in paraffin. Paraffin tissue blocks were sectioned at 5 µm and used for hematoxylin and eosin (H&E) staining, histomorphometry, and immunohistochemical analyses.

3.2.2.1.2 Organs for cryo sections

Mammary tumors, lungs, liver, kidneys, and spleen were snap-frozen in liquid nitrogen and stored at −80 °C until sectioning. We cut frozen tumors into 4–5 µm sections, placed them on pre-cooled microscope slides, fixed them in 80% methanol at 4 °C, followed by 100% acetone at −20 °C. Before staining, they were rinsed in PBS.

3.2.2.1.3 Organs for mRNA isolation

Pieces of primary mammary tumors and selected organs were rapidly excised, rinsed in PBS, snap-frozen in liquid nitrogen, and stored at −80 °C until RNA extraction.

3.2.2.1.4 Brain and cerebellar tissue collection

Following sacrifice, whole brains were removed, and cerebella were dissected from the remaining brain tissue. Brain tissue excluding the cerebellum and cerebellar tissue were processed separately for whole-tissue lysate preparation and subsequent Western blot analysis of redox-sensitive proteins. Tissue samples were kept on ice during processing and lysed immediately as described below.

3.2.2.2 Preparation of tumor lysates

Snap frozen mammary tumors from PyMT;WT, PyMT;DKO, PyMT;StfB and PyMT;CstC single knockout mice were homogenized in ice-cold lysis buffer using a Bullet Blender tissue homogenizer. For cathepsin activity measurements, tumors were homogenized in Tissue lysate buffer, whereas for immunoblotting, RIPA buffer was used; protein concentrations were determined and normalized before analysis.

3.2.2.3 Preparation of brain and cerebellar tissue lysates

Brain tissue excluding the cerebellum and cerebellar tissue were homogenized separately in ice-cold Nonidet P-40 (NP-40) lysis buffer containing 20 mM Tris–HCl (pH 7.4), 150 mM NaCl, 1 mM EDTA, 1% NP-40, 10% glycerol, 1 mM sodium orthovanadate, 10 mM sodium fluoride, and 10 mM β-glycerophosphate. The buffer was supplemented with a complete protease inhibitor cocktail and a phosphatase inhibitor cocktail (Sigma-Aldrich). Cell and tissue debris were removed by centrifugation, and protein concentrations in the supernatants were determined using the Bradford protein assay reagent (Bio-Rad). Equal amounts of protein were subsequently used for SDS-PAGE and Western blot analysis.

3.2.2.4 Preparation of primary PyMT tumor cells

We isolated primary PyMT tumor cells from transgenic PyMT mice mammary gland tumors as described earlier (Vasiljeva et al., 2006). Cells were grown in cDMEM. Cells

were maintained at 37 °C in a humidified incubator with 5% CO_2 and used for experiments up to passage 4.

3.2.3 Cell culture work

3.2.3.1 Cell lysates from primary PyMT tumor cells

For biochemical analyses, primary PyMT;WT and PyMT;DKO tumor cells were washed with ice-cold PBS and lysed in lysis buffer supplemented with protease inhibitors. Lysates were cleared by centrifugation, and supernatants were collected, protein concentrations determined, and samples either analyzed immediately or stored at −80 °C.

3.2.3.2 BrdU cell proliferation assay

To assess cell proliferation *in vitro*, primary PyMT;WT and PyMT;DKO tumor cells were seeded in 96-well plates at a density of 1×10^5 cells/mL and allowed to attach. Cells were labeled with BrdU for 2–4 h. BrdU incorporation into newly synthesized DNA was quantified using a BrdU cell proliferation kit according to the manufacturer's instructions, and absorbance was read at 450 nm with background subtraction at 540 nm on a microplate reader.

3.2.4 Gene expression and molecular analysis

3.2.4.1 Quantitative Real-Time PCR

Total RNA was isolated from frozen mammary tumors or other tissues using standard phenol- or column-based extraction methods, and complementary DNA (cDNA) was synthesized using reverse transcriptase and random primers. Quantitative Real-Time PCR (qPCR) was performed using gene-specific primers and a fluorescent DNA-binding dye or probe on a real-time PCR instrument, and relative gene expression levels were calculated with appropriate housekeeping genes as internal controls.

3.2.5 Protein analysis and biochemical assays

Cysteine cathepsin activity in tumor homogenates and primary tumor cell lysates was evaluated by measuring hydrolysis of the fluorogenic substrate Z-Phe-Arg-7-amido-4-methylcoumarin (Z-Phe-Arg-AMC) in the presence or absence of the broad-spectrum cysteine cathepsin inhibitor E64. For conditioned media, PyMT;WT and PyMT;DKO primary tumor cells were seeded in 12-well plates and incubated in PBS at 37 °C. Aliquots of supernatant were mixed with phosphate buffer and substrate. Fluorescence was read over time using a plate reader with excitation at 370 nm and emission at 460 nm.

3.2.6 Protein detection and characterization

3.2.6.1 Immunoblotting

Mammary tumor lysates from PyMT;WT and PyMT;DKO mice were resolved by SDS-PAGE and transferred onto polyvinylidene difluoride membranes. Membranes were probed with antibodies against stefin B (R&D Systems, Minneapolis, MN, USA; MAB1409, 1:5000), cystatin C (Abcam, Cambridge, UK; ab109508, 1:100,000) and phospho-AMPK alpha (Thr172) (Cell Signaling Technology, Danvers, MA, USA; #2535, rabbit monoclonal, 1:1000). Anti-β-actin (Sigma-Aldrich, St. Louis, MO, USA; A1978, mouse monoclonal,

1:5000) was used as a loading control. Membranes were incubated with appropriate secondary antibodies, followed by chemiluminescent detection. Band intensities were quantified by densitometry.

For Prx3 analysis in the LPS-induced neuroinflammation model, equal amounts of protein from brain and cerebellar tissue lysates were separated on 12.5% SDS-polyacrylamide gels and transferred for Western blot analysis. Membranes were probed with rabbit polyclonal anti-Prx3 antibody (Abcam, Cambridge, UK; ab73349) and mouse monoclonal anti-β-actin antibody (Sigma-Aldrich; A1978) as a loading control. Specific bands were visualized by enhanced chemiluminescence using ECL reagent. Band intensities were quantified by densitometry using ImageJ software, and Prx3 levels were expressed relative to the corresponding β-actin signal.

3.2.7 Histological and imaging methods

3.2.7.1 Histomorphometry

For volumetric measurement of total lung metastasis or disseminated tumor colonies in the lungs, the paraffin-embedded lungs were cut into 5-µm-thick slices from at least three different planes. After staining with hematoxylin and eosin, we identified metastatic foci by light microscopy. We determined the average metastasis size by computer-assisted measurement with Cellquest software (Olympus, Tokyo, Japan).

3.2.7.2 Histopathology

Histopathological examinations were performed on the liver, kidneys, spleen, and lungs to evaluate potential pathological changes in these organs. Tissue samples were fixed in 10% Neutral buffered Formalin, embedded in paraffin, sectioned at 5 µm thickness, and stained with hematoxylin and eosin (H&E) for microscopic evaluation. Sections were analyzed under a light microscope at 20x magnification, examining 20 fields of view (FOV) per sample. For each organ, tissue was collected from three distinct regions with a 100 µm spacing between sampling areas to ensure a comprehensive assessment of pathological alterations across different organ areas.

3.2.7.3 Tumor-stroma ratio

Tumor–stroma ratio (TSR) was assessed on sections stained with H&E of primary mammary tumors from PyMT;WT and PyMT;DKO mice. TSR (%) was calculated as tumor area/(tumor area + stroma area) × 100, using the mean value from five samples per group, with three fields of view per tumor analyzed at 10× magnification. Areas of tumor and stroma were quantified using regions of interest (ROIs) with CellSens software (Olympus).

3.2.7.4 Immunohistochemistry and immunofluorescence

3.2.7.4.1 Immunohistochemistry

Formalin-fixed, paraffin-embedded 5 µm thick tumor sections from PyMT;WT and PyMT;DKO mice were deparaffinized, rehydrated, and subjected to antigen retrieval in citrate buffer (pH 6.0). For macrophage markers, an additional pretreatment with Proteinase K was performed. After blocking endogenous peroxidase activity, sections were incubated with primary antibodies against Ki67, F4/80, CD86, and CD206, followed by detection using the Vectastain Elite ABC kit and visualization with DAB. Slides were counterstained with hematoxylin and then imaged on an Olympus IX81 bright-field

microscope. For each marker, we randomly selected five or ten high-power fields per tumor, which were quantified using ImageJ software. All image analysis was performed blinded to genotype.

3.2.7.4.2 Immunofluorescence

For immunofluorescence analysis, frozen tumor sections were processed as described above, stained with an antibody against the endothelial marker CD31 to assess the tumor vascularization, and then mounted in DAPI-containing antifade reagent. Immunofluorescence images were acquired with an Olympus IX81 microscope equipped with CellSens software (Olympus, Tokyo, Japan), and the CD31-positive area was quantified as a percentage of total tumor area in PyMT;WT and PyMT;DKO tumors.

3.2.7.5 Microscopy and image analysis

Bright-field images of H&E and immunohistochemically stained sections were acquired using an Olympus IX81 microscope with CellSens Imaging software (Olympus, Tokyo, Japan). For quantitative analyses of Ki67, TUNEL, F4/80, CD86, CD206, CD31, and lung metastases, five or ten randomly selected high-power fields per tumor or per organ were imaged and analyzed using ImageJ, with all evaluations performed in a genotype-blinded manner.

3.2.8 Pharmacological inhibition of cathepsins X and B in PyMT breast cancer models

3.2.8.1 Inhibitors and vehicle preparation

The triazole-based compound Z9, a selective reversible inhibitor of cathepsin X, was synthesized as described previously (U. P. Fonović et al., 2020). Nitroxoline, used as an inhibitor of cathepsin B, was obtained from Sigma-Aldrich (St. Louis, MO, USA). For in vivo administration, the compounds were prepared in 5% dimethyl sulfoxide (DMSO) in peanut oil. Mice in the vehicle control group received 5% DMSO in peanut oil according to the same treatment schedule.

3.2.8.2 FVB;PyMT transgenic mouse model and treatment

Female FVB/N transgenic mice expressing the polyoma middle T antigen under the control of the mouse mammary tumor virus long terminal repeat promoter [FVB/N-Tg(MMTV-PyMT)634Mul] were used as a spontaneous mammary tumor model. At 11 weeks of age, mice were randomly assigned to four groups (n=10 per group) and treated intraperitoneally every other day with vehicle (5% DMSO in peanut oil), Z9 (67.18 mg/kg), nitroxoline (40 mg/kg), or the combination of Z9 (67.18 mg/kg) and nitroxoline (40 mg/kg). The dose of Z9 was equimolar to the dose of nitroxoline. At 14 weeks of age, mice were euthanized, all mammary tumors were excised and weighed, and total tumor burden was calculated as cumulative mammary tumor weight per mouse. Lungs were dissected and processed for histomorphometric evaluation of pulmonary metastases.

3.2.8.3 Orthotopic MMTV-PyMT tumor model

The orthotopic mammary tumor model was established in female FVB/N mice by inoculation of $5x10^5$ primary MMTV-PyMT tumor cells in serum-free medium into the left inguinal mammary gland. When tumors reached a volume of approximately 125 mm^3,

tumor-bearing mice were randomly assigned to four groups (n=6 per group) and treated intraperitoneally every other day with vehicle (5% DMSO in peanut oil), Z9 (33.59 mg/kg), nitroxoline (20 mg/kg), or the combination of Z9 (33.59 mg/kg) and nitroxoline (20 mg/kg). Tumor dimensions were measured every other day using a caliper, and tumor volume was calculated as: V= (π $\times$a2$\times$b)/6.

3.2.9 Statistical analysis

Quantitative data are presented as mean $\pm$ standard error (SE) unless stated otherwise. Differences between PyMT;WT and PyMT;DKO groups were evaluated using Student's t-test for continuous variables, and Chi-square tests for proportions, with $p < 0.05$ considered statistically significant. To assess study robustness, post-hoc power analysis for the primary endpoint (cumulative tumor weight) was conducted using G*Power 3.1.

Chapter 4

Results

4.1 Analysis of PyMT Mammary Carcinomas

We characterized primary PyMT mammary tumors from wild-type (PyMT;WT) and stefin B and cystatin C double knockout (PyMT;DKO) female mice to determine how their simultaneous loss influences tumor development. First, we analyzed the expression of the inhibitors in mammary tumors, and then compared tumor onset, tumor growth dynamics, and cumulative tumor weight between PyMT;WT, and PyMT;DKO mice. Next, we evaluated tumor cell proliferation, cell death, angiogenesis, tumor-stroma ratio, and the development of pulmonary metastases to get a broader view of the impact of the two cysteine cathepsin inhibitors on tumor progression and spread.

4.1.1 Confirmation of stefin B and cystatin C depletion in tumors from PyMT;DKO mice

To confirm that both inhibitors are absent in our mouse model, we examined their expression in primary mammary tumors from PyMT;WT, PyMT;StfB^{-}/$^{-}$, PyMT;CstC^{-}/$^{-}$, and PyMT;DKO mice by Western blot analysis.
As presented in Figure 4, stefin B and cystatin C were both detectable in PyMT;WT samples, selectively absent in the corresponding single knockout cohorts, and completely lost in PyMT;DKO tumors, supporting successful genotype-specific depletion of both inhibitors.

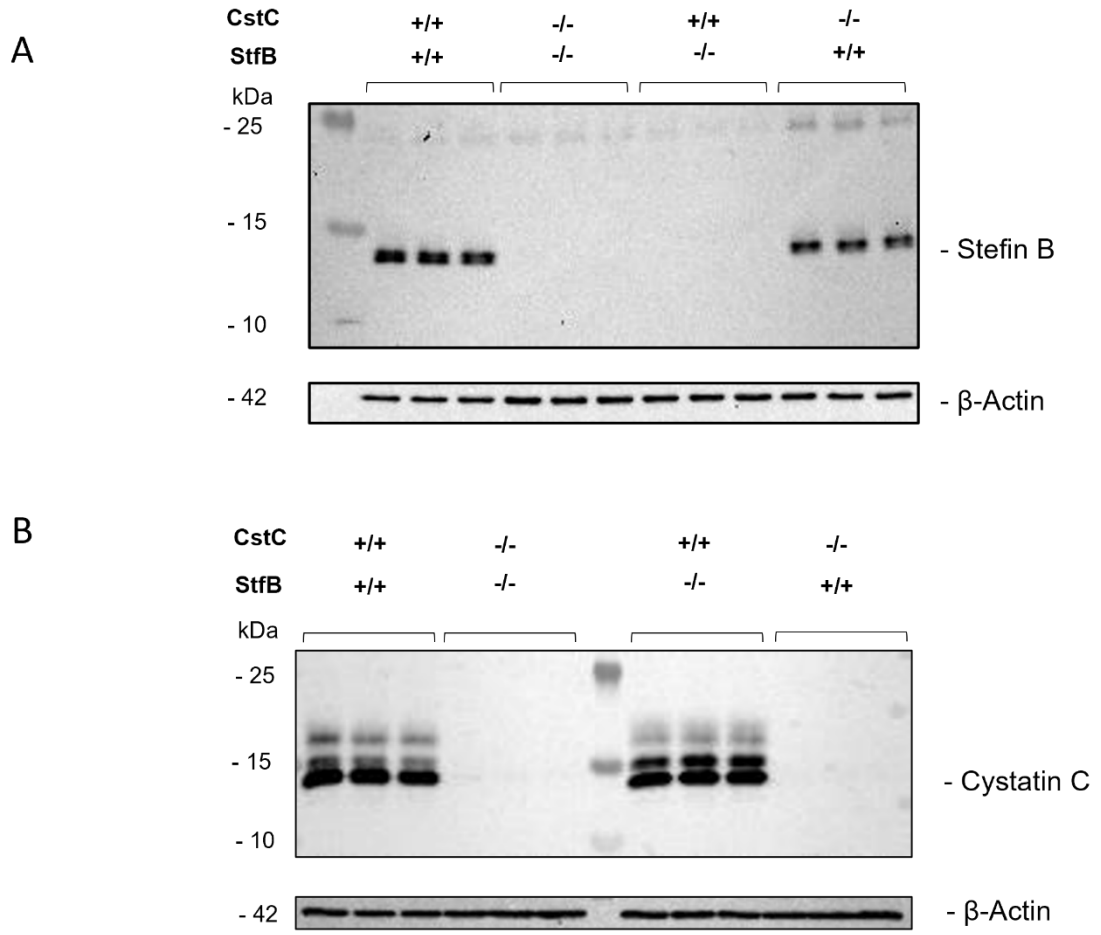


Figure 4: Stefin B and cystatin C expression in PyMT mammary tumors. (A) Western blot analysis of StfB in mammary tumors from PyMT;WT, PyMT;StfB^{-}/$^{-}$, PyMT;CstC^{-}/$^{-}$, and PyMT;DKO mice. StfB is present in PyMT;WT and PyMT;CstC^{-}/$^{-}$ tumors, but absent in PyMT;StfB^{-}/$^{-}$ and PyMT;DKO tumors. β-Actin was used as a loading control. (B) Western blot analysis of cystatin C (CstC) in the same tumor lysates. CstC is present in PyMT;WT and PyMT;StfB^{-}/$^{-}$ tumors, but absent in PyMT;CstC^{-}/$^{-}$ and PyMT;DKO tumors. β-Actin was used as a loading control.

To evaluate the impact of stefin B and cystatin C on tumor progression in the PyMT mammary mouse model, we compared the tumor growth kinetics in both groups of mice. We monitored tumor onset and tumor progression with palpation of all ten mammary glands, three times per week, starting at 30 days of age. For each animal, the onset of the first palpable tumor was defined as tumor onset, and differences between genotypes were evaluated based on the time to the first lesion.
In the PyMT;DKO cohort, females showed a slight but consistent delay in tumor onset compared with wild-type controls (Figure 5). The median time to the first detected tumor was 36 days in the control group and 38 days in the PyMT;DKO group. The Kaplan-Meier analysis of tumor-free survival confirmed a statistically significant difference between the groups ($p < 0.05$), indicating that simultaneous loss of both inhibitors slightly delays the tumor initiation *in vivo*.

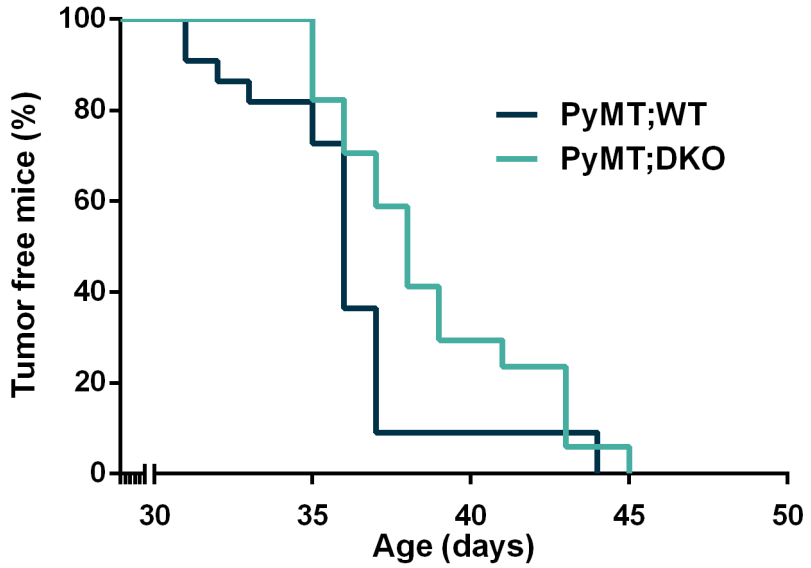


Figure 5: Delayed tumor onset in PyMT;DKO female mice. The Kaplan–Meier curves of tumor-free survival for PyMT;WT (n=22; dark blue line) and PyMT;DKO (n=17, turquoise line) female mice, showing a modest but significant delay in the occurrence of the first palpable mammary tumor. Statistical analysis suggests a significant difference in tumor-free survival between the two groups ($p < 0.05$), with the PyMT;DKO group showing a delayed onset of tumors and longer survival than PyMT;WT mice. The hazard ratio (HR) for PyMT;DKO versus PyMT;WT group was 0.59 (95% CI: 0.24–0.85). Differences were analyzed using the Mantel-Cox log-rank test.

4.1.2 Tumor size and weight assessment

To further evaluate how the combined loss of stefin B and cystatin C influences early tumor progression, we compared the size distribution of the first two palpable mammary tumors in PyMT;WT and PyMT;DKO mice 30 days after initial detection. Individual tumors were categorized as small (≤5 mm), medium (5–10 mm), and large (≥10 mm) based on caliper measurements to discover possible genotype-dependent differences in early tumor growth (Figure 6). PyMT;DKO females showed a clear shift toward smaller tumors, with a higher proportion in the small category and fewer tumors reaching ≥10 mm in diameter, compared to PyMT;WT mice. This suggests that the simultaneous loss of stefin B and cystatin C delays early tumor growth *in vivo*. The difference in tumor size distribution between the PyMT;WT and PyMT;DKO groups was statistically significant (chi-square test, $p < 0.01$), supporting a genotype-dependent reduction in early tumor growth.

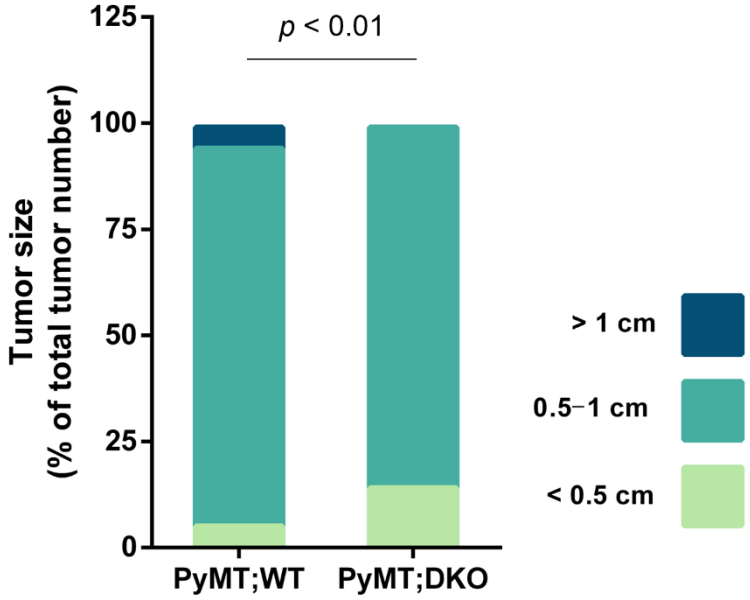


Figure 6: Tumor size distribution in PyMT;WT and PyMT;DKO female mice. The tumor size of two individual tumors 30 days after first detection with palpation from PyMT;WT (n=37) and PyMT;DKO (n=34) groups. p < 0.01 by the chi-square test.

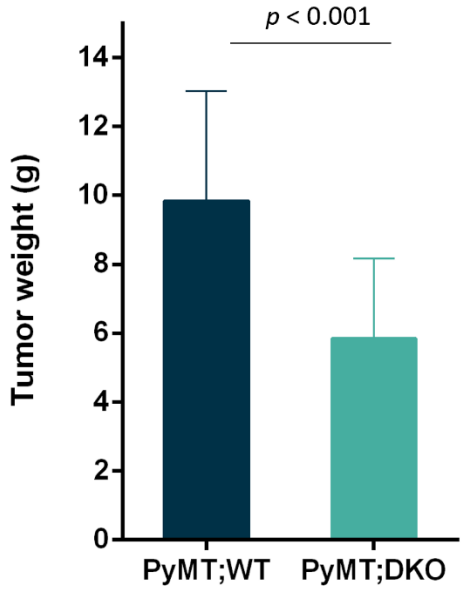


Figure 7: The cumulative tumor weight in PyMT;WT and PyMT;DKO female mice at 14 weeks of age. The total tumor weight per mouse for all mammary tumors was calculated for PyMT;WT (n = 13) and PyMT;DKO (n = 12) mice after tumor excision at necropsy. Differences were analyzed using Student's t-test, $p < 0.001$.

This reduction in tumor size was further accompanied *ex vivo* by quantifying the cumulative weight of all ten mammary tumors per mouse excised at 14 weeks of age. The quantification revealed an average tumor mass of 5.8 g in PyMT;DKO mice versus 9.8 g in PyMT;WT mice, corresponding to a 41% decrease in total tumor burden in the double-knockout group (Figure 7). Altogether, these data suggest that the combined loss of stefin

B and cystatin C markedly reduces primary mammary tumor growth in the PyMT mouse model.

4.1.3 Effect of stefin B and cystatin C deficiency on cell proliferation, cell death, and vascularization in PyMT mammary tumors

We next examined how the dual deficiency of stefin B and cystatin C affects key cellular processes driving tumor progression, focusing on cell proliferation and death in later-stage PyMT mammary adenocarcinomas. We assessed cell proliferation with immunohistochemical detection of the Ki67 nuclear marker in tumors from PyMT;WT and PyMT;DKO female mice at 14 weeks of age (Figure 8). Quantitative analysis revealed a markedly lower Ki67 proliferation index in PyMT;DKO tumors (6.6% Ki67-positive cells) compared with PyMT;WT tumors (24% Ki67-positive cells), which was in line with the reduced tumor size observed in the double-knockout group.

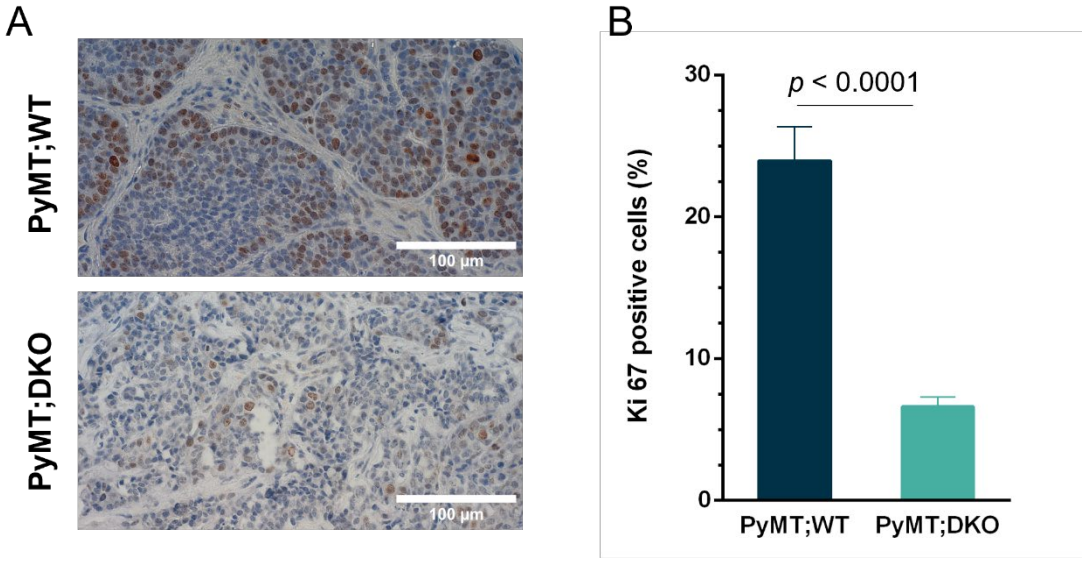


Figure 8: Effect of stefin B and cystatin C deficiency on tumor cell proliferation in PyMT mammary tumors. (A) Representative Ki67 immunohistochemical staining of primary mammary tumors from PyMT;WT and PyMT;DKO female mice at 14 weeks of age (scale bar: 100 µm). (B) Quantification of Ki67-positive nuclei shows a marked decrease in the proliferation index in PyMT;DKO tumors compared with PyMT;WT controls (PyMT;WT: n=11; PyMT;DKO: n=10). Differences were analyzed using Student's t-test, $p < 0.0001$.

We next analyzed whether altered tumor size in PyMT;DKO mice was associated with changes in tumor cell death. We quantified apoptotic cell death in primary mammary tumors by Terminal deoxynucleotidyl transferase dUTP nick end labeling (TUNEL) staining. Morphometric analysis of ten high-power fields per tumor showed that TUNEL-positive cells accounted for 5.8% of all nuclei in PyMT;DKO tumors versus 2.1% in PyMT;WT tumors (Figure 9), demonstrating a significant increase in apoptosis in the double-knockout group. These data suggest that enhanced cancer cell death, together with reduced proliferation, contributes to the smaller overall tumor burden observed in PyMT;DKO mice.

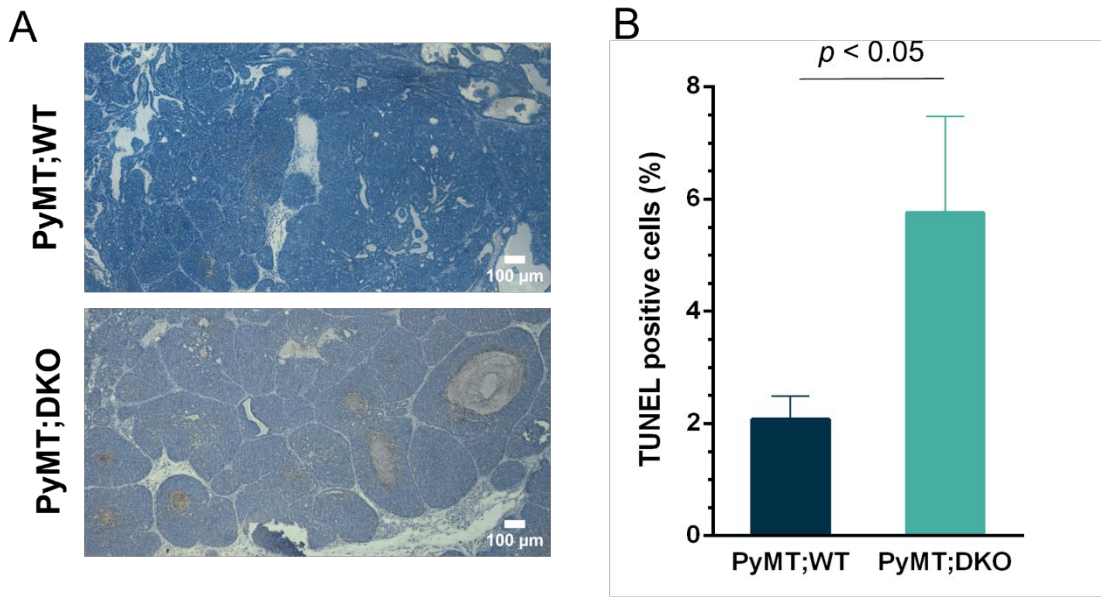


Figure 9: Cell death in PyMT mammary carcinomas from both genotypes, determined through TUNEL assays. Representative images (A) and quantification (B) of TUNEL-positive cells as a percentage of total cells in PyMT;WT (n=9) and PyMT;DKO (n=8) tumors. The TUNEL+ index was calculated from 10 high-power fields per tumor using computer-assisted data analysis in ImageJ. Differences were analyzed using Student's t-test. Scale bar: 100 µm.

As extensive cell death in rapidly growing malignant solid tumors can also result from hypoxia and nutrient deprivation due to insufficient blood supply (Lee et al., 2018; Yee & Li, 2021), we additionally examined tumor vascularization. Immunofluorescent staining for the endothelial marker CD31 (also known as platelet endothelial cell adhesion molecule-1 [PECAM-1]) and quantification of CD31-positive vessel area and density did not reveal significant differences between PyMT;WT and PyMT;DKO tumors (Figure 10), indicating that the combined loss of stefin B and cystatin C does not alter angiogenesis in this model. Together, these findings suggest that stefin B and cystatin C deficiency reduce primary tumor growth predominantly by shifting the balance towards decreased proliferation and increased apoptosis, rather than by limiting vascularization of the tumor.

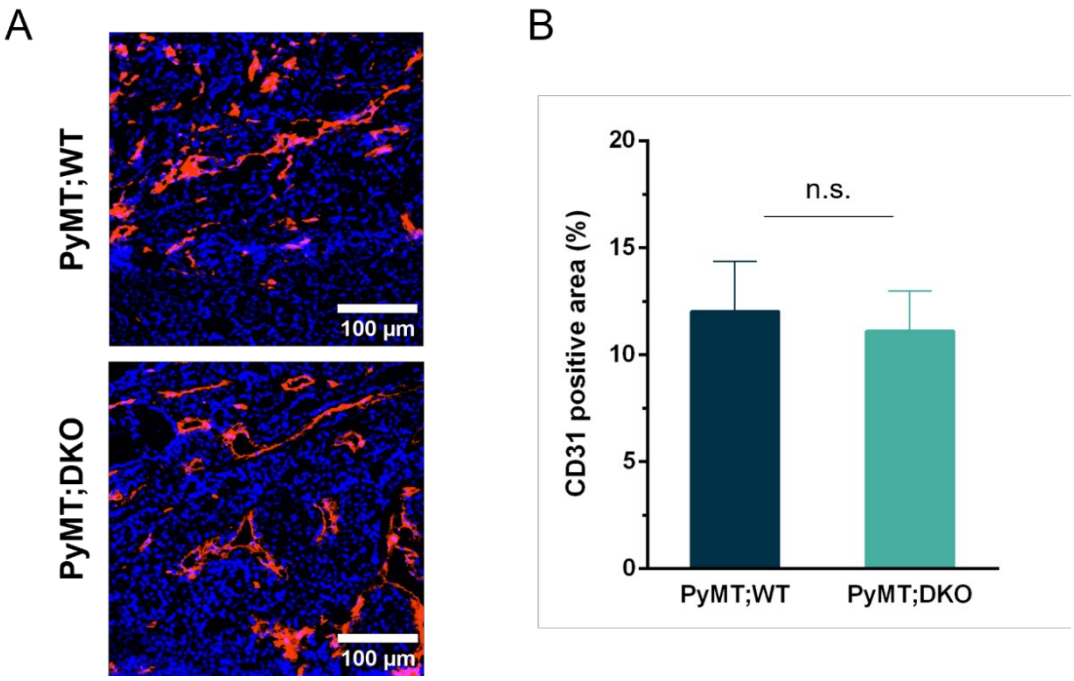


Figure 10: Tumor vascularization in PyMT;WT and PyMT;DKO mammary tumors. (A) Representative immunofluorescence images of tumor sections stained with the endothelial cell marker CD31 (red) and counterstained with DAPI (blue) from PyMT;WT and PyMT;DKO mice. Scale bar: 100 µm. (B) Quantification of CD31-positive area expressed as a percentage of total tumor area. No statistically significant difference in vascularization was observed between PyMT;WT, and PyMT;DKO tumors (n.s., not significant).

4.1.4 Evaluation of metastasis in PyMT mammary tumors

The expression of the PyMT oncogene in the mammary epithelium of the PyMT mouse breast cancer model drives the rapid development of multifocal adenocarcinomas. The majority of tumor-bearing mice develop lung metastasis by 14 weeks of age, making this model a reliable system for the investigation of metastatic disease *in vivo* (Guy et al., 1992). To determine if the dual loss of stefin B and cystatin C influences metastatic progression, we further quantified the burden of spontaneous pulmonary metastases in both groups of mice at 14 weeks of age. We performed histomorphometric analysis on lung sections stained with H&E obtained from three distinct tissue depths at 14 weeks of age to determine the number and size of metastatic lesions per 1 mm^2 of lung parenchyma in PyMT;WT and PyMT;DKO female mice. Metastatic foci were detected in all analyzed animals; however, the density of lung metastases per mm^2 was significantly lower in the PyMT;DKO group compared with PyMT;WT controls (0.26/mm^2 in PyMT;WT versus 0.05/mm^2 in PyMT;DKO), whereas the average size of individual metastatic lesions did not significantly differ between genotypes (Figure 11). These findings suggest that the combined loss of stefin B and cystatin C primarily impairs metastatic seeding or early colonization of the lung, leading to fewer metastatic foci, without substantially affecting the subsequent growth of established lung metastases.

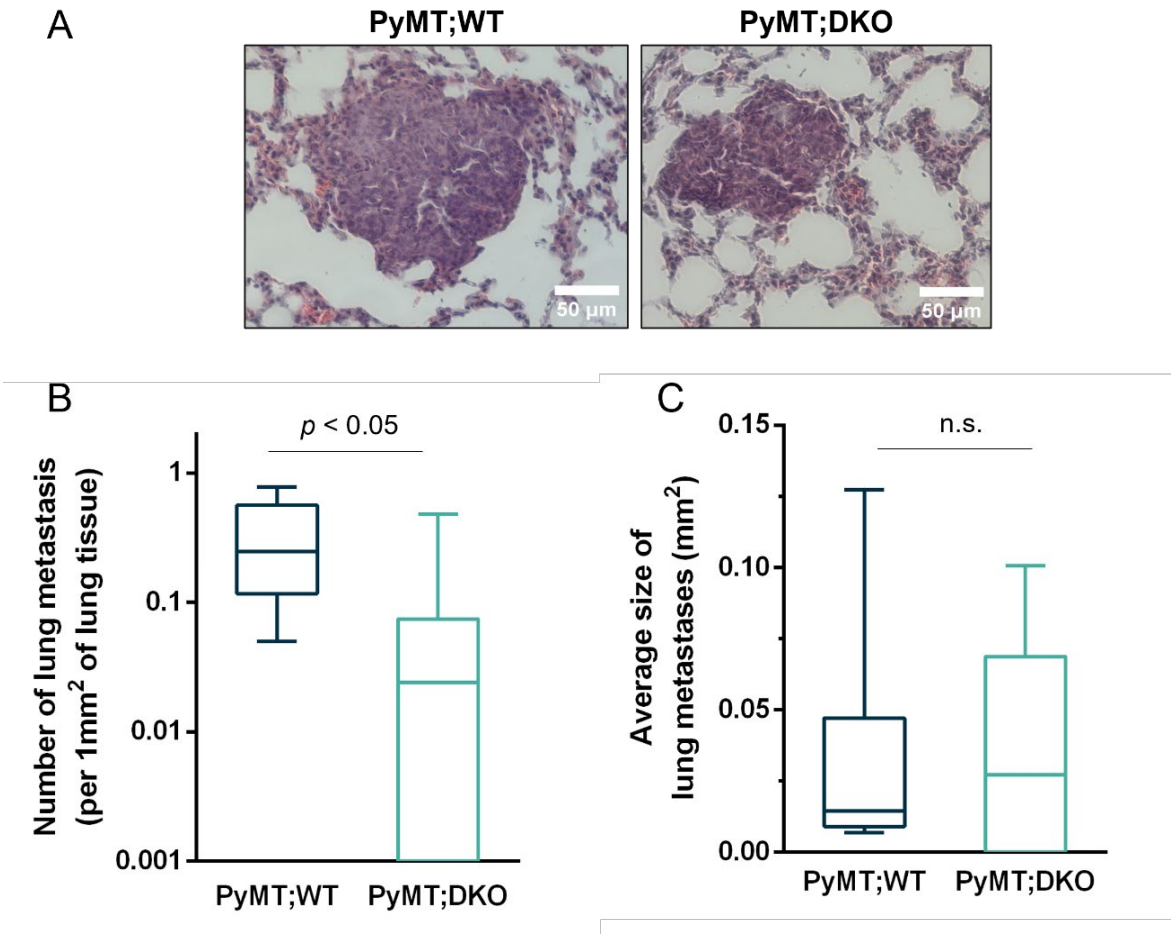


Figure 11: Effect of stefin B and cystatin C on pulmonary metastasis development in the PyMT breast cancer model. (A) Representative histological sections of lungs showing metastatic foci in PyMT;WT and PyMT;DKO female mice at 14 weeks of age (scale bar: 50 µm). (B) Histomorphometric analysis of the number of lung metastases in PyMT;WT (n=14) and PyMT;DKO (n=14) female mice at 14 weeks ($p < 0.05$). (C) Average size of individual lung metastases in PyMT;WT (n=14) and PyMT;DKO (n=14) mice, showing no statistically significant difference between genotypes (n.s., non-significant). Differences were analyzed using Student's t-test.

4.1.5 Histological characteristics of PyMT mammary carcinomas and organs

To assess if the simultaneous deficiency of stefin B and cystatin C affects the overall morphology of PyMT mammary tumors, we determined the tumor-stroma ratio on H&E-stained tumor sections. The tumor–stroma ratio (TSR) is defined as the proportion of tumor cells relative to stroma, and it has emerged as a simple histopathological parameter with prognostic relevance in several solid tumors, including breast cancer, where a high stromal content (stroma-high, low TSR) correlates with poorer outcome (van Pelt et al., 2018). In breast cancer, studies have shown that a high stromal content (stroma-high, low TSR) is associated with worse outcomes, especially in patients with triple-negative or high-grade disease (Jiang, Chen, & Liu, 2021; Vangangelt et al., 2020). Histological examination of PyMT mammary carcinomas revealed no significant differences in TSR between PyMT;WT and PyMT;DKO tumors (Figure 12), indicating that the overall tumor composition and stromal content were conserved regardless of genotype.

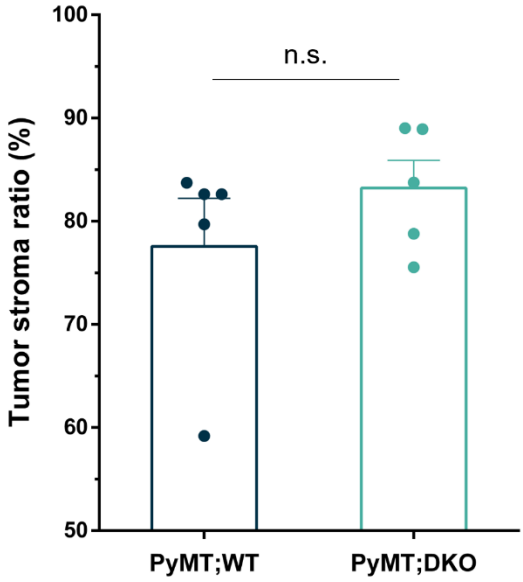


Figure 12: Tumor stroma ratio (TSR) in PyMT;WT and PyMT;DKO mammary tumors. The TSR (%) was calculated as the mean from 5 tissue sections per group, with 3 fields of view (FOV) examined per section at 10x magnification. Tumor and stroma areas were measured using CellSens software (Olympus).

We also evaluated the potential systemic effects of stefin B and cystatin C deficiency and performed a pathohistological examination of major organs (liver, kidney, lungs, and spleen) in PyMT;WT, PyMT;DKO, PyMT;StfB^{-}/$^{-}$, and PyMT;CstC^{-}/$^{-}$ mice. Histological examination of tissues from all groups revealed no major morphological abnormalities or genotype-specific differences (Figure 13), suggesting that stefin B and/or cystatin C deficiency does not appear to induce systemic pathological changes beyond those observed at the primary tumor site and changes in the number of pulmonary metastases.

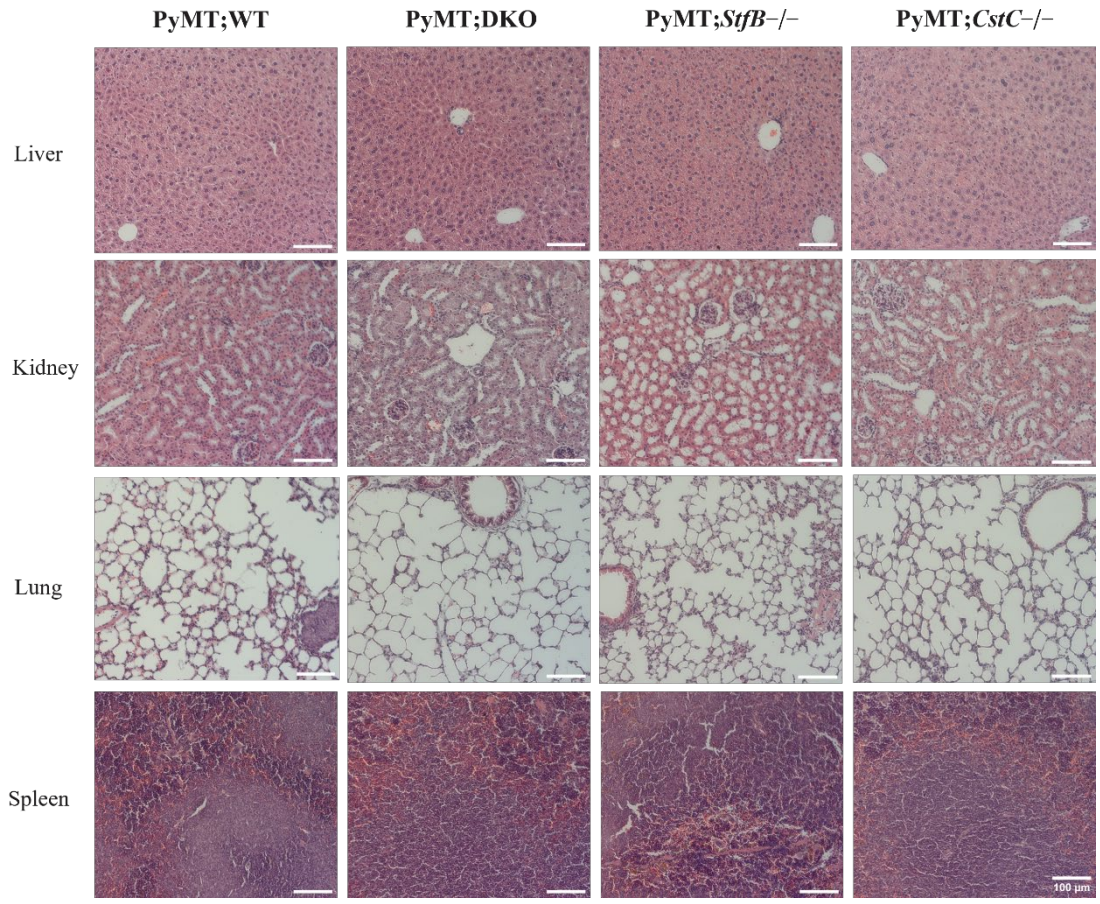


Figure 13: Histopathological examination of major organ tissues from different genotypes. Liver, kidney, lung, and spleen sections from PyMT;WT, PyMT;DKO, PyMT;StfB^{-}/$^{-}$, and PyMT;CstC^{-}/$^{-}$ mice were stained with hematoxylin and eosin, and comparative histopathological assessment was performed. Scale bar: 100 µm.

4.2 Analysis of PyMT Primary Tumor Cells

To further explain the role of stefin B and cystatin C on cell proliferation, we also analyzed primary PyMT tumor cells isolated from PyMT;WT and PyMT;DKO female transgenic mice.

4.2.1 *In vitro* proliferation of primary PyMT tumor cells

We next analysed the proliferation of primary PyMT tumor cells *in vitro* with a bromodeoxyuridine (BrdU) incorporation assay to assess whether the reduced tumor growth observed in PyMT;DKO mice reflects intrinsic differences in tumor cell proliferative capacity. Primary tumor cells isolated from PyMT;DKO mice showed significantly reduced proliferation compared to PyMT;WT cells ($p < 0.01$, Figure 14), suggesting that the combined deficiency of stefin B and cystatin C intrinsically impairs tumor cell proliferation, independently of the tumor microenvironment.

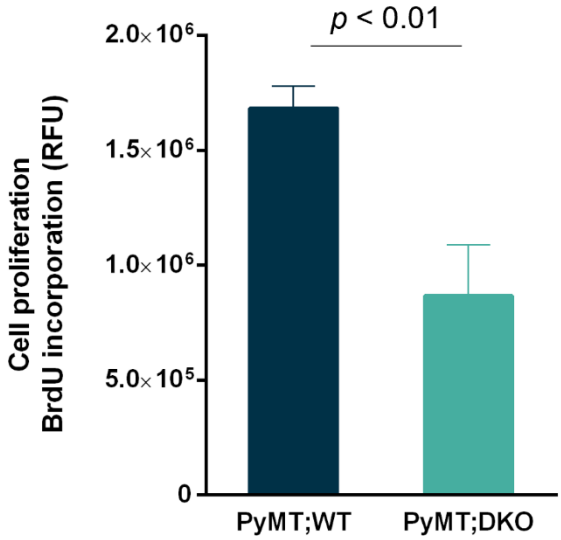


Figure 14: Reduced proliferation of primary PyMT;DKO tumor cells *in vitro*. BrdU incorporation assay of primary tumor cells isolated from PyMT;WT and PyMT;DKO mice. PyMT;DKO cells showed significantly reduced proliferation compared to PyMT;WT cells. Data are presented as mean ± SEM ($p < 0.01$).

4.3 Expression and Activity of Cysteine Cathepsins

Since cysteine cathepsins are key lysosomal proteases involved in tumor growth, invasion, and remodeling of the TME, we examined both expression and activity of major lysosomal cathepsins in PyMT mammary tumors to determine whether the observed tumor phenotypes in DKO mice reflect altered cathepsin regulation at the transcriptional or enzymatic level.

4.3.1 mRNA expression of cathepsins

We measured relative mRNA expression of cathepsins B, H, L, S and Z in primary mammary tumors by quantitative real-time PCR to evaluate whether deletion of stefin B and cystatin C affects transcription of individual cathepsins. Expression was normalized to the reference genes Atp5b (ATP synthase F1 subunit beta) and Ubc (ubiquitin C) and is shown relative to PyMT;WT, which was set to 1. Consistent with previous findings in single knockouts, we did not observe major differences in cathepsin transcript levels between PyMT;WT and PyMT;DKO group, except a modest but significant upregulation of CstS (Figure 15). These data suggest that the reduced tumor burden in DKO mice is not driven by altered cathepsin gene expression but rather by changes in cathepsin activity and downstream signaling.

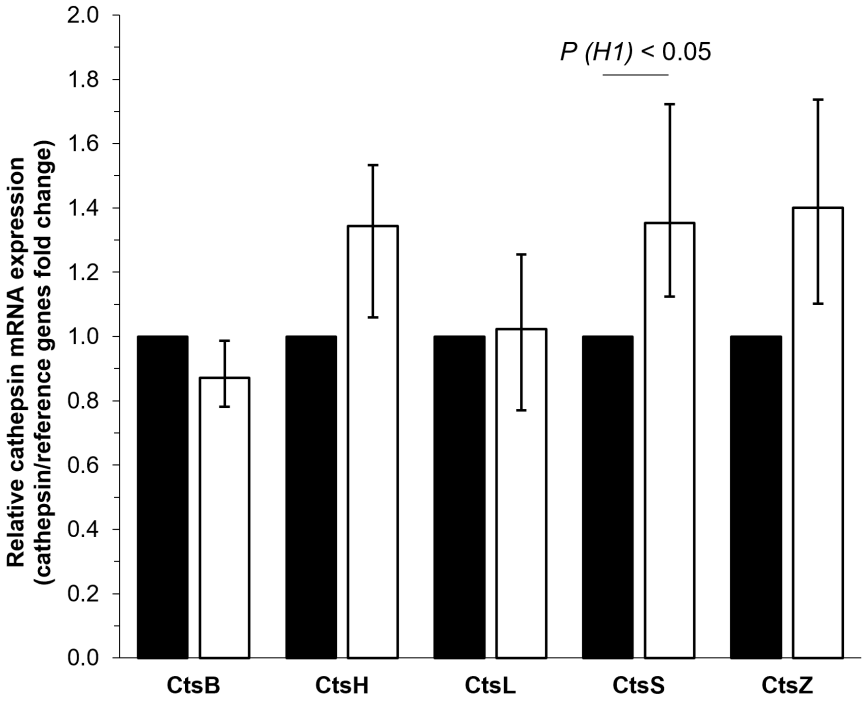


Figure 15: Expression of cysteine cathepsins in PyMT;WT (black, n=3) and PyMT;DKO (white, n=3) primary mammary tumors. Relative mRNA levels of cathepsin B (CtsB), cathepsin H (CtsH), cathepsin L (CtsL), cathepsin S (CtsS) and cathepsin Z (CtsZ) were determined by quantitative real-time PCR, normalized to reference genes (Atp5b, Ubc), and expressed relative to PyMT;WT (set to 1). Error bars represent 95% confidence intervals (CI) for expression ratios calculated by REST 2009 (randomisation test, 2000 iterations). CtsS is significantly upregulated in PyMT;DKO tumors compared with PyMT;WT (fold change 1.353, 95% CI 1.032–1.922, P(H1) = 0.011), whereas CtsB, CtsH, CtsL and CtsZ show no significant differences between genotypes.

4.3.2 Cathepsin activity in tumor tissue

Cysteine cathepsins are frequently upregulated and mislocalized in cancer, where their increased activity contributes to tumor progression by remodeling the extracellular matrix and modulating growth factor and cytokine signaling in the TME. Their proteolytic activity is normally controlled by endogenous inhibitors such as intracellular stefin B and extracellular cystatin C, so we next aimed to investigate how the combined loss of both inhibitors affects overall protease activity in the PyMT model. We therefore measured total cysteine cathepsin activity in PyMT tumor homogenates using the fluorogenic substrate Z-Phe-Arg-AMC and found significantly higher activity in PyMT;DKO tumors compared with PyMT;WT controls, as presented in Figure 16. These results are consistent with the loss of inhibitory function and support a shift toward a more proteolytically active tumor milieu in DKO mice.

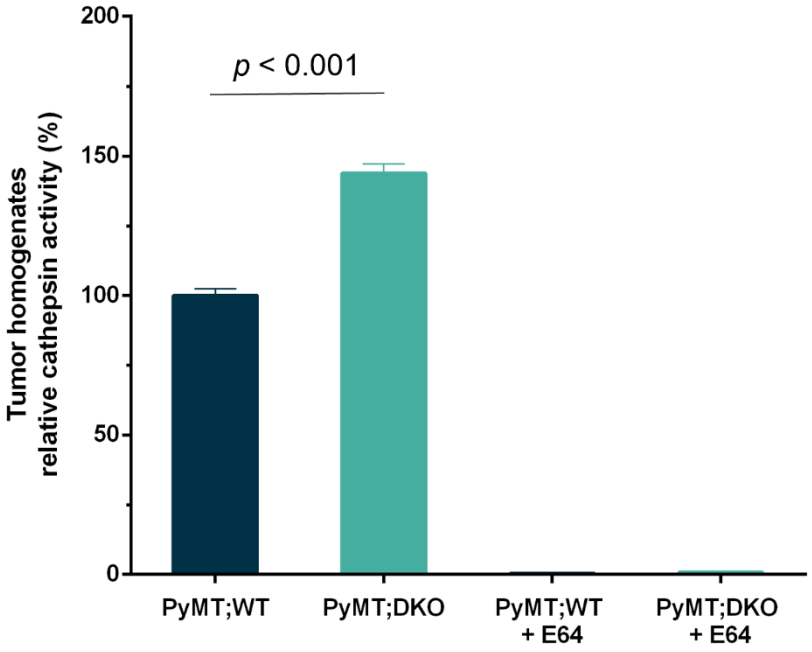


Figure 16: Relative cysteine cathepsin activity in tumor homogenates in PyMT;WT and PyMT;DKO mice. Activity was measured by Z-Phe-Arg-AMC hydrolysis in the presence or absence of the cysteine cathepsin inhibitor E64. The graph is showing significantly increased activity in PyMT;DKO tumors compared with PyMT;WT controls ($p < 0.001$).

4.3.3 Cathepsin activity in primary cell media and tumor lysates

Because cysteine cathepsins can act both within tumor cells and also in the extracellular space, where secreted proteases shape the TME, we next distinguished between intracellular and extracellular proteolytic compartments using primary PyMT tumor cells. Cathepsin activity measured in conditioned media from PyMT;DKO primary tumor cells was increased by approximately three-fold compared with media from PyMT;WT cells, whereas activity in corresponding cell lysates was not significantly altered between genotypes (Figure 17). This pattern supports the notion that the major consequence of stefin B and cystatin C loss in our model is an increase in extracellular cysteine cathepsin activity, rather than a global change in intracellular proteolysis. Together with the reduced tumor growth, lower proliferation, and increased apoptosis observed in PyMT;DKO tumors, these findings suggest that enhanced extracellular cathepsin activity in the absence of both inhibitors is compatible with, and may even contribute to, a remodeled microenvironment that ultimately restrains tumor progression in this setting.

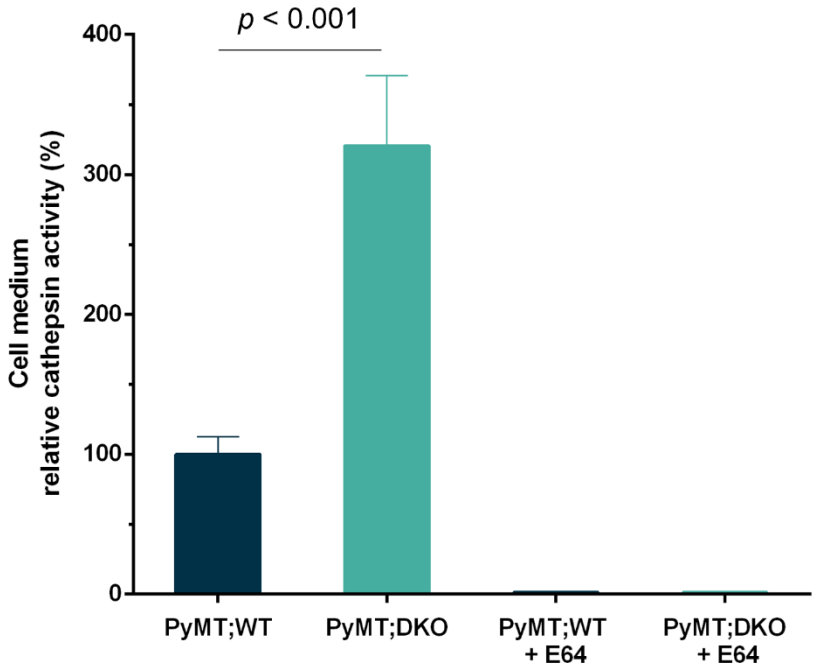


Figure 17: Relative cysteine cathepsin activity in conditioned media from primary PyMT;WT and PyMT;DKO tumor cells. The activity was measured by Z-Phe-Arg-AMC hydrolysis in the presence or absence of the cysteine cathepsin inhibitor E64. The graph is showing a marked increase in extracellular cathepsin activity in PyMT;DKO cultures compared with PyMT;WT controls ($p < 0.001$).

4.4 AMPK Activation in PyMT Mammary Tumors

To explore potential mechanisms underlying the altered tumor progression observed in DKO mice, we next analyzed activation of AMP-activated protein kinase (AMPK) in late-stage PyMT mammary tumors, since stefin B has recently been shown to be involved in AMPK-mechanistic target of rapamycin (mTOR)-dependent stress responses (Trstenjak-Prebanda et al., 2023). The AMPK–mTOR signaling pathway is a central regulator of cellular energy homeostasis and adaptation to stress. AMPK becomes activated under metabolic or oxidative stress. Once active, it promotes ATP-generating, catabolic pathways while suppressing anabolic processes, which are energy-consuming, in part through direct inhibition of mTOR, a key driver of protein synthesis and cell growth (Hardie, Ross, & Hawley, 2012; Herzig & Shaw, 2018). As a result, AMPK activation reduces cell proliferation and induces autophagy, enabling survival of cells under adverse conditions (Herzig & Shaw, 2018). Dysregulation of this pathway has important relevance for cancer, as it directly links cellular metabolic stress responses to the control of tumor growth and resistance to therapy (Faubert et al., 2013; Hardie et al., 2012).

4.4.1 Western blot analysis of phospho-AMPK (Thr172) and total AMPK in PyMT tumors

As presented in Figure 18, we detected a statistically significant increase in p-AMPK in PyMT;DKO tumors compared to the PyMT:WT group (p=0.03) by Western blot analysis. p-AMPK levels in single knockout tumors were within the range of controls. We also performed the Western blot analysis for total AMPK in mammary tumors, which served

as a control for overall AMPK protein abundance. We detected a significant increase in total AMPK in PyMT;DKO tumors (p=0.04) (Figure 19). Total AMPK was assessed as a supportive control for the p-AMPK analysis, and the concomitant increase in total AMPK and p-AMPK in PyMT;DKO tumors suggests that AMPK signaling is upregulated in this genotype. Taken together with the reduced proliferation and increased apoptosis in PyMT;DKO tumors, these data suggest that upregulated AMPK signaling may potentially contribute to mTOR suppression and altered cytokine networks in the DKO tumor microenvironment.

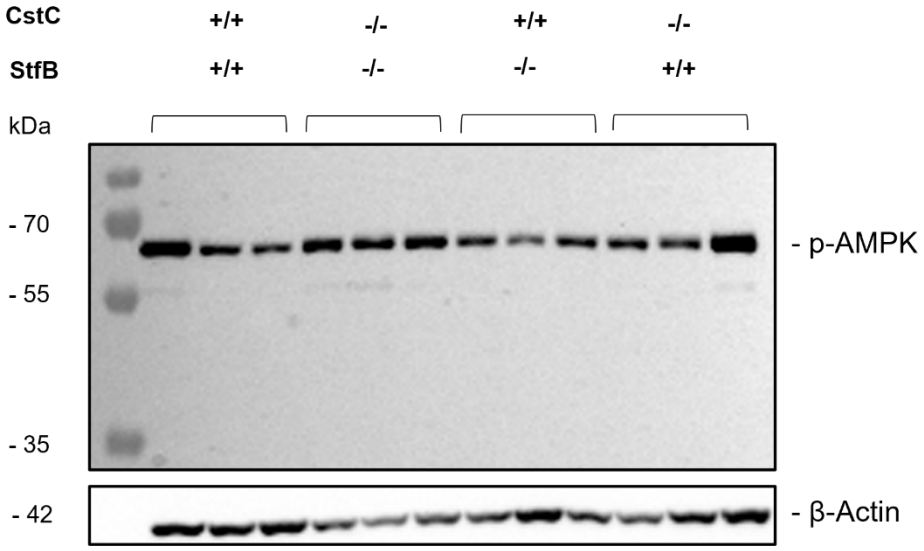


Figure 18: Comparison of p-AMPK expression between genotypes in PyMT mammary carcinomas. Representative Western blots show p-AMPK levels in tumors from PyMT;WT, PyMT;StfB−/−, PyMT;CstC−/−, and PyMT;DKO mice. β -actin served as a loading control.

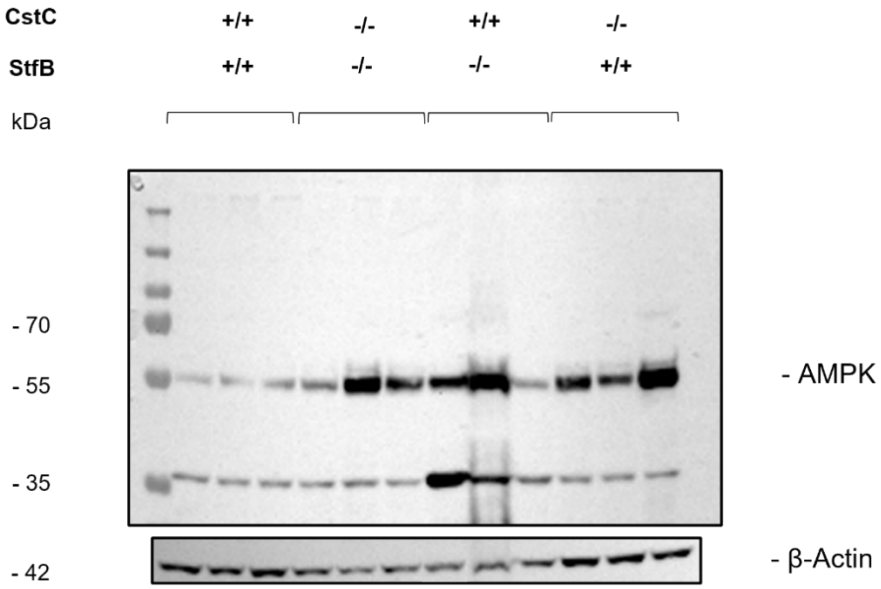


Figure 19: Total AMPK expression in PYMT mammary carcinomas in different genotypes. Representative Western blots show total AMPK levels in tumors from PyMT;WT,

PyMT;StfB−/−, PyMT;CstC−/−, and PyMT;DKO mice. β-actin served as a loading control.

4.5 Tumor Microenvironment and Immune Cell Infiltration

Since cysteine cathepsins and their inhibitors regulate antitumor immunity, we next investigated whether combined stefin B and cystatin C deficiency alters immune cell composition in PyMT tumors, with focus on tumor-associated macrophage (TAM) infiltration and polarization.

4.5.1 Immunohistochemical assessment of macrophage infiltration

Given the important role of macrophages in shaping the TME and affecting cancer progression, we first evaluated whether macrophage infiltration is altered in DKO mammary tumors. Tumor sections were immunohistochemically stained for F4/80, a well-established marker for murine macrophages. We detected a significantly higher proportion of F4/80-positive cells in PyMT;DKO tumors than in PyMT;WT controls (Figure 20), which suggests enhanced macrophage infiltration in the absence of both inhibitors.

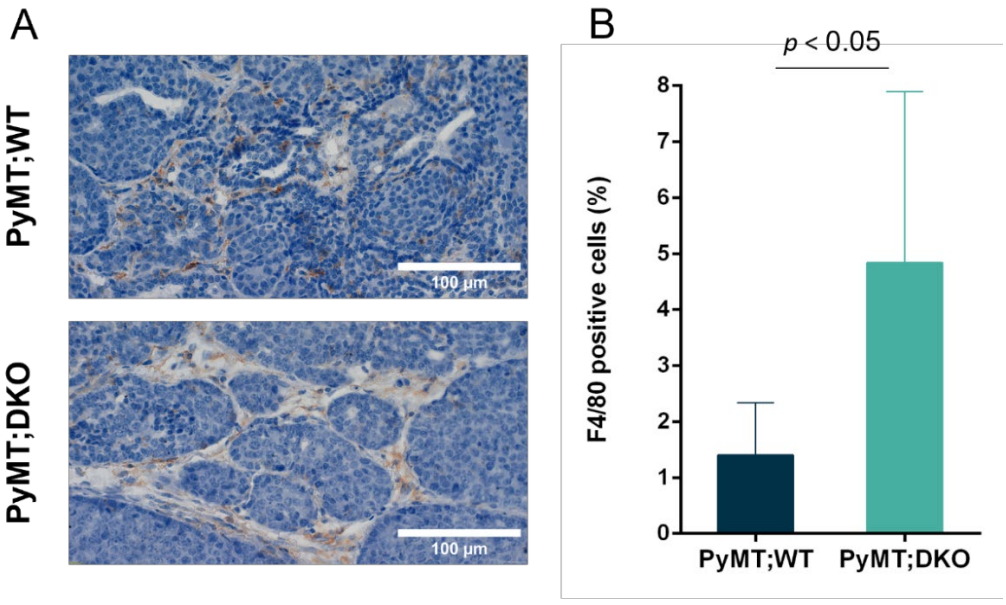


Figure 20: Effect of stefin B and cystatin C deficiency on macrophage infiltration in PyMT mammary tumors. (A) Representative microscopic images of immunohistochemical staining of F4/80, a broadly used marker for macrophages, in mammary tumors from PyMT;WT and PyMT;DKO mice. Scale bar: 100 µm. (B) Quantification of F4/80-positive cells as a percentage of total cells in PyMT;WT (n=5) and PyMT;DKO (n=5) tumors. Statistical significance was determined using Student's t-test.

4.5.2 Immunohistochemical detection of M1 and M2 macrophages

Since macrophage infiltration and polarization state determine their function within the TME and therefore highly affect the disease outcome in numerous pre-clinical models, including the PyMT breast cancer murine model (E. Y. Lin et al., 2001; Qian & Pollard, 2010), we next assessed whether the increased macrophage infiltration we observed is accompanied by a change in macrophage phenotype. We used CD86 and CD206 as markers

of classically activated M1 and alternatively activated M2 macrophages, respectively, and detected a significantly higher proportion of CD86-positive cells in PyMT;DKO tumors (Figure 21A, B). On the other hand, no significant difference in CD206-positive cells was observed between the groups (Figure 21C, D). These findings suggest an elevation of macrophage infiltration together with a shift toward an M1-dominated macrophage phenotype in DKO mammary tumors.

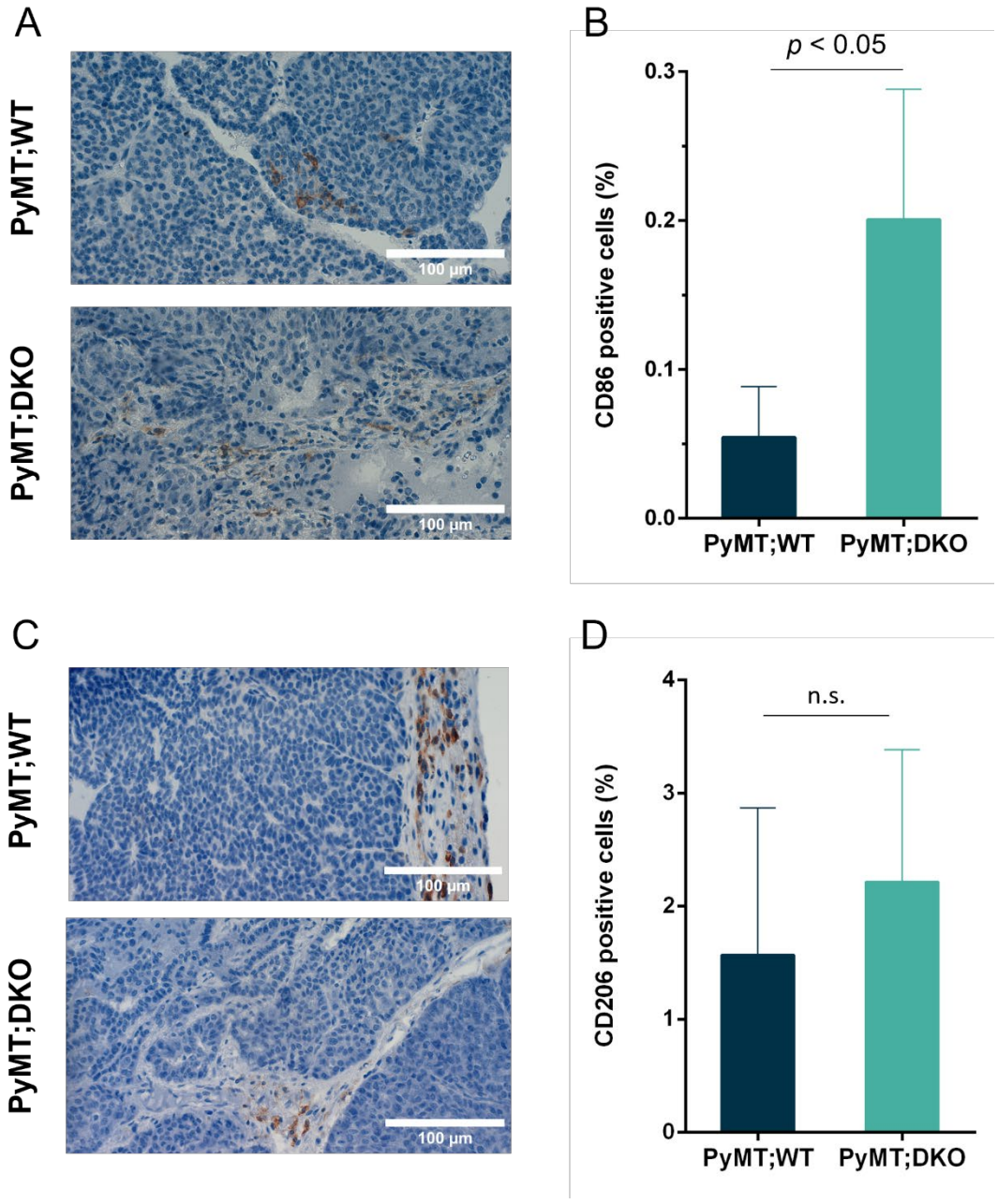


Figure 21: Effect of stefin B and cystatin C deficiency on macrophage polarization in PyMT mammary tumors. (A) Representative microscopic images of immunohistochemical staining of M1 macrophages using the CD86 marker in mammary tumors from PyMT;WT and PyMT;DKO mice with CD86 marker. Scale bar: 100 µm. (B) Quantification of CD86-positive cells as a percentage of total cells in PyMT;WT (n=5) and PyMT;DKO (n=5) tumors. (C) Representative immunohistochemical staining of M2 macrophages using the CD206 marker in mammary tumors from PyMT;WT and PyMT;DKO mice. Scale bar: 100 µm. (D) Quantification of CD206-positive cells as a percentage of total cells in

PyMT;WT (n=5) and PyMT;DKO (n=5) tumors. Statistical significance was determined using Student's t-test.

4.6 Comparison with Single-Knockout PyMT Breast Cancer Models

To place our observed effects of combined stefin B and cystatin C deficiency into context, we compared key tumor parameters from PyMT;DKO mice with previously published data from single stefin B and single cystatin C knockout studies in the same mouse breast cancer model (Butinar et al., 2014; Završnik et al., 2017). The comparison of these parameters is summarized in Table 1.

4.6.1 Tumor onset

In the stefin B single-knockout model, the first palpable mammary tumors appeared only slightly later than in wild-type mice, and this delay was not statistically significant, indicating that stefin B has little impact on tumor initiation in the PyMT mouse model (Butinar et al., 2014). Cystatin C deficiency similarly did not meaningfully alter the timing of tumor onset (Završnik et al., 2017). By contrast, combined stefin B and cystatin C deficiency significantly delayed tumor onset in PyMT;DKO mice (Matjan Štefin et al., 2026), showing that the disruption of intracellular and extracellular cathepsin regulation affects early tumor progression stronger than either of the single knockout alone.

4.6.2 Cumulative tumor weight

Both stefin B and cystatin C single knockouts reduced cumulative mammary tumor weight by approximately 23% compared with wild-type controls, but through distinct mechanisms. Stefin B deficiency primarily increased tumor cell death, whereas cystatin C deficiency mainly reduced proliferation (Butinar et al., 2014; Završnik et al., 2017). In PyMT;DKO mice, we observed a reduction in total tumor weight of about 41% (Matjan Štefin et al., 2026). The effect of either individual knockout was therefore exceeded by almost twice and suggests a complementary tumor-suppressive effect of simultaneous stefin B and cystatin C loss.

4.6.3 Cell proliferation

The observation in stefin B knockout study, in which stefin B did not significantly affect Ki67 levels or BrdU incorporation, supports the view that stefin B does not have a major role in driving cell proliferation (Butinar et al., 2014). In contrast, in the cystatin C deficiency study, the Ki67 and BrdU data were significantly reduced, consistent with a role for cystatin C in sustaining tumor cell proliferation (Završnik et al., 2017). In the DKO tumors, Ki67 levels were even more decreased and were the lowest among all included genotypes. This suggests the strongest impairment of proliferation when both inhibitors are missing (Matjan Štefin et al., 2026).

4.6.4 Apoptosis

Large TUNEL- and caspase-3–positive areas observed in stefin B-deficient tumors confirmed a clear increase in apoptosis compared with controls, supporting a cytoprotective role of stefin B against stress-induced cell death (Butinar et al., 2014). On the other hand, cystatin C deficiency was associated with slightly lower apoptotic rate, in order with its

primary impact on proliferation rather than survival (Završnik et al., 2017). In PyMT;DKO study, we detected a significantly elevated TUNEL index relative to wild-type, indicating that the pro-apoptotic effect of stefin B loss remains dominant in the DKO phenotype and that enhanced apoptosis likely contributes to reduced tumor burden (Matjan Štefin et al., 2026).

4.6.5 Angiogenesis

Between stefin B-deficient, cystatin C-deficient, and wild-type PyMT tumors, no significant differences in vessel density were detected by quantitative CD31 staining, indicating that neither inhibitor has a major effect on angiogenesis in this model (Butinar et al., 2014; Završnik et al., 2017). Consistent with this, we did not detect differences between groups in our study. PyMT;DKO tumors displayed similar CD31-positive vessel densities as wild-type tumors, suggesting that changes in tumor growth and metastasis are independent of gross alterations in vascularization (Matjan Štefin et al., 2026).

4.6.6 Lung metastasis

In the stefin B-knockout model, the number of pulmonary metastases did not significantly differ from wild-type, in line with its mainly intracellular role and limited influence on metastatic spread (Butinar et al., 2014). In contrast, cystatin C-deficient PyMT mice developed more lung metastases per unit lung area than wild-type animals, indicating that cystatin C normally restrains at least some steps of metastatic seeding or early colonization (Završnik et al., 2017). Surprisingly, in PyMT;DKO mice, we observed a marked reduction in pulmonary metastasis number compared with control animals. These results show that simultaneous stefin B loss counteracts the pro-metastatic effect of cystatin C deficiency and results in a phenotype that suppresses metastatic spread (Matjan Štefin et al., 2026).

The mean size of individual pulmonary metastases in both single-knockout studies remained comparable to wild-type controls, with only a slight tendency toward larger lesions in cystatin C-deficient mice (Završnik et al., 2017). In contrast, in PyMT;DKO lungs, we observed average metastasis sizes that were indistinguishable from wild-type despite the pronounced reduction in lesion number (Matjan Štefin et al., 2026). This data suggests that the loss of both inhibitors interferes primarily with metastatic seeding rather than the growth of metastatic colonies.

4.6.7 Cysteine cathepsin activity

Stefin B deficiency increased cysteine cathepsin activity in tumor lysates by about two-fold, reflecting the loss of a major cytosolic cathepsin inhibitor (Butinar et al., 2014). Deficiency of cystatin C similarly enhanced cathepsin activity in mammary tissue and tumors, consistent with its function as an important extracellular inhibitor (Završnik et al., 2017). In PyMT;DKO tumors, cathepsin activity was further elevated, indicating deregulated extra- and intracellular proteolysis. This increased activity aligned with an overall tumor-suppressive phenotype in the absence of both inhibitors (Matjan Štefin et al., 2026).

In the stefin B single-knockout study, extracellular cathepsin activity was not assessed (Butinar et al., 2014). Whereas in the cystatin C knockout, conditioned media from primary PyMT tumor cells showed clearly increased cathepsin activity, directly reflecting extracellular inhibition loss (Završnik et al., 2017). Analysis of conditioned media from PyMT;DKO tumor cells showed an even higher, approximately three-fold increase in

cathepsin activity compared with wild-type, underscoring the combined impact of removing both inhibitors on secreted protease activity (Matjan Štefin et al., 2026).

Table 1: Comparison of key tumor parameters across PyMT knockout breast cancer models. Results from stefin B single-knockout (PyMT;StfB^{-}/$^{-}$; StfB KO), cystatin C single-knockout (PyMT;CstC^{-}/$^{-}$; CstC KO), and double-knockout (PyMT;DKO) PyMT breast cancer models relative to wild-type (WT) controls (Butinar et al., 2014; Matjan Štefin et al., 2026; Završnik et al., 2017).

Parameter	PyMT;StfB^{-}/$^{-}$	PyMT;CstC^{-}/$^{-}$	PyMT;DKO
***IN VIVO* TUMOR PROGRESSION**			
Tumor onset	No significant delay	No significant delay	Significantly delayed (median day 38 vs. 36 in WT)
Cumulative tumor weight	Decreased by ~23% (6.5 g vs. 8.4 g in WT)	Decreased by ~23% (7.1 g vs. 9.2 g in WT)	Decreased by ~41% (5.8 g vs. 9.8 g in WT)
TUMOR CELL BIOLOGY			
***In situ* tumor cell proliferation (Ki67)**	No significant change	Moderately reduced (16.4% vs. 24% in WT)	Strongly reduced (6.6% vs. 24% in WT)
***In vitro* tumor cell proliferation (BrdU)**	No significant change	Reduced BrdU incorporation	Reduced BrdU incorporation
***In situ* tumor cell apoptosis (TUNEL)**	Significantly increased (7.5% vs. <1.5% in WT)	Slightly reduced (lower staining than WT)	Significantly increased (5.8% vs. 2.1% in WT)
***In vitro* tumor cell apoptosis (caspase 3)**	Increased cleaved caspase-3 signal	No major change	Not determined
Angiogenesis (CD31)	No significant change	No significant change	No significant change
METASTASIS			
Number of lung metastases (per mm² of lung tissue)	No significant change	Significantly increased (0.51 lesions/mm² vs.	Significantly reduced (0.05 lesions/mm² vs. 0.26 lesions/mm² in WT)

		0.26 lesions/mm² in WT)	
Size of lung metastasis	No significant change	No significant change	No significant change
PROTEOLYTIC ACTIVITY			
Total cathepsin activity in tumor homogenate	Moderately increased	Moderately increased	Strongly increased
Extracellular cathepsin activity in conditioned medium	Not determined	Moderately increased	Strongly increased

In summary, in PyMT;DKO mice, suppression of primary tumor burden and proliferation is more pronounced than in either single knockout. In addition, the number of lung metastases is uniquely reduced. These observations are accompanied by a shift in the immune microenvironment toward increased infiltration of M1 macrophages. All findings together suggest that stefin B and cystatin C exert complementary, non-redundant functions in the breast cancer model: stefin B mainly modulates stress-induced cell death, and cystatin C supports proliferative signaling. As a result, their cumulative loss reveals combined anti-tumor effects that exceeds the impact of either single-gene deficiency.

4.7 Pharmacological Inhibition of Cathepsins B and X Impairs Tumor Progression in MMTV-PyMT Breast Cancer Models

The analyses in PyMT;DKO mice demonstrated that concomitant loss of the endogenous cysteine cathepsin inhibitors stefin B and cystatin C substantially modifies primary tumor growth and metastatic dissemination. To complement these findings and to evaluate whether direct pharmacological targeting of tumor-promoting cysteine cathepsin activity can similarly restrict tumor progression, we examined the effects of the selective reversible cathepsin X inhibitor Z9, the cathepsin B inhibitor nitroxoline, and their combination in MMTV-PyMT-derived breast cancer models. These experiments were performed in both spontaneous FVB;PyMT transgenic mice and an orthotopic model established with primary MMTV-PyMT tumor cells (Mitrović et al., 2022).

4.7.1 Z9 and nitroxoline reduce mammary tumor burden in FVB;PyMT transgenic mice

To assess the effect of pharmacological cathepsin inhibition on tumor progression in vivo, eleven-week-old FVB;PyMT transgenic female mice were treated intraperitoneally every other day with vehicle, Z9, nitroxoline, or the combination of both inhibitors until 14 weeks of age. At the endpoint, all mammary tumors were excised and cumulative tumor weight was determined. Treatment with Z9, nitroxoline, or their combination significantly reduced total mammary tumor burden compared with vehicle-treated controls (Figure 22). However, combined treatment did not produce a further significant reduction in tumor weight relative to either single inhibitor.

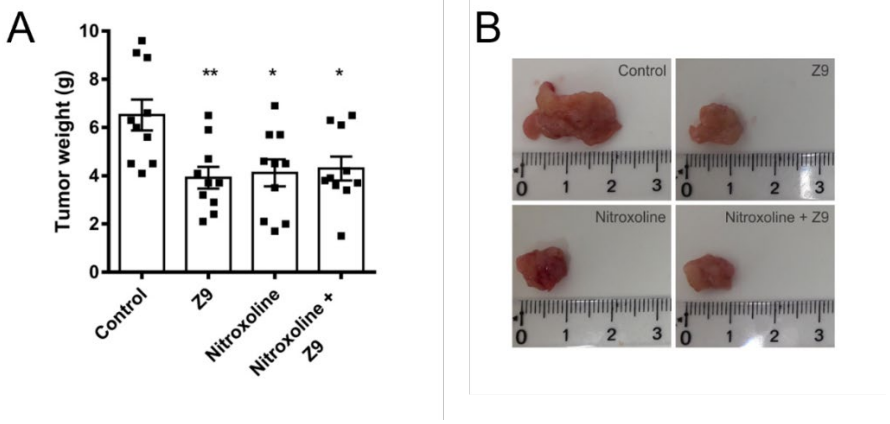


Figure 22: Z9 and nitroxoline reduce mammary tumor burden in FVB;PyMT transgenic mice. Eleven-week-old female FVB;PyMT transgenic mice were treated intraperitoneally every other day with vehicle (5% DMSO in peanut oil), the selective reversible cathepsin X inhibitor Z9 (67.18 mg/kg), the cathepsin B inhibitor nitroxoline (40 mg/kg), or the combination of Z9 (67.18 mg/kg) and nitroxoline (40 mg/kg). Mice were sacrificed at 14 weeks of age, and all mammary tumors were excised and weighed. (A) Cumulative mammary tumor weight per mouse was significantly reduced in the Z9-, nitroxoline-, and combination-treated groups compared with vehicle-treated controls. (B) Representative images of excised mammary tumors from the respective treatment groups. Data are presented as mean ± SEM. *p≤0.05, **p≤0.01.

4.7.2 Z9 and nitroxoline reduce pulmonary metastatic burden in FVB;PyMT transgenic mice

To determine whether pharmacological cathepsin inhibition also affects metastatic progression, pulmonary metastases were quantified in H&E-stained lung sections from treated FVB;PyMT mice. Z9, nitroxoline, and combined treatment significantly reduced both the number and mean cross-sectional area of lung metastatic lesions compared to vehicle treatment (Figure 23). As observed for primary tumor burden, the combination did not result in a further significant reduction in metastasis relative to treatment with either inhibitor alone. These findings support the conclusion that pharmacological inhibition of either CatX or CatB can impair spontaneous metastatic progression in the FVB;PyMT model.

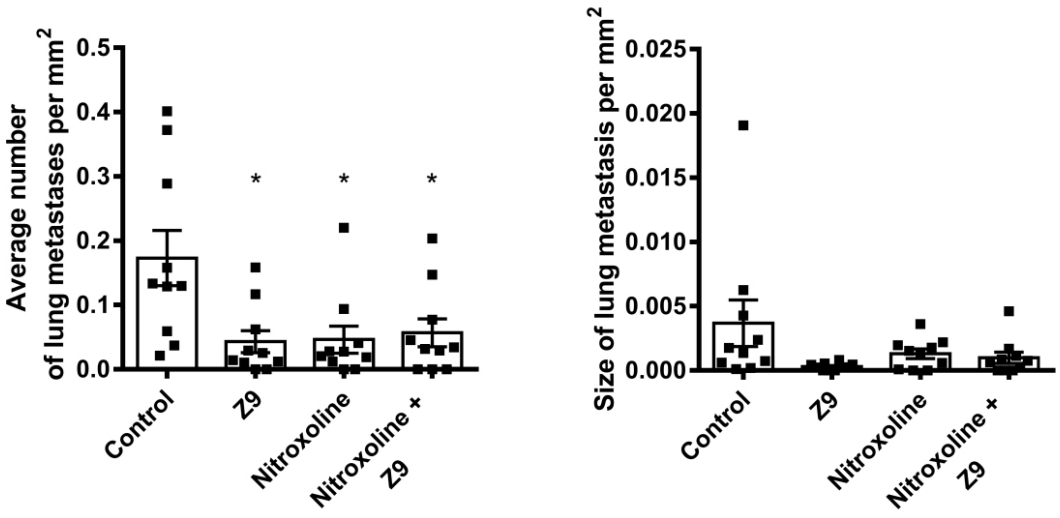
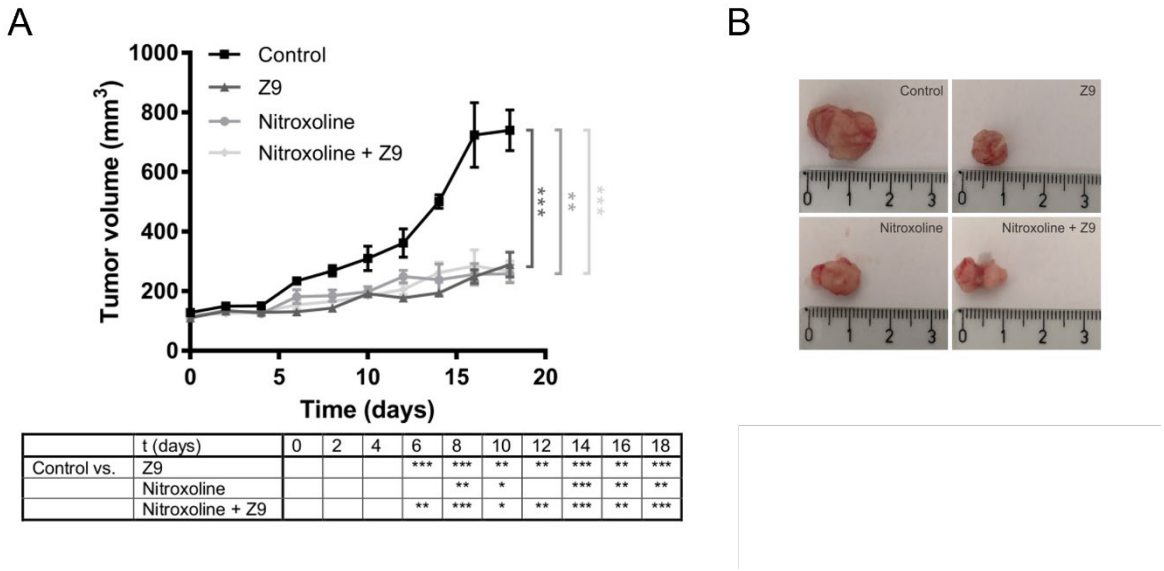


Figure 23: Z9 and nitroxoline reduce pulmonary metastatic burden in FVB;PyMT transgenic mice. At 14 weeks of age, lungs were collected from vehicle-, Z9-, nitroxoline-, and Z9/nitroxoline-treated FVB;PyMT transgenic mice. Paraffin-embedded lung sections were stained with hematoxylin and eosin, and pulmonary metastatic lesions were evaluated by histomorphometric analysis. The number of pulmonary metastases per mm^2 of lung tissue and the mean cross-sectional area of individual metastases were significantly reduced in all inhibitor-treated groups compared to vehicle-treated controls. Data are presented as mean ± SEM. *$p \leq 0.05$

4.7.3 Pharmacological inhibition of cathepsins B and X suppresses tumor growth in an orthotopic MMTV-PyMT model

To confirm the antitumor activity of Z9 in an independent PyMT-derived model, primary MMTV-PyMT tumor cells were injected orthotopically into the left inguinal mammary gland of syngeneic FVB mice. When tumor volume reached approximately 125 mm^3, mice were treated every other day with vehicle, Z9, nitroxoline, or the combination of both inhibitors. Tumor growth was monitored throughout the treatment period. Z9, nitroxoline, and combined treatment each significantly reduced orthotopic tumor growth compared to vehicle treatment (Figure 24). As in the transgenic model, simultaneous CatX and CatB inhibition did not confer an additional significant reduction in tumor growth compared to individual treatments.



	t (days)	0	2	4	6	8	10	12	14	16	18
Control vs.	Z9				***	***	**	**	***	**	***
	Nitroxoline					**	*		***	**	**
	Nitroxoline + Z9				**	***	*	**	***	**	***

Figure 24: Z9 and nitroxoline impair tumor growth in an orthotopic MMTV-PyMT breast cancer model. Orthotopic mammary tumors were established in female FVB mice. When tumor volume reached approximately 125 mm^3, mice were treated intraperitoneally every other day with vehicle (5% DMSO in peanut oil), Z9 (33.59 mg/kg), nitroxoline (20 mg/kg), or the combination of Z9 (33.59 mg/kg) and nitroxoline (20 mg/kg). (A) Tumor volume was measured every other day throughout treatment. Z9, nitroxoline, and combined treatment significantly reduced tumor growth compared with vehicle treatment; the table suggests the time points at which statistically significant differences relative to controls were observed. (B) Representative images of orthotopic tumors collected from each treatment group. Data are presented as mean ± SEM. *p≤0.05, **p≤0.01, ***p≤0.001.

Collectively, these experiments demonstrate that pharmacological inhibition of CatX by Z9 and CatB by nitroxoline impairs primary tumor growth and pulmonary metastatic progression in MMTV-PyMT breast cancer models. The concordant effects observed in spontaneous FVB;PyMT tumors and the orthotopic model support a tumor-promoting role for both cathepsin activities in vivo. In contrast, combined treatment did not provide a measurable additional benefit over either single inhibitor under the conditions used in these in vivo experiments.

4.8 Stefin B deficiency and mitochondrial redox response during LPS-induced neuroinflammation

To complement the tumor-focused studies and obtain a broader view of the biological consequences of stefin B deficiency, we investigated mitochondrial redox regulation in a non-tumor model of LPS-induced neuroinflammation. Peroxiredoxin 3 (Prx3) is a mitochondria-specific antioxidant protein involved in the removal of mitochondrial reactive oxygen species and protection against oxidative damage.

In brain tissue from untreated animals, Prx3 protein levels did not significantly differ between wild-type and stefin B-deficient mice (Figure 25A). Following LPS challenge, however, Prx3 levels were significantly higher in brain lysates from stefin B-deficient mice compared with wild-type controls (Figure 25B, E). A different pattern was observed in the

cerebellum, where stefin B-deficient mice exhibited significantly elevated Prx3 levels already under basal conditions (Figure 25C, F). Higher Prx3 levels in stefin B-deficient mice compared with wild-type animals were also observed following LPS challenge (Figure 25D, F). No significant differences in Prx3 levels between untreated and LPS-treated animals were detected within either genotype.

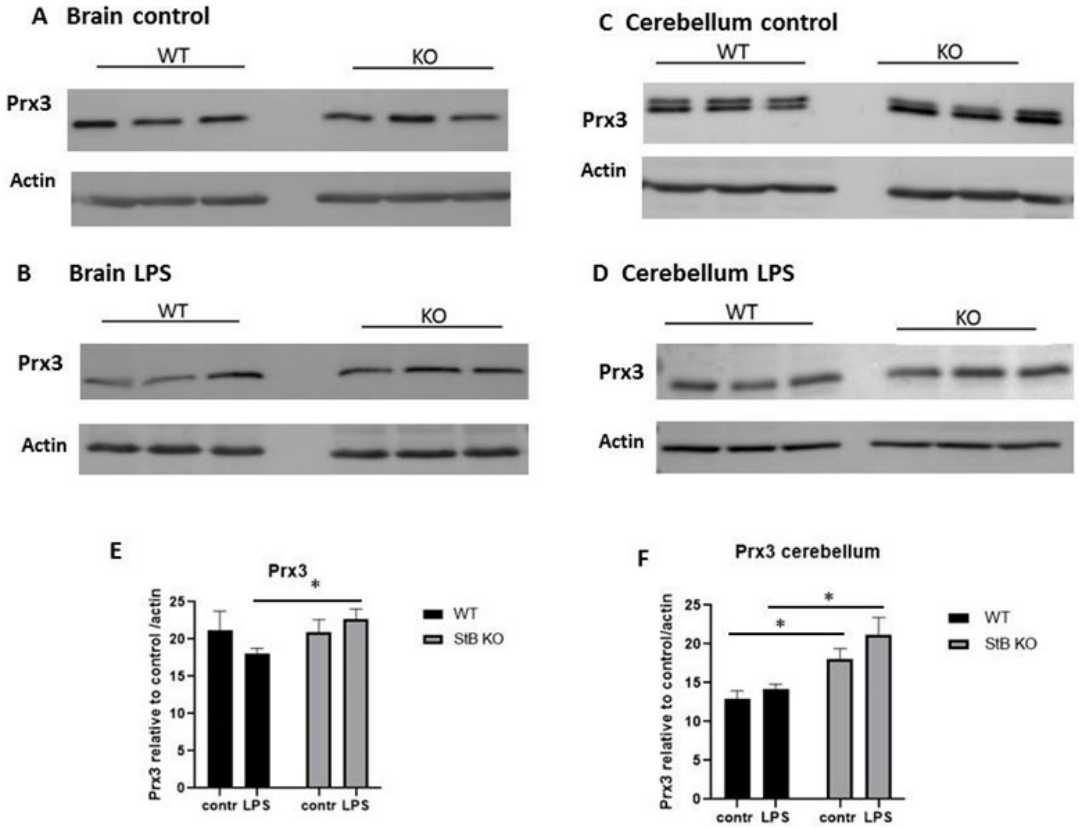


Figure 25: Peroxiredoxin 3 (Prx3) expression in brain and cerebellar tissue of stefin B-deficient (StfB KO) and wild-type (WT) mice under basal conditions and during LPS-induced neuroinflammation. (A, B) Western blot analysis of Prx3 and β-actin in brain lysates from untreated control (A) and LPS-treated (3 mg/kg, 4 h) (B) WT and StfB KO mice. (C, D) Western blot analysis of Prx3 and β-actin in cerebellar lysates from untreated (C) and LPS-treated (D) WT and StfB KO mice. (E, F) Densitometric quantification of Prx3 protein levels in brain (E) and cerebellar (F) lysates relative to β-actin. Prx3 expression is significantly increased in brain tissue of LPS-treated StfB KO mice compared with WT controls and is elevated in cerebellar tissue of StfB KO mice both under basal conditions and after LPS challenge ($^*p < 0.05$).

These results demonstrate that stefin B deficiency is associated with altered mitochondrial antioxidant status, particularly in the cerebellum, and with genotype-dependent differences in Prx3 expression during inflammatory stress. The increased Prx3 levels are consistent with an adaptive response to altered mitochondrial redox homeostasis in the absence of stefin B.

Chapter 5

Discussion

In this research, we investigated the combined role of stefin B and cystatin C in breast cancer progression using their double-knockout in the PyMT mouse model. Our aim was to examine how the simultaneous genetic ablation of both inhibitors, and therefore the disruption of control of cysteine cathepsins' proteolytic activity, influences tumor growth dynamics and the tumor microenvironment.

Cysteine cathepsins have long been known as important mediators of cancer progression. Mainly due to their elevated activity in the tumor microenvironment and their ability to promote invasion, angiogenesis, and immune escape (V. Turk et al., 2012). Their proteolytic activity is tightly controlled by endogenous inhibitors of the cystatin superfamily, including the intracellular stefin B and the extracellular cystatin C (V. Turk et al., 2008). Both have been involved in multiple diseases, including cancer. Beyond their well-established role as protease inhibitors, several studies suggest that they have protease-independent signalling functions such as modulating immune cell activation, cytokine production, and cell survival pathways. Additionally, their distinct localization provide these two inhibitors with specific characteristics that affect tumor biology via pathways other than direct protease inhibition (Leto, Crescimanno, & Flandina, 2018). Cystatin C has been shown to modulate dendritic cell maturation, MHC II–mediated antigen presentation and polarizing cytokine production, and inflammasome activation, all of which impact anti-tumor T-cell responses (Biasizzo et al., 2021; Magister & Kos, 2013). Stefin B has furthermore been implicated in the regulation of oxidative and lysosomal stress responses, NLRP3 inflammasome activation and apoptosis in myeloid cells (Kopitar-Jerala, 2015b; Katarina Maher et al., 2014; Trstenjak-Prebanda et al., 2023).

While the individual contributions of these inhibitors to tumor biology have been studied previously, their combined impact on breast cancer progression remained unexplored before this work. In the present study, we showed that simultaneous deficiency of stefin B and cystatin C in the PyMT mouse model results in delayed tumor onset, reduced tumor growth, decreased proliferation, increased apoptosis, and fewer lung metastases, accompanied by an altered composition of the tumor immune microenvironment (Matjan Štefin et al., 2026). In most analyses, we compared the double knockout PyMT female mice (PyMT;DKO) with PyMT wild-type controls (PyMT;WT). When possible, we also included tissues from single knockout cohorts from previous studies.

One of the main findings of this study was that the simultaneous deficiency of stefin B and cystatin C had a stronger inhibitory impact on tumor growth than the loss of either one of them alone. When we analysed tumor growth dynamics, we first observed that the combined deficiency of stefin B and cystatin C in PyMT;DKO mice resulted in delayed tumor onset and significantly reduced tumor growth compared to PyMT;WT controls. At 14 weeks, the cumulative tumor weight per mouse was reduced by 41% in PyMT;DKO

animals compared to controls. When we compared our data with previously reported single knockout data, we observed much stronger tumor growth suppression in the PyMT;DKO phenotype. Stefin B deletion alone reduced cumulative tumor weight by approximately 23%, and cystatin C deletion produced a similar ~23% reduction (Butinar et al., 2014; Završnik et al., 2017). Our results suggest that stefin B and cystatin C restrain tumor progression through parallel mechanisms, and that their combined depletion reveals synergistic tumor-suppressive effects. First, the stronger reduction in tumor burden in the double-knockout model compared with either single knockouts supports the idea that stefin B and cystatin C act through complementary rather than redundant pathways. Second, a single inhibitor deficiency produces only a moderate effect, whereas the combined loss of both inhibitors expression results in a much greater decrease in tumor burden. Thus, we can conclude that both inhibitors contribute to distinct but cooperating pro-tumorigenic mechanisms. The observed enhancement likely reflects the coordinated disruption of stefin B-mediated stress resistance (Butinar et al., 2014) and cystatin C-mediated growth support (Završnik et al., 2017), although the exact molecular mechanism of this synergy remains to be fully defined. Similarly, clinical data from colorectal cancer patients showed that elevated serum levels of both stefin B and cystatin C were associated with advanced disease stage and poor survival (Janko Kos et al., 2000). Together, these data further support the concept that the combined activity of these inhibitors can promote tumor progression.

Based on the activity measurements using synthetic cathepsin substrates, we detected a significant increase in substrate cleavage in PyMT;DKO tumors compared to PyMT;WT tumors, and observed an approximately 3-fold increase in activity in conditioned medium from PyMT;DKO primary tumor cells. These findings confirm that both stefin B and cystatin C are notable regulators of protease activity in this mouse model. Furthermore, the addition of the broad-spectrum cathepsin inhibitor E64 confirmed that the measured activity was referable specifically to cysteine cathepsins. Despite this markedly elevated extracellular proteolytic activity, PyMT;DKO tumors were smaller and grew more slowly, demonstrating that increased cathepsin activity does not translate into enhanced tumor progression in this context (Vasiljeva & Turk, 2008). One possible explanation is that unrestrained extracellular cathepsin activity in the absence of cystatin C cleaves and inactivates pro-survival extracellular signaling molecules, including growth factor receptor complexes or 14-3-3-associated complexes, as previously described in the cystatin C single-knockout model (Završnik et al., 2017). In addition, excessive pericellular proteolysis may destabilize integrin–ECM adhesion complexes and release ECM-bound growth factors in a non-productive manner and disrupt spatially organized survival signaling and, paradoxically, promote cell detachment and stress rather than sustained proliferation (Gocheva et al., 2006; Mohamed & Sloane, 2006). An alternative, not mutually exclusive, interpretation is that the increased apoptotic and immune-mediated pressure described below overrides any potential pro-tumorigenic effect of elevated matrix degradation (Vasiljeva & Turk, 2008).

Another key observation in late-stage PyMT;DKO tumors was a significant reduction of proliferation index, detected by immunohistochemical quantification of Ki67, which aligns with the smaller tumor size in the DKO group. This was further confirmed by BrdU incorporation assays on primary tumor cells that similarly demonstrated decreased proliferation in DKO cultures. These results are in agreement with previous work in the cystatin C single-knockout PyMT mice, where decreased proliferation was detected both *ex vivo* and *in vitro* and was correlated with altered p38 MAPK activation and decreased levels of secreted 14-3-3 proteins. These findings suggest a role of cystatin C in regulating growth-factor-related signaling beyond cathepsin inhibition (Završnik et al., 2017). Cystatin C has additionally been proposed to modulate TGF-β signaling and pathways

related to EMT, thus supporting tumor cell proliferation and survival in a context-dependent manner (Cox, 2009).

In addition to reduced proliferation of tumor cells, we detected a significantly higher rate of apoptotic cell death in PyMT;DKO tumors by TUNEL staining. Histological analysis showed more islands of dead cells in DKO tumors than in controls, in line with previous findings in stefin B-deficient PyMT tumors demonstrating increased sensitivity to oxidative and lysosomal stress (Butinar et al., 2014). Under physiological conditions, stefin B protects cells from inappropriate release of cathepsins into the cytosol by stabilizing lysosomal membranes. Therefore, in its absence, lysosomal permeabilization can occur under oxidative stress, allowing cathepsins to enter the cytoplasm and cleave Bcl-2 family members such as BH3-interacting domain death agonist (Bid), B-cell lymphoma-extra large (Bcl-xL), and myeloid cell leukemia-1 (Mcl-1). With Bid conversion to truncated Bid (tBid), activation of intrinsic apoptosis via caspases-3 and -7 occurs (Butinar et al., 2014). Stefin B also exhibits protease-independent cytoprotective effects by stabilizing FLIP, which interferes with death receptor signaling by competing with caspase-8 for FADD binding (Yang et al., 2010). These mechanisms explain why stefin B deficiency can sensitize tumor cells to both intrinsic and extrinsic apoptotic stimuli and are consistent with the increased apoptosis we observed in PyMT;DKO tumors.

Because reduced tumor size can also result from impaired tumor vascularization (Esteves, Monteiro, & Duarte, 2021), we next evaluated whether cystatin C and stefin B depletion affects angiogenesis in PyMT tumors. Quantitative analysis of CD31-positive vessels revealed no statistically significant difference in average vessel density between the two groups. These data ruled out impaired angiogenesis as the possible cause for the reduced size of PyMT;DKO tumors. Moreover, these data were consistent with previous observations in the cystatin C single-knockout PyMT model, where no major changes in vascular density were detected as well (Završnik et al., 2017). The reduced tumor burden in DKO mice is therefore more likely due to the combination of decreased proliferation and increased apoptosis than to alterations in tumor vascularization. Similarly to CD31 results, we did not observe any significant differences when evaluating the tumor-stroma ratio (TSR) in PyMT;DKO and PyMT;WT tumor sections. The reduced tumor burden in DKO mice, therefore, likely reflects cellular rather than structural remodeling of the tumor microenvironment.

The capability of the PyMT breast cancer mouse model to form pulmonary metastases spontaneously provides a useful framework for studying the mechanisms that control tumor dissemination. Histomorphometric analysis of lung sections at 14 weeks showed that PyMT;DKO mice had significantly fewer pulmonary metastases per unit area than PyMT;WT mice. Interestingly, the average size of individual metastatic lesions did not differ significantly between genotypes. This finding suggests that the combined absence of stefin B and cystatin C primarily interferes with early steps of metastasis, such as survival in circulation, extravasation, or initial colonization of the lung, rather than with the growth of already established metastatic foci. These findings contrast with the phenotypes of single knockouts, in which stefin B loss does not markedly affect metastasis and cystatin C loss promotes metastatic dissemination in the PyMT breast cancer mouse model (Butinar et al., 2014; Završnik et al., 2017). Comparable context-dependent effects of cystatin C on invasion and metastasis have been reported elsewhere. In prostate cancer, for example, downregulation of cystatin C enhanced tumor cell invasion (Abrahamson et al., 2003; Wegiel et al., 2009), whereas in K14-HPV16 transgenic mice, cystatin C deficiency promoted epidermal dysplasia and accelerated skin tumor development through increased proliferation, angiogenesis, and reduced apoptosis (Yu et al., 2010). In lung cancer, tissue and serum cystatin levels showed more complex connections with prognosis (Werle et al., 2006), further showing that its impact on metastatic behavior is highly dependent on tumor

type and microenvironment. As metastasis is a multistep process influenced by tumor cell-intrinsic properties and host factors such as immune surveillance and the "seed-and-soil" compatibility of distant organs (Balkwill, Capasso, & Hagemann, 2012; Gajewski, Schreiber, & Fu, 2013; Hanahan & Weinberg, 2011), the reduced metastatic burden in DKO mice likely reflects a combination of lowered proliferation of tumor cells, enhanced apoptosis, and a remodeled microenvironment that is less permissive for metastatic seeding.

The tumor microenvironment (TME) is a dynamic and complex ecosystem composed of cancer cells, stromal cells, immune cells, blood vessels, ECM, and soluble mediators that collectively shape tumor progression, angiogenesis, immune evasion, and resistance to therapy (Balkwill et al., 2012; Gajewski et al., 2013; Hanahan & Weinberg, 2011). Among immune cells within tumors, tumor-associated macrophages (TAMs) are key regulators of cancer progression and have already been studied in the PyMT model (E. Y. Lin et al., 2001; Qian & Pollard, 2010). In our study, we observed an increase in F4/80-positive macrophages in PyMT;DKO tumors compared to PyMT;WT tumors. More importantly, immunohistochemical analysis of macrophage polarization markers showed an increase in CD86-positive M1 macrophages in DKO tumors, with no related increase in CD206-positive M2 macrophages. This suggests a shift of the TME toward a more pro-inflammatory, tumor-suppressive state, more dominated by M1-like rather than M2-like TAMs, which typically prevail in many solid tumors and promote tumor progression through immunosuppression, angiogenesis, and tissue remodeling (Barbay et al., 2015; Bied, Ho, Ginhoux, & Blériot, 2023; R. Huang et al., 2024).

The observation of a tumor suppressive TME in PyMT;DKO tumors is of particular interest for several reasons. First, M1-polarized macrophages can display direct anti-tumor functions through the production of inflammatory mediators, reactive oxygen and nitrogen species, and cytotoxic activity against tumor cells (Chen et al., 2023; Hallam, Escorcio-Correia, Soper, Schultheiss, & Hagemann, 2009). Second, while the mechanisms underlying this M1 shift are not yet fully elucidated, it has been shown that cystatin C deficiency can modulate macrophage cytokine profiles and inflammatory responses, including regulation of TNF-α and IL-10 production (Frendéus, Wallin, Janciauskiene, & Abrahamson, 2009; K. Maher et al., 2014). Our observation of increased M1 macrophage infiltration aligns with very recent findings in pancreatic cancer models, where cystatin C knockout reduced tumor growth and altered the tumor immune microenvironment by lowering the recruitment of immunosuppressive TREM2+ macrophages (Kleeman et al., 2023). Although those studies mainly reported decreased pro-tumorigenic macrophage populations, whereas our PyMT;DKO model shows increased M1 populations, both observations converge on a remodeling of the tumor microenvironment toward an anti-tumor state. Additionally, given that stefin B has been involved in AMPK-dependent regulation of inflammasome activation and IL-18 release in macrophages (Kopitar-Jerala, 2015b; Trstenjak-Prebanda et al., 2023), it is plausible that the altered AMPK activation observed in DKO tumors contributes to reprogramming of macrophage population through crosstalk between metabolic stress pathways and inflammatory cytokine production. This hypothesis, although, remains to be tested experimentally. Thus, the simultaneous loss of stefin B and cystatin C appears to disrupt signaling networks that normally recruit and polarize TAMs toward a pro-tumorigenic state, creating conditions particularly unfavorable to survival and proliferation of tumor cells.

Our results, together with previous single-knockout data, strongly support the view that stefin B and cystatin C contribute to tumor progression through both protease-dependent and protease-independent mechanisms (Butinar et al., 2014; Završnik et al., 2017). The protease-independent functions of each inhibitor are particularly relevant in this context. First, stefin B provides cytoprotection against oxidative damage by

stabilizing lysosomal membranes and confers resistance to death receptor signaling through stabilization of FLIP; in addition, stefin B has been implicated in AMPK/mTOR-regulated autophagy and inflammasome control in macrophages (Butinar et al., 2014; Kopitar-Jerala, 2015a; Trstenjak-Prebanda et al., 2023). Second, cystatin C maintains growth-promoting signals in part through the support of 14-3-3 protein secretion, modulation of TGF-β signaling and EMT-related pathways. It has also been shown to affect macrophage cytokine profiles, recruitment of tumor-promoting immune cells, and NLRP3 inflammasome activation (Biasizzo et al., 2021; Cox, 2009; Frendéus et al., 2009; Kleeman et al., 2023; Magister & Kos, 2013; Završnik et al., 2017). Recent work in LPS-stimulated macrophages has shown that stefin B promotes activation of AMPK and suppresses mTORC1 signaling, thereby enhancing mitophagy and limiting NLRP3 inflammasome activation (Trstenjak-Prebanda et al., 2023). In PyMT;DKO tumors, we detected a selective increase in p-AMPK levels that was not observed in either single knockout. These data suggest a potential role for the combined loss of both inhibitors in modulating cellular stress responses via the AMPK pathway in a context-dependent manner. Thus, the DKO phenotype, characterized with reduced tumor growth and proliferation, enhanced apoptosis, elevated cathepsin activity, M1 macrophage polarization, and reduced metastatic colonization, likely reflects the simultaneous impairment of several interconnected pro-tumorigenic circuits rather than solely a consequence of unregulated proteolysis (Vasiljeva & Turk, 2008).

The pharmacological inhibition studies included in this thesis provide a complementary perspective on the cysteine cathepsin system in mammary tumor progression. In the FVB;PyMT transgenic model, treatment with the selective cathepsin X inhibitor Z9, the cathepsin B inhibitor nitroxoline, or their combination significantly reduced mammary tumor burden and pulmonary metastatic number and size compared with vehicle-treated controls. This antitumor effect was confirmed in an independent orthotopic MMTV-PyMT model, where Z9, nitroxoline, and combined treatment similarly suppressed tumor growth (Mitrović et al., 2022). These findings suggest that pharmacological inhibition of either cathepsin B or cathepsin X is sufficient to impair tumor progression in vivo.

Notably, although combined inhibition enhanced suppression of tumor cell migration and spheroid growth in vitro, it did not further reduce tumor growth or metastasis beyond either inhibitor alone *in vivo* (Mitrović et al., 2022), suggesting that compensatory interactions between cathepsins B and X identified in isolated cells do not necessarily translate into additive effects within the complex tumor microenvironment.

At first sight, this contrasts with the PyMT;DKO phenotype in the present study: whereas direct inhibition of the tumor-promoting cathepsins B and X reduced tumor growth, loss of the endogenous inhibitors stefin B and cystatin C, which increased overall cysteine cathepsin activity, was likewise associated with reduced tumor growth and metastatic burden. This apparent paradox reflects the fact that these approaches act at different regulatory levels: nitroxoline and Z9 directly block selected cathepsins, whereas stefin B and cystatin C deficiency removes broad-acting endogenous regulators with additional protease-independent effects on oxidative stress, cell survival, inflammatory signaling, and immune-cell behavior.

Furthermore, the Z-Phe-Arg-AMC activity assay used in PyMT;DKO tumor homogenates and conditioned media reflects overall cysteine cathepsin activity and cannot resolve the individual contribution, localization, or substrate specificity of particular cathepsins. The DKO phenotype therefore cannot be interpreted simply as a consequence of increased cathepsin B or X activity; rather, it reflects the combined effect of altered protease balance and the protease-independent functions of these endogenous inhibitors. Together, these comparisons underscore that the balance between cysteine cathepsins and their endogenous inhibitors, rather than total proteolytic activity alone, determines the outcome for tumor progression.

The analysis of stefin B deficiency in the LPS-induced neuroinflammation model provides additional context for the stress-related functions of stefin B outside the tumor setting. Increased Prx3 expression in the cerebellum of untreated stefin B-deficient mice and in the brain and cerebellum following LPS challenge is consistent with altered mitochondrial redox homeostasis and may reflect a compensatory antioxidant response to increased mitochondrial oxidative stress (Trstenjak Prebanda et al., 2021). These findings support a broader role of stefin B in cellular adaptation to oxidative and inflammatory stress, beyond its direct inhibition of cysteine cathepsins. This is relevant to the present cancer study because oxidative stress and inflammatory signaling are also important components of the tumor microenvironment and can influence tumor cell survival and immune-cell function. However, the neuroinflammation findings should be regarded as complementary mechanistic evidence and do not directly demonstrate that Prx3 or the same redox response is responsible for the tumor phenotype observed in PyMT;DKO mice.

However, several limitations should be taken into considerations in the interpretation of our findings. We conducted the study in a single transgenic mammary cancer model at a single time point, in a late stage of mammary carcinomas (14 weeks of age). It therefore remains to be determined to what extent the observed mechanisms apply to earlier or later stages of breast cancer development, to other breast cancer subtypes, or, ultimately, to other tumor types. Next, the specific signaling pathways connecting the combined loss of stefin B and cystatin C to the observed changes in TAM polarization and metastatic seeding remain incompletely characterized and explained and the contributions of individual cytokines, including IL-10, TNF-α, and IL-18 (Frendéus et al., 2009), are still an area for further investigation. Furthermore, an increase in p-AMPK was detected in DKO tumors; the upstream events potentially connecting DKO-induced AMPK activation to downstream mTOR suppression, cytokine remodeling, and macrophage polarization remain to be resolved. The question that is also still not clear is whether the activation of AMPK precedes or follows the immune microenvironment shift. Future studies should therefore address detailed evaluation of AMPK/mTOR and related stress signaling in DKO tumors, cytokine profiling of the both tumor and immune compartments, and testing if pharmacological or genetic modulation of these pathways can mimic or reverse the DKO phenotype - alone or in combination with traditional therapeutic strategies.

Overall, our research study shows that dual loss of stefin B and cystatin C suppresses tumor progression in PyMT breast cancer model, consistent with context-dependent, pro-tumorigenic roles of these inhibitors *in vivo*. Rather than being uniformly protective, stefin B and cystatin C appear to support tumor metabolism and a microenvironment that permits tumor growth and dissemination. In the PyMT;DKO model, their combined depletion unmasks a pronounced tumor-suppressive phenotype that exceeds the effects of either single-gene deficiency (Butinar et al., 2014; Završnik et al., 2017). Our findings challenge the traditional view of cystatins as uniformly protective in cancer. However, although combined stefin B and cystatin C deficiency reduced primary tumor growth and metastatic burden, it did not prevent mammary tumor development. The present findings therefore identify the stefin B–cystatin C regulatory axis, as well as its downstream proteolytic, stress-response, and immune-regulatory pathways, as priorities for further mechanistic and preclinical investigation, rather than directly supporting systemic dual inhibition of stefin B and cystatin C as a therapeutic strategy.

Chapter 6

Conclusions

In this thesis, we showed that combined stefin B and cystatin C deficiency in the PyMT mouse model affects mammary tumor progression. Loss of both inhibitors, included in our study, reduced primary tumor growth and pulmonary metastases and also by altered key cellular and microenvironmental features, including tumor cell proliferation, apoptosis and macrophage polarization. We therefore confirmed that balanced inhibition of cysteine cathepsins at both the intracellular and extracellular level is important for controlling primary tumor growth. Specifically, our findings revealed, that the dual inhibitor deficiency significantly reduces tumor cell proliferation, increases apoptosis, and promotes macrophage infiltration with a shift toward M1 polarization, supporting a role for both inhibitors in shaping the tumor immune microenvironment.

We also demonstrated that simultaneous loss of stefin B and cystatin C reduces the number of pulmonary metastases. This suggests that disruption of cathepsin regulation impairs metastatic seeding or early colonization rather than the growth of metastatic lesions.

By comparing our results with previously reported single-knockout PyMT mouse models, we showed that the double-knockout phenotype exceeds the effects of individual gene deletions. This highlights complementary rather than redundant functions of stefin B and cystatin C in breast cancer. These results together redefine the functional paradigm of cystatin family inhibitors in breast cancer and demonstrate a potential context-dependent tumor-promoting role rather than a uniformly protective function.

As complementary approaches, pharmacological inhibition of cathepsin B with nitroxoline and cathepsin X with Z9 reduced mammary tumor growth and metastatic progression in MMTV-PyMT breast cancer models. In addition, analysis of stefin B-deficient mice in an LPS-induced neuroinflammation model revealed altered expression of Prx3, further supporting a broader role of stefin B in mitochondrial redox regulation and cellular responses to inflammatory stress.

References

Abrahamson, M., Alvarez-Fernandez, M., & Nathanson, C.-M. (2003). Cystatins. *Biochemical Society Symposia, 70*, 179-199. doi:10.1042/bss0700179 %J Biochemical Society Symposia

Allison, E., Edirimanne, S., Matthews, J., & Fuller, S. J. (2023). Breast Cancer Survival Outcomes and Tumor-Associated Macrophage Markers: A Systematic Review and Meta-Analysis. *Oncol Ther, 11*(1), 27-48. doi:10.1007/s40487-022-00214-3

Attalla, S., Taifour, T., Bui, T., & Muller, W. (2021). Insights from transgenic mouse models of PyMT-induced breast cancer: recapitulating human breast cancer progression in vivo. *Oncogene, 40*(3), 475-491. doi:10.1038/s41388-020-01560-0

Bakir, B., Chiarella, A. M., Pitarresi, J. R., & Rustgi, A. K. (2020). EMT, MET, Plasticity, and Tumor Metastasis. *Trends Cell Biol, 30*(10), 764-776. doi:10.1016/j.tcb.2020.07.003

Balkwill, F. R., Capasso, M., & Hagemann, T. (2012). The tumor microenvironment at a glance. *J Cell Sci, 125*(Pt 23), 5591-5596. doi:10.1242/jcs.116392

Barbay, V., Houssari, M., Mekki, M., Banquet, S., Edwards-Lévy, F., Henry, J. P., . . . Brakenhielm, E. (2015). Role of M2-like macrophage recruitment during angiogenic growth factor therapy. *Angiogenesis, 18*(2), 191-200. doi:10.1007/s10456-014-9456-z

Biasizzo, M., Trstenjak-Prebanda, M., Dolinar, K., Pirkmajer, S., Završnik, J., Turk, B., & Kopitar-Jerala, N. (2021). Cystatin C Deficiency Increases LPS-Induced Sepsis and NLRP3 Inflammasome Activation in Mice. *10*(8), 2071.

Bied, M., Ho, W. W., Ginhoux, F., & Blériot, C. (2023). Roles of macrophages in tumor development: a spatiotemporal perspective. *Cellular & Molecular Immunology, 20*(9), 983-992. doi:10.1038/s41423-023-01061-6

Bray, F., Laversanne, M., Sung, H., Ferlay, J., Siegel, R. L., Soerjomataram, I., & Jemal, A. (2024). Global cancer statistics 2022: GLOBOCAN estimates of incidence and mortality worldwide for 36 cancers in 185 countries. *CA Cancer J Clin, 74*(3), 229-263. doi:10.3322/caac.21834

Breznik, B., Mitrović, A., T, T. L., & Kos, J. (2019). Cystatins in cancer progression: More than just cathepsin inhibitors. *Biochimie, 166*, 233-250. doi:10.1016/j.biochi.2019.05.002

Butinar, M., Prebanda, M. T., Rajković, J., Jerič, B., Stoka, V., Peters, C., . . . Vasiljeva, O. (2014). Stefin B deficiency reduces tumor growth via sensitization of tumor cells to oxidative stress in a breast cancer model. *Oncogene, 33*(26), 3392-3400. doi:10.1038/onc.2013.314

Chen, S., Saeed, A. F. U. H., Liu, Q., Jiang, Q., Xu, H., Xiao, G. G., . . . Duo, Y. (2023). Macrophages in immunoregulation and therapeutics. *Signal Transduction and Targeted Therapy, 8*(1), 207. doi:10.1038/s41392-023-01452-1

Christofori, G. (2006). New signals from the invasive front. *Nature, 441*(7092), 444-450. doi:10.1038/nature04872

Coll, E., Botey, A., Alvarez, L., Poch, E., Quintó, L., Saurina, A., . . . Darnell, A. (2000). Serum cystatin C as a new marker for noninvasive estimation of glomerular filtration rate and as a marker for early renal impairment. *Am J Kidney Dis, 36*(1), 29-34. doi:10.1053/ajkd.2000.8237

Cox, J. L. (2009). Cystatins and cancer. *Front Biosci (Landmark Ed), 14*(2), 463-474. doi:10.2741/3255

Čeru, S., Konjar, Š., Maher, K., Repnik, U., Križaj, I., Benčina, M., . . . Kopitar-Jerala, N. (2010). Stefin B interacts with histones and cathepsin L in the nucleus. *J Biol Chem, 285*(13), 10078-10086. doi:10.1074/jbc.M109.034793

DeLa Cadena, R. A., & Colman, R. W. (1991). Structure and functions of human kininogens. *Trends Pharmacol Sci, 12*(7), 272-275. doi:10.1016/0165-6147(91)90569-e

DeNardo, D. G., Barreto, J. B., Andreu, P., Vasquez, L., Tawfik, D., Kolhatkar, N., & Coussens, L. M. (2009). CD4+ T Cells Regulate Pulmonary Metastasis of Mammary Carcinomas by Enhancing Protumor Properties of Macrophages. *Cancer Cell, 16*(2), 91-102. doi:https://doi.org/10.1016/j.ccr.2009.06.018

Dennemärker, J., Lohmüller, T., Mayerle, J., Tacke, M., Lerch, M. M., Coussens, L. M., . . . Reinheckel, T. (2010). Deficiency for the cysteine protease cathepsin L promotes tumor progression in mouse epidermis. *Oncogene, 29*(11), 1611-1621. doi:10.1038/onc.2009.466

Diepenbruck, M., & Christofori, G. (2016). Epithelial-mesenchymal transition (EMT) and metastasis: yes, no, maybe? *Current opinion in cell biology, 43*, 7-13. doi:10.1016/j.ceb.2016.06.002

Ervin, H., & Cox, J. L. (2005). Late stage inhibition of hematogenous melanoma metastasis by cystatin C over-expression. *Cancer Cell International, 5*(1), 14. doi:10.1186/1475-2867-5-14

Esteves, M., Monteiro, M. P., & Duarte, J. A. (2021). The effects of vascularization on tumor development: A systematic review and meta-analysis of pre-clinical studies. *Crit Rev Oncol Hematol, 159*, 103245. doi:10.1016/j.critrevonc.2021.103245

Faubert, B., Boily, G., Izreig, S., Griss, T., Samborska, B., Dong, Z., . . . Jones, R. G. (2013). AMPK is a negative regulator of the Warburg effect and suppresses tumor growth in vivo. *Cell Metab, 17*(1), 113-124. doi:10.1016/j.cmet.2012.12.001

Fischer, K. R., Durrans, A., Lee, S., Sheng, J., Li, F., Wong, S. T., . . . Gao, D. (2015). Epithelial-to-mesenchymal transition is not required for lung metastasis but contributes to chemoresistance. *Nature, 527*(7579), 472-476. doi:10.1038/nature15748

Fluck, M. M., & Schaffhausen, B. S. (2009). Lessons in signaling and tumorigenesis from polyomavirus middle T antigen. *Microbiol Mol Biol Rev, 73*(3), 542-563, Table of Contents. doi:10.1128/mmbr.00009-09

Fonović, M., & Turk, B. (2014). Cysteine cathepsins and their potential in clinical therapy and biomarker discovery. *8*(5-6), 416-426. doi:https://doi.org/10.1002/prca.201300085

Fonović, U. P., Knez, D., Hrast, M., Zidar, N., Proj, M., Gobec, S., & Kos, J. (2020). Structure-activity relationships of triazole-benzodioxine inhibitors of cathepsin X. *European Journal of Medicinal Chemistry, 193*, 112218. doi:https://doi.org/10.1016/j.ejmech.2020.112218

Frendéus, K. H., Wallin, H., Janciauskiene, S., & Abrahamson, M. (2009). Macrophage responses to interferon-gamma are dependent on cystatin C levels. *Int J Biochem Cell Biol, 41*(11), 2262-2269. doi:10.1016/j.biocel.2009.05.005

Frese, K. K., & Tuveson, D. A. (2007). Maximizing mouse cancer models. *Nat Rev Cancer, 7*(9), 645-658. doi:10.1038/nrc2192

Gajewski, T. F., Schreiber, H., & Fu, Y.-X. (2013). Innate and adaptive immune cells in the tumor microenvironment. *Nature Immunology, 14*(10), 1014-1022. doi:10.1038/ni.2703

Gocheva, V., Wang, H. W., Gadea, B. B., Shree, T., Hunter, K. E., Garfall, A. L., . . . Joyce, J. A. (2010). IL-4 induces cathepsin protease activity in tumor-associated macrophages to promote cancer growth and invasion. *Genes Dev, 24*(3), 241-255. doi:10.1101/gad.1874010

Gocheva, V., Zeng, W., Ke, D., Klimstra, D., Reinheckel, T., Peters, C., . . . Joyce, J. A. (2006). Distinct roles for cysteine cathepsin genes in multistage tumorigenesis. *Genes Dev, 20*(5), 543-556. doi:10.1101/gad.1407406

Gogineni, V. R., Gupta, R., Nalla, A. K., Velpula, K. K., & Rao, J. S. (2012). uPAR and cathepsin B shRNA impedes TGF-β1-driven proliferation and invasion of meningioma cells in a XIAP-dependent pathway. *Cell Death & Disease, 3*(12), e439-e439. doi:10.1038/cddis.2012.170

Gounaris, E., Tung, C. H., Restaino, C., Maehr, R., Kohler, R., Joyce, J. A., . . . Khazaie, K. (2008). Live imaging of cysteine-cathepsin activity reveals dynamics of focal inflammation, angiogenesis, and polyp growth. *PLoS One, 3*(8), e2916. doi:10.1371/journal.pone.0002916

Grubb, A., & Löfberg, H. (1982). Human gamma-trace, a basic microprotein: amino acid sequence and presence in the adenohypophysis. *Proc Natl Acad Sci U S A, 79*(9), 3024-3027. doi:10.1073/pnas.79.9.3024

Guy, C. T., Cardiff, R. D., & Muller, W. J. (1992). Induction of mammary tumors by expression of polyomavirus middle T oncogene: a transgenic mouse model for metastatic disease. *Mol Cell Biol, 12*(3), 954-961. doi:10.1128/mcb.12.3.954-961.1992

Hallam, S., Escorcio-Correia, M., Soper, R., Schultheiss, A., & Hagemann, T. (2009). Activated macrophages in the tumour microenvironment-dancing to the tune of TLR and NF-kappaB. *J Pathol, 219*(2), 143-152. doi:10.1002/path.2602

Hanahan, D. (2022). Hallmarks of Cancer: New Dimensions. *Cancer Discovery, 12*(1), 31-46. doi:10.1158/2159-8290.CD-21-1059 %J Cancer Discovery

Hanahan, D., & Coussens, L. M. (2012). Accessories to the crime: functions of cells recruited to the tumor microenvironment. *Cancer Cell, 21*(3), 309-322. doi:10.1016/j.ccr.2012.02.022

Hanahan, D., & Weinberg, R. A. (2000). The hallmarks of cancer. *Cell, 100*(1), 57-70. doi:10.1016/s0092-8674(00)81683-9

Hanahan, D., & Weinberg, R. A. (2011). Hallmarks of cancer: the next generation. *Cell, 144*(5), 646-674. doi:10.1016/j.cell.2011.02.013

Harbeck, N., Penault-Llorca, F., Cortes, J., Gnant, M., Houssami, N., Poortmans, P., . . . Cardoso, F. (2019). Breast cancer. *Nature Reviews Disease Primers, 5*(1), 66. doi:10.1038/s41572-019-0111-2

Hardie, D. G., Ross, F. A., & Hawley, S. A. (2012). AMPK: a nutrient and energy sensor that maintains energy homeostasis. *Nat Rev Mol Cell Biol, 13*(4), 251-262. doi:10.1038/nrm3311

Harris, M. A., Savas, P., Virassamy, B., O'Malley, M. M. R., Kay, J., Mueller, S. N., . . . Loi, S. (2024). Towards targeting the breast cancer immune microenvironment. *Nature Reviews Cancer, 24*(8), 554-577. doi:10.1038/s41568-024-00714-6

He, Y., Liu, Q., Luo, Z., Hu, Q., Wang, L., & Guo, Z. (2025). Role of Tumor-Associated Macrophages in Breast Cancer Immunotherapy. *Front Biosci (Landmark Ed), 30*(4), 26995. doi:10.31083/fbl26995

Herzig, S., & Shaw, R. J. (2018). AMPK: guardian of metabolism and mitochondrial homeostasis. *Nat Rev Mol Cell Biol, 19*(2), 121-135. doi:10.1038/nrm.2017.95

Huang, C., Lu, J., Yang, J., Wang, Z., Hang, D., & Fu, Z. (2024). Associations of serum cystatin C concentrations with total mortality and mortality of 12 site-specific cancers. *Front Mol Biosci, 11*, 1209349. doi:10.3389/fmolb.2024.1209349

Huang, R., Kang, T., & Chen, S. (2024). The role of tumor-associated macrophages in tumor immune evasion. *J Cancer Res Clin Oncol, 150*(5), 238. doi:10.1007/s00432-024-05777-4

Hüsemann, Y., Geigl, J. B., Schubert, F., Musiani, P., Meyer, M., Burghart, E., . . . Klein, C. A. (2008). Systemic spread is an early step in breast cancer. *Cancer Cell, 13*(1), 58-68. doi:10.1016/j.ccr.2007.12.003

Jääskeläinen, M. M., Tumelius, R., Hämäläinen, K., Rilla, K., Oikari, S., Rönkä, A., . . . Auvinen, P. (2024). High Numbers of CD163+ Tumor-Associated Macrophages Predict Poor Prognosis in HER2+ Breast Cancer. *Cancers (Basel), 16*(3). doi:10.3390/cancers16030634

Jakoš, T., Pišlar, A., Jewett, A., & Kos, J. (2019). Cysteine Cathepsins in Tumor-Associated Immune Cells. *Front Immunol, 10*, 2037. doi:10.3389/fimmu.2019.02037

Janowski, R., Kozak, M., Jankowska, E., Grzonka, Z., Grubb, A., Abrahamson, M., & Jaskolski, M. (2001). Human cystatin C, an amyloidogenic protein, dimerizes through three-dimensional domain swapping. *Nat Struct Biol, 8*(4), 316-320. doi:10.1038/86188

Jiang, P., Chen, Y., & Liu, B. (2021). Prognostic Efficacy of Tumor-Stroma Ratio in Women With Breast Cancer: A Meta-Analysis of Cohort Studies. *Volume 11 - 2021*. doi:10.3389/fonc.2021.731409

Jolly, M. K., Boareto, M., Huang, B., Jia, D., Lu, M., Ben-Jacob, E., . . . Levine, H. (2015). Implications of the Hybrid Epithelial/Mesenchymal Phenotype in Metastasis. *Front Oncol, 5*, 155. doi:10.3389/fonc.2015.00155

Joyce, J. A., Baruch, A., Chehade, K., Meyer-Morse, N., Giraudo, E., Tsai, F. Y., . . . Hanahan, D. (2004). Cathepsin cysteine proteases are effectors of invasive growth and angiogenesis during multistage tumorigenesis. *Cancer Cell, 5*(5), 443-453. doi:10.1016/s1535-6108(04)00111-4

Kaur, G., Mohan, P., Pawlik, M., DeRosa, S., Fajiculay, J., Che, S., . . . Levy, E. (2010). Cystatin C rescues degenerating neurons in a cystatin B-knockout mouse model of progressive myoclonus epilepsy. *Am J Pathol, 177*(5), 2256-2267. doi:10.2353/ajpath.2010.100461

Kim, J., Harper, A., McCormack, V., Sung, H., Houssami, N., Morgan, E., . . . Fidler-Benaoudia, M. M. (2025). Global patterns and trends in breast cancer incidence and mortality across 185 countries. *Nat Med, 31*(4), 1154-1162. doi:10.1038/s41591-025-03502-3

Kleeman, S. O., Thakir, T. M., Demestichas, B., Mourikis, N., Loiero, D., Ferrer, M., . . . Janowitz, T. (2023). Cystatin C is glucocorticoid responsive, directs recruitment of Trem2+ macrophages, and predicts failure of cancer immunotherapy. *Cell Genomics, 3*(8), 100347. doi:https://doi.org/10.1016/j.xgen.2023.100347

Kolwijck, E., Massuger, L. F., Thomas, C. M., Span, P. N., Krasovec, M., Kos, J., & Sweep, F. C. (2010). Cathepsins B, L and cystatin C in cyst fluid of ovarian tumors. *J Cancer Res Clin Oncol, 136*(5), 771-778. doi:10.1007/s00432-009-0716-z

Konduri, S. D., Yanamandra, N., Siddique, K., Joseph, A., Dinh, D. H., Olivero, W. C., . . . Rao, J. S. (2002). Modulation of cystatin C expression impairs the invasive and tumorigenic potential of human glioblastoma cells. *Oncogene, 21*(57), 8705-8712. doi:10.1038/sj.onc.1205949

Kopitar-Jerala, N. (2015a). Innate Immune Response in Brain, NF-Kappa B Signaling and Cystatins. *Front Mol Neurosci, 8*, 73. doi:10.3389/fnmol.2015.00073

Kopitar-Jerala, N. (2015b). The Role of Stefin B in Neuro-inflammation. *Front Cell Neurosci, 9*, 458. doi:10.3389/fncel.2015.00458

Kopitz, C., Anton, M., Gansbacher, B., & Krüger, A. (2005). Reduction of experimental human fibrosarcoma lung metastasis in mice by adenovirus-mediated cystatin C overexpression in the host. *Cancer Res, 65*(19), 8608-8612. doi:10.1158/0008-5472.Can-05-1572

Kos, J., Krašovec, M., Cimerman, N., Nielsen, H. J., Christensen, I. J., & Brünner, N. (2000). Cysteine Proteinase Inhibitors Stefin A, Stefin B, and Cystatin C in Sera from Patients with Colorectal Cancer: Relation to Prognosis1. *Clinical Cancer Research, 6*(2), 505-511.

Kos, J., & Lah, T. T. (1998). Cysteine proteinases and their endogenous inhibitors: target proteins for prognosis, diagnosis and therapy in cancer (review). *Oncol Rep, 5*(6), 1349-1361. doi:10.3892/or.5.6.1349

Kramer, L., Turk, D., & Turk, B. (2017). The Future of Cysteine Cathepsins in Disease Management. *Trends Pharmacol Sci, 38*(10), 873-898. doi:10.1016/j.tips.2017.06.003

Lalioti, M. D., Antonarakis, S. E., & Scott, H. S. (2003). The epilepsy, the protease inhibitor and the dodecamer: progressive myoclonus epilepsy, cystatin b and a 12-mer repeat expansion. *Cytogenetic and Genome Research, 100*(1-4), 213-223. doi:10.1159/000072857 %J Cytogenetic and Genome Research

Lalmanach, G., Naudin, C., Lecaille, F., & Fritz, H. (2010). Kininogens: More than cysteine protease inhibitors and kinin precursors. *Biochimie, 92*(11), 1568-1579. doi:10.1016/j.biochi.2010.03.011

Lapidus, R. G., Nass, S. J., & Davidson, N. E. (1998). The Loss of Estrogen and Progesterone Receptor Gene Expression in Human Breast Cancer. *Journal of Mammary Gland Biology and Neoplasia, 3*(1), 85-94. doi:10.1023/A:1018778403001

Lee, S. Y., Ju, M. K., Jeon, H. M., Jeong, E. K., Lee, Y. J., Kim, C. H., . . . Kang, H. S. (2018). Regulation of Tumor Progression by Programmed Necrosis. *Oxid Med Cell Longev, 2018*, 3537471. doi:10.1155/2018/3537471

Lehtinen, M. K., Tegelberg, S., Schipper, H., Su, H., Zukor, H., Manninen, O., . . . Lehesjoki, A.-E. (2009). Cystatin B Deficiency Sensitizes Neurons to Oxidative Stress in Progressive Myoclonus Epilepsy, EPM1. *29*(18), 5910-5915. doi:10.1523/JNEUROSCI.0682-09.2009 %J The Journal of Neuroscience

Leto, G., Crescimanno, M., & Flandina, C. (2018). On the role of cystatin C in cancer progression. *Life Sci, 202*, 152-160. doi:10.1016/j.lfs.2018.04.013

Li, Y., Liu, F., Cai, Q., Deng, L., Ouyang, Q., Zhang, X. H. F., & Zheng, J. (2025). Invasion and metastasis in cancer: molecular insights and therapeutic targets. *Signal Transduct Target Ther, 10*(1), 57. doi:10.1038/s41392-025-02148-4

Lin, E. Y., Jones, J. G., Li, P., Zhu, L., Whitney, K. D., Muller, W. J., & Pollard, J. W. (2003). Progression to malignancy in the polyoma middle T oncoprotein mouse breast cancer model provides a reliable model for human diseases. *Am J Pathol, 163*(5), 2113-2126. doi:10.1016/s0002-9440(10)63568-7

Lin, E. Y., Nguyen, A. V., Russell, R. G., & Pollard, J. W. (2001). Colony-Stimulating Factor 1 Promotes Progression of Mammary Tumors to Malignancy. *Journal of Experimental Medicine, 193*(6), 727-740. doi:10.1084/jem.193.6.727 %J Journal of Experimental Medicine

Lin, Y. Y., Chen, Z. W., Lin, Z. P., Lin, L. B., Yang, X. M., Xu, L. Y., & Xie, Q. (2016). Tissue Levels of Stefin A and Stefin B in Hepatocellular Carcinoma. *Anat Rec (Hoboken), 299*(4), 428-438. doi:10.1002/ar.23311

Liu, Z., Chen, J., Ren, Y., Liu, S., Ba, Y., Zuo, A., . . . Han, X. (2024). Multi-stage mechanisms of tumor metastasis and therapeutic strategies. *Signal Transduction and Targeted Therapy, 9*(1), 270. doi:10.1038/s41392-024-01955-5

Löser, R., & Pietzsch, J. (2015). Cysteine cathepsins: their role in tumor progression and recent trends in the development of imaging probes. *Front Chem, 3*, 37. doi:10.3389/fchem.2015.00037

Magister, S., & Kos, J. (2013). Cystatins in immune system. *J Cancer, 4*(1), 45-56. doi:10.7150/jca.5044

Maglione, J. E., Moghanaki, D., Young, L. J., Manner, C. K., Ellies, L. G., Joseph, S. O., . . . MacLeod, C. L. (2001). Transgenic Polyoma middle-T mice model premalignant mammary disease. *Cancer Res, 61*(22), 8298-8305.

Maher, K., Jerič Kokelj, B., Butinar, M., Mikhaylov, G., Manček-Keber, M., Stoka, V., . . . Kopitar-Jerala, N. (2014). A Role for Stefin B (Cystatin B) in Inflammation and Endotoxemia*. *Journal of Biological Chemistry, 289*(46), 31736-31750. doi:https://doi.org/10.1074/jbc.M114.609396

Maher, K., Završnik, J., Jerič-Kokelj, B., Vasiljeva, O., Turk, B., & Kopitar-Jerala, N. (2014). Decreased IL-10 expression in stefin B-deficient macrophages is regulated by the MAP kinase and STAT-3 signaling pathways. *FEBS Lett, 588*(5), 720-726. doi:10.1016/j.febslet.2014.01.015

Marra, A., Trapani, D., Viale, G., Criscitiello, C., & Curigliano, G. (2020). Practical classification of triple-negative breast cancer: intratumoral heterogeneity, mechanisms of drug resistance, and novel therapies. *npj Breast Cancer, 6*(1), 54. doi:10.1038/s41523-020-00197-2

Matjan Štefin, P., Završnik, J., Butinar, M., Mikhaylov, G., Turk, B., & Vasiljeva, O. (2026). Stefin B and Cystatin C Deficiency Suppresses Tumor Growth and Alters Tumor Microenvironment in a Breast Cancer Model. *15*(4), 360.

McGranahan, N., & Swanton, C. (2017). Clonal Heterogeneity and Tumor Evolution: Past, Present, and the Future. *Cell, 168*(4), 613-628. doi:10.1016/j.cell.2017.01.018

Mikhaylov, G., Klimpel, D., Schaschke, N., Mikac, U., Vizovisek, M., Fonovic, M., . . . Vasiljeva, O. (2014). Selective Targeting of Tumor and Stromal Cells By a Nanocarrier System Displaying Lipidated Cathepsin B Inhibitor. *53*(38), 10077-10081. doi:https://doi.org/10.1002/anie.201402305

Mikhaylov, G., Mikac, U., Magaeva, A., Itin, V., Naiden, E., Psakhye, I., . . . Vasiljeva, O. (2011). Ferri-liposomes as an MRI-visible drug-delivery system for targeting tumours and their microenvironment. *Nature nanotechnology, 6*, 594-602. doi:10.1038/nnano.2011.112

Mirković, B., Markelc, B., Butinar, M., Mitrović, A., Sosič, I., Gobec, S., . . . Kos, J. (2015). Nitroxoline impairs tumor progression in vitro and in vivo by regulating cathepsin B activity. *Oncotarget, 6*(22), 19027-19042. doi:10.18632/oncotarget.3699

Mitrović, A., Završnik, J., Mikhaylov, G., Knez, D., Pečar Fonović, U., Matjan Štefin, P., . . . Kos, J. (2022). Evaluation of novel cathepsin-X inhibitors in vitro and in vivo and their ability to improve cathepsin-B-directed antitumor therapy. *Cell Mol Life Sci, 79*(1), 34. doi:10.1007/s00018-021-04117-w

Mohamed, M. M., & Sloane, B. F. (2006). Multifunctional enzymes in cancer. *Nature Reviews Cancer, 6*(10), 764-775. doi:10.1038/nrc1949

Munir, M. T., Kay, M. K., Kang, M. H., Rahman, M. M., Al-Harrasi, A., Choudhury, M., . . . Rahman, S. M. (2021). Tumor-Associated Macrophages as Multifaceted Regulators of Breast Tumor Growth. *Int J Mol Sci, 22*(12). doi:10.3390/ijms22126526

Mussap, M., & Plebani, M. (2004). Biochemistry and clinical role of human cystatin C. *Crit Rev Clin Lab Sci, 41*(5-6), 467-550. doi:10.1080/10408360490504934

Nakabayashi, H., Hara, M., & Shimuzu, K. (2005). Clinicopathologic significance of cystatin C expression in gliomas. *Hum Pathol, 36*(9), 1008-1015. doi:10.1016/j.humpath.2005.06.021

Nieto, M. A., Huang, R. Y., Jackson, R. A., & Thiery, J. P. (2016). EMT: 2016. *Cell, 166*(1), 21-45. doi:10.1016/j.cell.2016.06.028

Olafsson, I., & Grubb, A. (2000). Hereditary cystatin C amyloid angiopathy. *Amyloid, 7*(1), 70-79. doi:10.3109/13506120009146827

Olson, O. C., & Joyce, J. A. (2015). Cysteine cathepsin proteases: regulators of cancer progression and therapeutic response. *Nat Rev Cancer, 15*(12), 712-729. doi:10.1038/nrc4027

Pattengale, P. K., Stewart, T. A., Leder, A., Sinn, E., Muller, W., Tepler, I., . . . Leder, P. (1989). Animal models of human disease. Pathology and molecular biology of spontaneous neoplasms occurring in transgenic mice carrying and expressing activated cellular oncogenes. *Am J Pathol, 135*(1), 39-61.

Pennacchio, L. A., Bouley, D. M., Higgins, K. M., Scott, M. P., Noebels, J. L., & Myers, R. M. (1998). Progressive ataxia, myoclonic epilepsy and cerebellar apoptosis in cystatin B-deficient mice. *Nat Genet, 20*(3), 251-258. doi:10.1038/3059

Qian, B.-Z., & Pollard, J. W. (2010). Macrophage Diversity Enhances Tumor Progression and Metastasis. *Cell, 141*(1), 39-51. doi:https://doi.org/10.1016/j.cell.2010.03.014

Qiu, X., Zhao, T., Luo, R., Qiu, R., & Li, Z. (2022). Tumor-Associated Macrophages: Key Players in Triple-Negative Breast Cancer. *Volume 12 - 2022*. doi:10.3389/fonc.2022.772615

Quail, D. F., & Joyce, J. A. (2013). Microenvironmental regulation of tumor progression and metastasis. *Nat Med, 19*(11), 1423-1437. doi:10.1038/nm.3394

Radisky, E. S. (2024). Extracellular proteolysis in cancer: Proteases, substrates, and mechanisms in tumor progression and metastasis. *J Biol Chem, 300*(6), 107347. doi:10.1016/j.jbc.2024.107347

Reinheckel, T., Peters, C., Krüger, A., Turk, B., & Vasiljeva, O. (2012). Differential Impact of Cysteine Cathepsins on Genetic Mouse Models of De novo Carcinogenesis: Cathepsin B as Emerging Therapeutic Target. *Front Pharmacol, 3*, 133. doi:10.3389/fphar.2012.00133

Ribatti, D. (2017). Epithelial-mesenchymal transition in morphogenesis, cancer progression and angiogenesis. *Exp Cell Res, 353*(1), 1-5. doi:10.1016/j.yexcr.2017.02.041

Sami, A., & Raza, A. (2024). Reprogramming the tumor microenvironment - macrophages emerge as key players in breast cancer immunotherapy. *Front Immunol, 15*, 1457491. doi:10.3389/fimmu.2024.1457491

Sevenich, L., Schurigt, U., Sachse, K., Gajda, M., Werner, F., Müller, S., . . . Reinheckel, T. (2010). Synergistic antitumor effects of combined cathepsin B and cathepsin Z deficiencies on breast cancer progression and metastasis in mice. *Proc Natl Acad Sci U S A, 107*(6), 2497-2502. doi:10.1073/pnas.0907240107

Shen, Q., & Brown, P. H. (2005). Transgenic mouse models for the prevention of breast cancer. *Mutat Res, 576*(1-2), 93-110. doi:10.1016/j.mrfmmm.2004.10.013

Sokol, J. P., Neil, J. R., Schiemann, B. J., & Schiemann, W. P. (2005). The use of cystatin C to inhibit epithelial-mesenchymal transition and morphological transformation stimulated by transforming growth factor-beta. *Breast Cancer Res, 7*(5), R844-853. doi:10.1186/bcr1312

Sokol, J. P., & Schiemann, W. P. (2004). Cystatin C antagonizes transforming growth factor beta signaling in normal and cancer cells. *Mol Cancer Res, 2*(3), 183-195.

Stavrou, M., & Constantinidou, A. (2024). Tumor associated macrophages in breast cancer progression: implications and clinical relevance. *Front Immunol, 15*, 1441820. doi:10.3389/fimmu.2024.1441820

Stoka, V., Vasiljeva, O., Nakanishi, H., & Turk, V. (2023). The Role of Cysteine Protease Cathepsins B, H, C, and X/Z in Neurodegenerative Diseases and Cancer. *Int J Mol Sci, 24*(21). doi:10.3390/ijms242115613

Strojan, P., Anicin, A., Svetic, B., Pohar, M., Smid, L., & Kos, J. (2007). Stefin a and stefin B: markers for prognosis in operable squamous cell carcinoma of the head and neck. *Int J Radiat Oncol Biol Phys, 68*(5), 1335-1341. doi:10.1016/j.ijrobp.2007.02.004

Sung, H., Ferlay, J., Siegel, R. L., Laversanne, M., Soerjomataram, I., Jemal, A., & Bray, F. (2021). Global Cancer Statistics 2020: GLOBOCAN Estimates of Incidence and Mortality Worldwide for 36 Cancers in 185 Countries. *71*(3), 209-249. doi:https://doi.org/10.3322/caac.21660

Škerget, K., Taler-Verčič, A., Bavdek, A., Hodnik, V., Čeru, S., Tušek-Žnidarič, M., . . . Žerovnik, E. (2010). Interaction between Oligomers of Stefin B and Amyloid-β in Vitro and in Cells*. *Journal of Biological Chemistry, 285*(5), 3201-3210. doi:https://doi.org/10.1074/jbc.M109.024620

Taglieri, N., Koenig, W., & Kaski, J. C. (2009). Cystatin C and Cardiovascular Risk. *Clinical Chemistry, 55*(11), 1932-1943. doi:10.1373/clinchem.2009.128397 %J Clinical Chemistry

Tizon, B., Sahoo, S., Yu, H., Gauthier, S., Kumar, A. R., Mohan, P., . . . Levy, E. (2010). Induction of Autophagy by Cystatin C: A Mechanism That Protects Murine Primary Cortical Neurons and Neuronal Cell Lines. *PLoS One, 5*(3), e9819. doi:10.1371/journal.pone.0009819

Trstenjak-Prebanda, M., Biasizzo, M., Dolinar, K., Pirkmajer, S., Turk, B., Brault, V., . . . Kopitar-Jerala, N. (2023). Stefin B Inhibits NLRP3 Inflammasome Activation via AMPK/mTOR Signalling. *Cells, 12*(23). doi:10.3390/cells12232731

Trstenjak Prebanda, M., Matjan-Štefin, P., Turk, B., & Kopitar-Jerala, N. (2021). Altered Expression of Peroxiredoxins in Mouse Model of Progressive Myoclonus Epilepsy upon LPS-Induced Neuroinflammation. *Antioxidants (Basel), 10*(3). doi:10.3390/antiox10030357

Tummalapalli, P., Spomar, D., Gondi, C. S., Olivero, W. C., Gujrati, M., Dinh, D. H., & Rao, J. S. (2007). RNAi-mediated abrogation of cathepsin B and MMP-9 gene expression in a malignant meningioma cell line leads to decreased tumor growth, invasion and angiogenesis. *Int J Oncol, 31*(5), 1039-1050. doi:10.3892/ijo.31.5.1039

Turk, B., Turk, D., & Salvesen, G. S. (2002). Regulating cysteine protease activity: essential role of protease inhibitors as guardians and regulators. *Curr Pharm Des, 8*(18), 1623-1637. doi:10.2174/1381612023394124

Turk, B., Turk, D., & Salvesen, G. S. (2005). Regulating Cysteine Protease Activity: Essential Role of Protease Inhibitors as Guardians and Regulators. *Medicinal*

Chemistry Reviews - Online (Discontinued), 2(4), 283-297. doi:http://dx.doi.org/10.2174/1567203054637524

Turk, V., & Bode, W. (1991). The cystatins: Protein inhibitors of cysteine proteinases. *285*(2), 213-219. doi:https://doi.org/10.1016/0014-5793(91)80804-C

Turk, V., Stoka, V., & Turk, D. (2008). Cystatins: biochemical and structural properties, and medical relevance. *Front Biosci, 13*, 5406-5420. doi:10.2741/3089

Turk, V., Stoka, V., Vasiljeva, O., Renko, M., Sun, T., Turk, B., & Turk, D. (2012). Cysteine cathepsins: from structure, function and regulation to new frontiers. *Biochim Biophys Acta, 1824*(1), 68-88. doi:10.1016/j.bbapap.2011.10.002

van Pelt, G. W., Kjær-Frifeldt, S., van Krieken, J., Al Dieri, R., Morreau, H., Tollenaar, R., . . . Mesker, W. E. (2018). Scoring the tumor-stroma ratio in colon cancer: procedure and recommendations. *Virchows Arch, 473*(4), 405-412. doi:10.1007/s00428-018-2408-z

Vangangelt, K. M. H., Green, A. R., Heemskerk, I. M. F., Cohen, D., van Pelt, G. W., Sobral-Leite, M., . . . Mesker, W. E. (2020). The prognostic value of the tumor-stroma ratio is most discriminative in patients with grade III or triple-negative breast cancer. *Int J Cancer, 146*(8), 2296-2304. doi:10.1002/ijc.32857

Vasiljeva, O., Korovin, M., Gajda, M., Brodoefel, H., Bojic, L., Krüger, A., . . . Reinheckel, T. (2008). Reduced tumour cell proliferation and delayed development of high-grade mammary carcinomas in cathepsin B-deficient mice. *Oncogene, 27*(30), 4191-4199. doi:10.1038/onc.2008.59

Vasiljeva, O., Papazoglou, A., Krüger, A., Brodoefel, H., Korovin, M., Deussing, J., . . . Reinheckel, T. (2006). Tumor cell-derived and macrophage-derived cathepsin B promotes progression and lung metastasis of mammary cancer. *Cancer Res, 66*(10), 5242-5250. doi:10.1158/0008-5472.can-05-4463

Vasiljeva, O., Reinheckel, T., Peters, C., Turk, D., Turk, V., & Turk, B. (2007). Emerging roles of cysteine cathepsins in disease and their potential as drug targets. *Curr Pharm Des, 13*(4), 387-403. doi:10.2174/138161207780162962

Vasiljeva, O., & Turk, B. (2008). Dual contrasting roles of cysteine cathepsins in cancer progression: Apoptosis versus tumour invasion. *Biochimie, 90*(2), 380-386. doi:https://doi.org/10.1016/j.biochi.2007.10.004

Vidak, E., Javoršek, U., Vizovišek, M., & Turk, B. (2019). Cysteine Cathepsins and their Extracellular Roles: Shaping the Microenvironment. *Cells, 8*(3). doi:10.3390/cells8030264

Vizovišek, M., Fonović, M., & Turk, B. (2019). Cysteine cathepsins in extracellular matrix remodeling: Extracellular matrix degradation and beyond. *Matrix Biology, 75-76*, 141-159. doi:https://doi.org/10.1016/j.matbio.2018.01.024

Wang, B., Sun, J., Kitamoto, S., Yang, M., Grubb, A., Chapman, H. A., . . . Shi, G. P. (2006). Cathepsin S controls angiogenesis and tumor growth via matrix-derived angiogenic factors. *J Biol Chem, 281*(9), 6020-6029. doi:10.1074/jbc.M509134200

Wang, C., Lin, Y., Zhu, H., Zhou, Y., Mao, F., Huang, X., . . . Li, C. (2022). The Prognostic and Clinical Value of Tumor-Associated Macrophages in Patients With Breast Cancer: A Systematic Review and Meta-Analysis. *Front Oncol, 12*, 905846. doi:10.3389/fonc.2022.905846

Wegiel, B., Jiborn, T., Abrahamson, M., Helczynski, L., Otterbein, L., Persson, J. L., & Bjartell, A. (2009). Cystatin C is downregulated in prostate cancer and modulates invasion of prostate cancer cells via MAPK/Erk and androgen receptor pathways. *PLoS One, 4*(11), e7953. doi:10.1371/journal.pone.0007953

Werle, B., Schanzenbächer, U., Lah, T. T., Ebert, E., Jülke, B., Ebert, W., . . . Kos, J. (2006). Cystatins in non-small cell lung cancer: tissue levels, localization and relation to prognosis. *Oncol Rep, 16*(4), 647-655.

Withana, N. P., Blum, G., Sameni, M., Slaney, C., Anbalagan, A., Olive, M. B., . . . Parker, B. S. (2012). Cathepsin B inhibition limits bone metastasis in breast cancer. *Cancer Res, 72*(5), 1199-1209. doi:10.1158/0008-5472.Can-11-2759

Wyckoff, J. B., Wang, Y., Lin, E. Y., Li, J.-f., Goswami, S., Stanley, E. R., . . . Condeelis, J. (2007). Direct Visualization of Macrophage-Assisted Tumor Cell Intravasation in Mammary Tumors. *Cancer Res, 67*(6), 2649-2656. doi:10.1158/0008-5472.CAN-06-1823 %J Cancer Research

Yadati, T., Houben, T., Bitorina, A., & Shiri-Sverdlov, R. (2020). The Ins and Outs of Cathepsins: Physiological Function and Role in Disease Management. *Cells, 9*(7). doi:10.3390/cells9071679

Yang, F., Tay, K. H., Dong, L., Thorne, R. F., Jiang, C. C., Yang, E., . . . Zhang, X. D. (2010). Cystatin B inhibition of TRAIL-induced apoptosis is associated with the protection of FLIP(L) from degradation by the E3 ligase itch in human melanoma cells. *Cell Death Differ, 17*(8), 1354-1367. doi:10.1038/cdd.2010.29

Yee, P. P., & Li, W. (2021). Tumor necrosis: A synergistic consequence of metabolic stress and inflammation. *Bioessays, 43*(7), e2100029. doi:10.1002/bies.202100029

Yu, W., Liu, J., Shi, M. A., Wang, J., Xiang, M., Kitamoto, S., . . . Shi, G.-P. (2010). Cystatin C Deficiency Promotes Epidermal Dysplasia in K14-HPV16 Transgenic Mice. *PLoS One, 5*(11), e13973. doi:10.1371/journal.pone.0013973

Završnik, J., Butinar, M., Prebanda, M. T., Krajnc, A., Vidmar, R., Fonović, M., . . . Vasiljeva, O. (2017). Cystatin C deficiency suppresses tumor growth in a breast cancer model through decreased proliferation of tumor cells. *Oncotarget, 8*(43), 73793-73809. doi:10.18632/oncotarget.17379

Zhang, C., He, Y., Liu, X., Xie, J., Fang, M., Yang, X., . . . Zhang, C. C. (2025). Oligomeric cystatin C supports the immunosuppressive activity of myeloid cells through interaction with inhibitory receptors. *Signal Transduction and Targeted Therapy, 10*(1), 368. doi:10.1038/s41392-025-02462-x

Zhang, G. P., Yue, X., & Li, S. Q. (2020). Cathepsin C Interacts with TNF- α /p38 MAPK Signaling Pathway to Promote Proliferation and Metastasis in Hepatocellular Carcinoma. *Cancer Res Treat, 52*(1), 10-23. doi:10.4143/crt.2019.145

Zhang, W., Zi, M., Sun, L., Wang, F., Chen, S., Zhao, Y., . . . Xu, Y. (2019). Cystatin C regulates major histocompatibility complex-II–peptide presentation and extracellular signal-regulated kinase-dependent polarizing cytokine production by bone marrow-derived dendritic cells. *97*(10), 916-930. doi:https://doi.org/10.1111/imcb.12290

Bibliography

Publications Related to the Thesis

Journal Articles

Matjan Štefin, P., Završnik, J., Butinar, M., Mikhaylov, G., Turk, B., & Vasiljeva, O. (2026). Stefin B and Cystatin C Deficiency Suppresses Tumor Growth and Alters Tumor Microenvironment in a Breast Cancer Model. *15*(4), 360.

Mitrović, A., Završnik, J., Mikhaylov, G., Knez, D., Pečar Fonović, U., Matjan Štefin, P., . . . Kos, J. (2022). Evaluation of novel cathepsin-X inhibitors in vitro and in vivo and their ability to improve cathepsin-B-directed antitumor therapy. Cell Mol Life Sci, 79(1), 34. doi:10.1007/s00018-021-04117-w

Trstenjak Prebanda, M., Matjan-Štefin, P., Turk, B., & Kopitar-Jerala, N. (2021). Altered Expression of Peroxiredoxins in Mouse Model of Progressive Myoclonus Epilepsy upon LPS-Induced Neuroinflammation. Antioxidants (Basel), 10(3). doi:10.3390/antiox10030357

Conference Papers

Vidmar, R., Vizovišek, M., Sever, T., Matjan Štefin, P., Mikhaylov, G., Reinheckel, T., Turk, B., & Fonović, M. (2021). Legumain as a modulator of immune response. FEBS Open Bio, 11(Suppl. 1), 166. https://doi.org/10.1002/2211-5463.13205

Vidmar, R., Vizovišek, M., Sever, T., Kolarič, M., Matjan-Štefin, P., Mikhaylov, G., Kozak, A., Reinheckel, T., Turk, B., & Fonović, M. (2022). Emerging role of legumain in innate immune response – potential link to anti-inflammatory effects. In A. Kozak (Ed.) *Proteolysis at the interface between health and disease: FEBS ICGEB 2022 Advanced Course, 18–21 September, Bled, Slovenia: Book of abstracts* (p. 25).

Kozak, A., Mikhaylov, G., Matjan-Štefin, P., Khodakivskyi, P., Turk, B., Goun, E., & Vasiljeva, O. (2022). A new cathepsin D targeting system based on liposome-bound pepstatin A. In A. Kozak (Ed.) *Proteolysis at the interface between health and disease: FEBS ICGEB 2022 Advanced Course, 18–21 September, Bled, Slovenia: Book of abstracts* (p. 53).

Sinožić, T., Matjan-Štefin, P., Sever, T., & Turk, B. (2024). Application of a tissue decellularization method in colorectal cancer protein biomarker research. In V. Stoka (Ed.) *Proteolysis at the interface between health and disease: FEBS 2024 advanced course, Bled, Slovenia, 14–18 September 2024: Programme and book of abstracts* (pp. 54–55).

Lavrih, E., Matjan-Štefin, P., Turk, B., & Mikhaylov, G. (2024). Protease inhibitors in combination with nanosized drug delivery system for retinal neurodegeneration. In V. Stoka (Ed.) *Proteolysis at the interface between health and disease: FEBS 2024 advanced course, Bled, Slovenia, 14–18 September 2024: Programme and book of abstracts* (pp. 50–51).

Matjan-Štefin, P., Završnik, J., Butinar, M., Mikhaylov, G., Turk, B., & Vasiljeva, O. (2024). Stefin B and cystatin C deficiency suppresses tumor growth and alters tumor microenvironment. In V. Stoka (Ed.) *Proteolysis at the interface between health and disease: FEBS 2024 advanced course, Bled, Slovenia, 14–18 September 2024: Programme and book of abstracts* (p. 52).

Podlipec, R., Krišelj, A., Matjan-Štefin, P., Usaar, S., & Humar, M. (2025). Optične resonance v lipidnih kapljicah maščobnih celic za natančno sledenje dinamike bioloških procesov. In J. Stergar, I. Lengar, & P. Ziherl (Eds.), *14. slovenska fizikalna konferenca: Zbornik povzetkov, Brdo pri Kranju, 10. oktober 2025* (p. 11). Fakulteta za matematiko in fiziko.

Podlipec, R., Krišelj, A., Matjan-Štefin, P., Usaar, S., & Humar, M. (2025). Nanometer-precision tracking of adipocyte dynamics via single–lipid droplet whispering-gallery microresonators. ACS Sensors, 10, 511–521. doi:10.1021/acssensors.5c03272

Other Publications

Podlipec, R., Krišelj, A., Matjan-Štefin, P., Usaar, S., & Humar, M. (2025). Nanometer-precision tracking of adipocyte dynamics via single–lipid droplet whispering-gallery microresonators. ACS Sensors, 10, 511–521. doi:10.1021/acssensors.5c03272

Biography

The author of this thesis, Petra Matjan Štefin, obtained her Veterinary Medicine degree in 2018 at the Faculty of Veterinary Medicine, University of Ljubljana. In October 2019, she enrolled in the Nanosciences and Nanotechnologies programme at the Jožef Stefan International Postgraduate School under the supervision of Dr. Georgy Mikhaylov. In the same year, she started working as a young researcher at the Jožef Stefan Institute Department of Biochemistry, Molecular and Structural Biology. Her doctoral dissertation research focused on the role of stefin B and cystatin C simultaneous removal on cancer progression and tumor microenvironment using a breast cancer mouse model. Since October 2024, she has been working as an assistant researcher at the same department at the Jožef Stefan Institute, with a focus on *in vivo* cancer studies.